

Microheterogeneity and individual differences of human urinary *N*-glycome under normal physiological conditions.

2023

Hend Ahmed Mohamed Aly Zedan

Doctoral Program of Life and Food Sciences

Graduate school of Science and Technology

Niigata University

LIST OF CONTENTS

Abbreviations

Acknowledgment

1.1. Abstract	1
1.2. Introduction	2-4
1.3. Material and Methods	5-7
1.4. Results and Discussion	8-22
1.5. Conclusion	23-25
1.6. Figures	26-55
1.7. Tables	56-63
1.8. References	64-69

LIST OF ABBREVIATIONS

PA	pyridylamino residue
DEAE HPLC	diethylaminoethyl- High Performance Liquid Chromatography
LC	Liquid Chromatography
(RP)-LC	reversed-phase Liquid Chromatography
HILIC	hydrophilic interaction Liquid Chromatography
(PGC)-LC	porous graphitized carbon Liquid Chromatography
MS	Mass Spectrometry
MS/MS	Tandem Mass Spectrometry
m/z	Mass to Charge ratio
PTM	Post-translation modifications
N	neutral
A1	mono-sialylated
A2	di-sialylated
A3	tri-sialylated
A4	tetra- sialylated
ASGPR	asialoglycoprotein receptor
ManR	mannose receptor

ACKNOWLEDGEMENT

I would like to express my deepest gratitude to my supervisor, Prof. Shunji Natsuka, for his unwavering support, guidance, and encouragement throughout my PhD journey. His expertise and invaluable insights have been instrumental in shaping my research and have provided me with the opportunity to grow both intellectually and professionally.

I would also like to thank Prof. Tadashi Yamamoto for providing me the urine samples. In addition to, his invaluable feedback and suggestions, which helped me to improve my research and my thesis.

I am also grateful to my colleagues in professor Natsuka's lab for their support and co-operation.

I would like to extend my sincere thanks and appreciation to my dear husband. In particular for his continuous and valuable support to me during my studies.

Finally, I would like to thank my family and loved ones for their unwavering support and encouragement. This achievement would not have been possible without their love and support.

Thank you all.

Abstract: Urine is considered an outstanding biological fluid for biomarker discovery, reflecting both systemic and urogenital physiology. However, analyzing the *N*-glycome in urine in detail has been challenging due to the low abundance of glycans attached to glycoproteins compared to free oligosaccharides. Therefore, this study aims to thoroughly analyze urinary *N*-glycome using LC-MS/MS. The *N*-glycans were released using hydrazine and labeled with 2-aminopyridine (PA), followed by anion-exchange fractionation before LC-MS/MS analysis. A total of 109 *N*-glycans were identified and quantified, of which 58 were identified and quantified repeatedly in at least 80% of samples and accounted for approximately 85% of the total urinary glycome signal. Interestingly, a comparison between urine and serum *N*-glycome revealed that approximately 50% of the urinary glycome could originate from the kidney and urinary tract, where they were exclusively identified in urine, while the remaining 50% were common in both. Additionally, a correlation was found between age/sex and the relative abundances of urinary *N*-glycome, with more age-related changes observed in women than men. The results of this study provide a reference for human urine *N*-glycome profiling and structural annotations.

Keywords: HPLC; multistage mass spectrometry; *N*-glycans; urine; serum

1. Introduction

N-glycosylation is considered one of the most common co- and post-translational protein modifications [1, 2]. Approximately 50% of human proteins are likely to be *N*-glycosylated, with some estimations approaching 70% [3]. Unlike nucleic acid and protein synthesis, *N*-glycosylation is not a template-driven process, as diverse glycosyltransferase and glycosidase enzymes control the attachment of the oligosaccharides to some asparagine residues of the protein backbone [4]. *N*-glycans are involved in numerous physiological processes, including protein folding, cell signaling, immune reactions, host–pathogen interactions, protein trafficking, and so forth [5]. The variation of the *N*-glycome profile reflects the physiological and pathological status of cells and may be associated with different diseases' onset and progression [5].

In the context of biomarker discovery, different *N*-glycome studies are focused on building a baseline reference from human tissues or biofluids under normal physiological conditions, which can be used for the comparison with future *N*-glycome studies under disease conditions. For example, Kaijie Xiao et al. identified 214 distinct *N*-glycan structures with a spectrum-level false discovery rate $\leq 1\%$ from human normal liver LO2 seed cells [6]. They reported that 37% of identified *N*-glycans was fucosylated, 13% was sialylated, 32% was sialylated-fucosylated, and only 4% was oligomannose-containing *N*-glycans. Additionally, the glycome profiles of IgG-depleted and nondepleted plasma samples were demonstrated under normal physiological conditions, and they identified 50 and 106 independent glycan ions before and after IgG-depletion, respectively [7].

In urine, Haiying Li et al. identified 116 *N*-glycan compositions. Additionally, they performed quantitative comparisons of the most repetitive 46 glycan compositions between different age and sex groups. They showed significant differences between the adult male and female cohorts [8].

However, the previous studies investigated urinary *N*-glycome under normal physiological conditions in the context of biomarker discovery. They generally identified glycans at the composition level, without assessing further structural aspects that may differentiate glycan isomers with the same composition.

Of note, only using MS-MS/MS data is not sufficient for this purpose, and further dimensions might be required. Research reported that liquid chromatography (LC)-MS techniques, such as hydrophilic interaction-LC (HILIC) [9], porous graphitized carbon (PGC)-LC [10], and reversed-phase (RP)-LC [11, 12] are often more suitable approaches for this purpose.

However, the isomeric separation of PA-*N*-glycans on a C18 column outperforms other LC methods in discriminating the glycan isomers with different branching structures based on their elution time, as pyridylamino residue (PA) is small and less hydrophobic than other labeling methods, such as 2-AB or 2-AA, which makes the contribution of the glycan itself to the retention relatively high and results in better separation of different species and deducing more structural information on the glycan [13, 14]. Thus, to investigate the structural features of the human *N*-glycome, and discriminate among glycan isoforms under normal physiological conditions in urine and serum, PA-Glycans were dually fractionated by anion-exchange HPLC and reversed-phase (RP)-LC before MS-MS/MS analysis.

Additionally, considering these identified structural features, I aim to investigate the variations among genders and different ages in urine. Moreover, a comparative analysis of urinary and serum

glycome was conducted to distinguish between *N*-glycan structures originating from the kidney or urinary tract and those originating from the circulation system.

2. Materials and Methods

2.1. Protein Extraction and Purification from Urine Samples

Urine samples from 12 healthy individuals, including 6 males with an average age of 32 years and 6 females with an average age of 30 years (Table 1), were obtained. The urine samples were collected and immediately placed in ice boxes, followed by centrifugation at 1000 rpm for 10 min at 4 °C to eliminate debris. The samples were then stored at -20 °C for further processing. The methanol/chloroform (4:1) extraction method [15] was used to extract glycoproteins from the urine.

2.2. Preparation of PA-Glycans

Urinary *N*-linked glycans were liberated from glycoproteins by hydrazinolysis, according to the method described before [16, 17]. Briefly, the lyophilized samples were subjected to heat at 100 °C for 12 h with anhydrous hydrazine. Repeated evaporations were applied to the samples to remove hydrazine. The released glycans were re-*N*-acetylated with acetic anhydride in a saturated sodium bicarbonate solution and then passed through a Dowex 50Wx2 (H⁺) cation exchanger (Dow Chemicals, Midland, MI, USA) to remove sodium ions. The reducing ends of the liberated glycans were tagged with the fluorophore 2-aminopyridine using reductive amination [18, 19]. To analyze human serum *N*-glycans, 5 μL of pooled healthy human serum was purchased from CosmoBio (Tokyo, Japan). The method used was the same as for the urine samples.

2.3. Purification of PA-Glycans

To remove the excess reagents and contaminants, three consecutive purification methods were applied: water-saturated phenol/chloroform (1:1, v/v) extraction, gel filtration (1 × 8 cm, TSK-gel

Toyopearl HW-40F; Tosoh, Tokyo, Japan), and solid-phase extraction with a graphite carbon cartridge (GL-Pak Carbograph 150 mg; GL Sciences, Tokyo, Japan). These methods were reported elsewhere [12, 20].

2.4. Anion-Exchange HPLC for PA-Glycan Separation

Prior to LC-MS analysis, the samples were fractionated according to the number of negative charges using anion-exchange HPLC, in which PA-glycans were separated on a TSK-gel diethylaminoethyl (DEAE)-5PW column (0.75×7.5 cm; Tosoh, Tokyo, Japan) using a Waters Alliance HPLC system with a Waters 2475 fluorescence detector (Milford, MA, USA) in the methods previously reported [12].

2.5. LC-MS Analysis

PA-glycans were analyzed using a Dionex U3000 HPLC system and an ESI-probe coupled to a LTQ XL linear ion trap mass spectrometer (Thermo Scientific, San Jose, CA, USA). PA-glycans were separated by reversed-phase LC on an Inert-Sustain AQ-C18 column (2.1×150 mm) at a flow rate of 0.2 mL/min at 30 °C. Elution was performed using Eluent A (0.2% formic acid) and Eluent B (20% acetonitrile in 0.2% formic acid). The column was equilibrated with Eluent A, and 3 min after sample injection, the proportion of Eluent B was increased linearly from 0 to 25% over 100 min, and then to 100% over 5 min. The elution times of the PA-*N*-glycans by reversed-phase HPLC were standardized and converted to glucose unit values by comparison with the elution times of PA-isomaltooligosaccharides, as described before [12].

MS and MS/MS data were collected in a data-dependent mode, and the top five full MS peaks in each scan event were selected for MS/MS analysis. Collision-induced dissociation was used for

MS/MS analysis. The data were recorded and analyzed using the Xcalibur 2.2 software (Thermo Fisher Scientific, Waltham, Massachusetts, U.S.).

2.6. Data Analysis

To identify the *N*-glycans, the analyzed ions were compared against an in-house glycan library [12, 14] using various factors, such as precursor ion mass, elution time, glucose unit, MS2 fragment ions, and published structures. To calculate the relative abundance of each glycan in a sample, the glycan area was expressed as a percentage of the glycome area of the A2G(4)2S(6)2 glycan, which represents the most abundant glycan in both urine and serum samples. Individual glycan structures were named using the Oxford nomenclature [21, 22], in which different symbols are used to represent specific features of the structure. For example, the letter A indicates the number of antennae (GlcNAc) on the trimannosyl core present, F represents fucose, B denotes the presence of a bisecting *N*-acetylglucosamine, G represents galactoses, and S indicates sialic acids.

Statistical analysis was conducted using the Wilcoxon test to compare the data, with $p < 0.05$ indicating significance. Additionally, a correlation test was used to investigate the relationship between the relative abundances of identified glycans and age, with $p < 0.05$ considered significant. All plots were created using the ggplot2 package in R. A bootstrapping technique was used to validate significantly differentiated glycans between males and females, as well as glycans significantly correlated with age. This method was also used to detect newly significant glycans that were not identified in the original data (false negatives).

3. Results and Discussion

3.1. Structure Analysis of *N*-Glycans

To obtain a *N*-glycome profile based on reversed-phase HPLC and mass spectrometry from urine under normal physiological conditions, hydrazinolysis was utilized to release *N*-glycans from urinary glycoproteins. These *N*-glycans were then labeled with pyridylamino residue (PA), which is a useful glycan labeling method for improving the separation ability of glycans in reversed-phase HPLC. The PA-glycans from glycoproteins in urine were separated into different fractions based on their sialylation levels—neutral(N), mono-sialylated(A1), di-sialylated(A2), tri-sialylated(A3), and tetra-sialylated(A4)—using anion-exchange HPLC (Figure 1).

Each fraction was then further separated on reversed-phase HPLC (Figure 2) and analyzed using ESI-MS.

In general, mass spectrometry can differentiate between glycans based on their *m/z* values. As a result, I was able to identify 67 distinct compositions, which can be grouped into 6 different categories according to their primary constituents. Sialylated and fucosylated glycans made up the majority of urinary glycans (45.05%), followed by sialylated-afucosylated (19.78%), neutral fucosylated (16.48%), high mannose (HM) (8.79%), asialylated-afucosylated (excluding HM) (5.49%), and sulfated (4.4%) fractions (Figure 3A). Analysis of the sialic acid count distribution for sialylated glycans revealed that mono-sialylated glycans were the most common, representing 56.1% and 66.67% of sialylated-fucosylated and sialylated-afucosylated glycans, respectively. In contrast, tri-sialylated glycans were the least common among all sialylated glycans, representing

only 7.32% and 5.56% of sialylated-fucosylated and sialylated-afucosylated glycans, respectively (Figure 3 B,C).

Overall, our findings align with those of Haiying Li et al. [8]. They examined the glycome of healthy volunteers and showed that most urinary glycans were both sialylated and fucosylated, while sulfated glycans were present in only small amounts.

Earlier studies highlighted the significance of the primary constituents of the glycans identified in the normal physiological condition of the urinary glycome profile. The presence of sialic acid has been shown to be crucial for various biological functions, as the removal of sialic acid from uromodulin has been found to result in a loss of its ability to inhibit crystal aggregation and growth [23]. Moreover, it was reported that high mannose glycans in uromodulin play a significant role in the urinary defense against bacterial infections [24, 25].

Since mass spectrometry alone faces challenges in unraveling the glycan structure and differentiating between glycan isomers with varying branching structures, the elution time and glucose unit were utilized to determine the structural details of glycans and distinguish between various glycan isoforms with the same mass according to the empirical additivity rule of unit contribution [12].

I applied this rule to determine how each monosaccharide contributed positively or negatively to retention on C18 columns, taking into account the monosaccharide type, position, and glycosidic linkages. With this approach, I successfully identified and quantified 109 distinct *N*-glycan structures corresponding to 67 glycan compositions from urine samples using LC-MS/MS analysis.

These identified *N*-glycans displayed a uniform elution profile across all samples, which is useful in accurately determining their structural characteristics and distinguishing between glycan isoforms.

For example, I observed differences in the elution times of M7[6] and M7[3] glycans (H7Hn2PA1) in the N-fraction, attributed to the addition of a terminal mannose to α 1,6 or α 1,3 core mannose antennae, respectively, where the former had a tendency to elute earlier by approximately three minutes. Similarly, differences in the elution times of A2G(4)2[3]S(6)1 and A2G(4)2[3]S(3)1 glycan isoforms with the same composition (N1H5Hn4PA1) in the A1 fraction were attributed to the contribution of α 2,6-NeuAc or α 2,3-NeuAc, respectively, with the former eluting earlier by approximately five to six minutes (Figure 4).

Applying the empirical additivity rules by comparing the elution positions of the N-fraction PA-*N*-glycans on reversed-phase LCs suggests that the addition of core Fuc contributes positively to the retention by 10 - 12 min. In contrast, the addition of one α 1,3-Fuc residue with bisecting on a branch made a substantial negative contribution to retention (10- 15 min). Moreover, the addition of bisecting GlcNAc contributes positively to the retention by 16 -17 min (Figure 4).

Interestingly, the existence of a methyl group in Fucoses made them relatively hydrophobic compared to other *N*-glycans monosaccharides. In core-fucosylated glycans, the interaction of the PA label and fucose with the C18 stationary phase is more likely to be stronger, leading to increasing their retention.

In contrast, when the fucose is positioned at the opposite side of the PA-label (on one of the antennae), the interaction with the C18 stationary phase is less strong, leading to decreasing their retention [26].

In A1 and A2 fraction glycans, the addition of α 2,3-NeuAc contributed positively to the retention in the range of 6–8 min (without bisecting GlcNAc, with or without core Fuc), whereas the addition of α 2,6-NeuAc attached to LacNAc on α 3-Man made a smaller contribution to retention, which was less positive (0–2 min, without bisecting GlcNAc, with or without core Fuc) (Figure 4). Of note, the results obtained from applying empirical additivity rules are highly consistent with previous studies describing the separation of PA-labeled glycans with C18 columns [12, 27, 28].

3.2. *The Origin of the Urinary Glycome*

It was estimated that 70% of the human urinary proteome could originate from the kidney and the urinary tract, whereas the remaining 30% comes from various systemic organs and is then filtered by the glomerulus [29]. However, the origin of the glycans present in urine has never been investigated. Thus, in this section, I aim to investigate the origin of the urinary glycome. The results obtained from the serum and urinary glycome comparison showed that ~50% of the urine glycome may originate from the kidney and urinary tract, where it was absent in serum (Table 2). In agreement with our finding, Haiying Li et al. compared urinary identified glycans in their study with the published *N*-glycome of human serum/plasma, and they reported that 50% of the urine *N*-glycome was not present in the serum/plasma glycome [8]. This emphasizes the potential of using the urinary glycome as a source of new biomarkers for kidney and urinary tract diseases.

Since uromodulin is the most abundant protein in urine, and it was estimated that glycans represent ~30% of its weight [30, 31], I postulated that a high portion of the identified glycans that originated from the kidney and urinary tract could be released from uromodulin. On the other hand, ~30 % of serum glycans were represented uniquely in serum only (Table 3).

Most of the unique glycans in serum are sialylated *N*-glycans. These glycans may lose their terminal sialic acid residues during blood circulation through the action of neuraminidase (sialidase). Such cleavage exposes the galactose residues and generated galactose-terminated glycoproteins, known as asialoglycoproteins (ASGPRs), which can be completely taken up after binding to asialoglycoproteins receptors (ASGPRs) in the liver [32] or renal tubules [33]. These receptors might contribute to the removal of sialoglycoproteins from the serum via endocytosis.

Additionally, other less common unique glycans in serum, such as high mannose glycans, can be cleared by the mannose receptor (ManR) in the liver because they can bind to glycoproteins with oligomannose-type glycans [34].

The relative abundance of common glycans in urine and serum was calculated as a percent of A2G(4)2S(6)2 glycan(N2H5Hn4PA1), as it represents the most abundant glycan in urine and serum samples (Figure 5). Of note, A2G(4)2S(6)2 glycan represents 35% and 18% of the total serum and urine glycome signal, respectively.

Interestingly, the relative abundance of the majority of common glycans in both urine and serum was elevated in urine compared to serum. These urine-elevated glycans may be released from proteins that are enriched or enhanced in the kidney and urinary tract. For example, the M6 glycan was approximately 14 times more abundant in urine than in serum. Conversely, some glycans, such as F(6)A2[6]G(4)1 and F(6)A2, were found at higher relative abundances in serum than in urine, increasing by approximately 9 and 2 times, respectively. This dual contribution of shared glycans to both the serum and urine glycome may be due to incomplete or partial reabsorption (Figure 5).

In agreement with our findings, Li et al. identified the M6 composition (H6Hn2) as the 2nd highest relative abundance (9.45%) in the enriched uromodulin fraction compared with low relative abundance (0.62) in the depleted uromodulin fraction, showing that the majority of urinary M6 may be released from the enriched kidney protein (uromodulin) [35]. Oppositely, the F(6)A2 composition (H3Hn4dH1PA1) was identified in the uromodulin-enriched fraction with low relative abundance (0.02) compared to that of the uromodulin-depleted fraction (0.15), showing the possibility of release mainly from other tissue-enriched or enhanced plasma proteins [35].

3.3. Annotating the Structure of the Core Glycome in Urine

Of note, 58 of all identified glycans showed a tendency to be identified and quantified in at least 80% of urine samples; I named them in this manuscript as “the urinary core glycome”, and they accounted for ~85% of the total urinary glycome amount (they are shown with a blue background in Table 2 and in Figure 6).

Investigating the distribution of the relative abundances for the glycans of core glycome across urine samples showed that A2G(4)2S(6)2 was the most abundant glycan, accounting for 18% of the total urinary glycome, and it increased more than twofold over the other most abundant glycans in the other fractions M6 and M2. Glyconnect data showed that A2G(4)2S(6)2 with a composition of N2H5Hn4PA1 could be released from the most abundant proteins in serum and the plasma-like immunoglobulins Plasminogen, Serotransferrin, and Fibrinogen (<https://glyconnect.expasy.org/browser/structures/1378> (6 September 2022)).

I analyzed the structural features of the core glycome in different fractions, as they could be attributed to its precursor protein function. In the neutral fraction, 22 out of the 58 core glycans

were identified and quantified. The most abundant structure was M6, followed by M2, M3, F(6)M2, and M5. Each of them has a relative abundance above 20% of the A2G(4)2S(6)2 signal. On the other hand, other glycans have a relative abundance of less than 20% of the A2G(4)2S(6)2 signal (Figure 6). However, they tend to be identified repeatedly in at least 80% of samples, indicating their crucial role in different biological activities under normal physiological conditions. As shown in Table 2, 11 neutral glycans in the core glycome were fucosylated (neutral fucosylated type), and 10 glycans (N-9-1, 9-2, 11, 12, 14, 16-1, 18, 19, 20, and 21) (Table 2) were fucosylated only on the core (α 1,6-Fuc), whereas glycan (N-10) was triply fucosylated at the core and branches.

Additionally, partial structure information of the identified glycans can be deduced using MS/MS spectra, as it can validate the existence and location of certain structural features in the identified glycans using some characteristic fragment ions, such as core fucose characteristic fragment ions or bisecting GlcNAc characteristic fragment ions (Figure 7). The presence of the core fucose for these N fraction glycans was validated with MS/MS data based on the existence of the core fucose characteristic fragment ions of $m/z = 649.4$ (HexNAc2Fuc1-PA(1H⁺)) or $m/z = 325.0$ (HexNAc2Fuc1-PA(2H⁺)) (Figure 7—N-11, N-12, and N-14).

Overall, 7 out of 11 fucosylated glycans were galactosylated (N-10, 12, 14, 16, 19, 20, and 21) (Table 2), whereas the afucosylated glycans in the neutral fraction (high mannose and asialylated-afucosylated (excluding HM) types) were agalactosylated (N-1 to 6-3), and only 3 were galactosylated (N-8, 15, and 17-1). Of note, seven glycans in the neutral fraction have bisecting GlcNAc glycans (N-10, 15, and 17-1 to 21).

The presence of the bisecting GlcNAc for these glycans was validated with MS/MS data based on the existence of the bisecting GlcNAc characteristic fragment ions of $m/z = 1014.3$ (HexNAc1-Hex-HexNAc2Fuc1-PA(1H⁺)) (Figure 7—N-21).

In the mono-sialylated (A1) fraction, 19 glycans were identified and quantified as the core glycome. The top 3 abundant glycans in the A1 fraction were F(6)A2G(4)2[3]S(6)1, A2G(4)2[3]S(6)1, and F(6)A2G(4)2[6]S(3)1, as each of them had a relative abundance above 10% of the A2G(4)2S(6)2 glycan signal. On the other hand, M5A1[3]G(4)1S(6)1 and M4A1[3]G(4)1S(6)1 were the least abundant core glycans in the A1 fraction. In total, 11 mono-sialylated glycans (A1-8-1, 9, 14-1, 14-2, 15, 17, 19, 20, 21, 24, and 26) were core-fucosylated (sialylated-fucosylated type).

The existence of the core fucose for these A1 glycans was validated with MS/MS data based on the existence of the core fucose characteristic fragment ion of $m/z = 649.4$ (HexNAc2Fuc1-PA(1H⁺)) (Figure 7—A1-9, A-14, A1-15, A1-24).

While the other 8 glycans (A1-2-1, 2-2, 3, 5, 6, and 10 to 12) were afucosylated (sialylated-afucosylated type), most of the glycans contained type 2 LacNAc (Gal β 1-4GlcNAc) antennae, a common structure of vertebrate glycans, and some were modified by bisecting GlcNAc (A1-24, 26). The existence of bisecting GlcNAc for these A1 glycans was validated from MS/MS data based on the existence of the bisecting GlcNAc characteristic fragment ions of $m/z = 1014.3$ (HexNAc1-Hex-HexNAc2Fuc1-PA(1H⁺)) (Figure 7—A1-24).

The type 2 LacNAc of these glycans was frequently sialylated by α 2,6-linkage rather than α 2,3-linkage.

Among the mono-sialylated glycans, sialylation occurred mainly on the α 1,3-Man arm. Some glycans (A1-8-1, 14-2, 17) had LacdiNAc (GalNAc β 1-4GlcNAc) antenna.

The existence of LacdiNAc (GalNAc β 1-4GlcNAc) sequences in these A1 glycans was characterized by B ion fragments at $m/z = 407$ (HexNAc2) (Figure 7—A1-14-2, A1-17). Moreover,

the LacdiNAc-NeuAc1 sequence in the F(6)A2GalNAc2[3]S(6)1 glycan was characterized by a B ion fragment at $m/z = 698.2$ (HexNAc2 NeuAc1) (Figure 7—A1-17).

In general, the existence of sialic acid in A1 glycans was elucidated based on a characteristic fragment ion of $m/z = 657.2$ ((NeuAc-Hex-HexNAc1) (1H⁺)) (Figure 7—A1-2-1 to A1-12, A1-15, A1-24).

In the di-sialylated (A2) fraction, nine glycans were identified and quantified. The most abundant glycan in the A2 fraction and all glycomes was A2G(4)2S(6)2, as it represented ~18% of the total glycome signal. F(6)A2G(4)2S(3)2 and F(6)A2G(4)2S(6)2 represented the 2nd and 3rd most abundant glycans, respectively. The afucosylated form from F(6)A2G(4)2S(3)2 was identified as the least abundant core glycan in the A2 fraction. A total of 6 di-sialylated glycans (A2-7-2, 8, and 9 to 12) were fucosylated (sialylated-fucosylated type), and the remaining 3 glycans (A2-2, 4, and 7) were afucosylated (sialylated-afucosylated type). All glycans had type 2 LacNAc antennae, and 2 glycans (A2-7-2 and 9) also had LacdiNAc antenna. The existence of LacdiNAc antenna in these A2 glycans was characterized by a B ion fragment at $m/z = 698.2$ (HexNAc2 NeuAc1) (Figure 7—A2-9).

In general, the presence of di-sialic acids in A2 fraction glycans can be elucidated using the characteristic fragment ions of $m/z = 900.8$ ((NeuAc2-Hex5-HexNAc2) (2H⁺)) or $m/z = 1799.3$ ((NeuAc2-Hex5-HexNAc2) (1H⁺)) (Figure 7—A2-2, A2-8).

In the tri-sialylated (A3) fraction, 5 glycans (A3-2, 4, 13, 14, and 15) were identified and quantified in the core glycome. A total of 4 glycans out of 5 (A3-2 and A3-13 to 15) were fucosylated (sialylated-fucosylated type), while A3G(4)3S3_1 was afucosylated (sialylated-afucosylated type).

All of these glycans had a tri-antennary structure, with two branches (Gal β 1-4GlcNAc) originating from α 1-3 core mannose.

The presence of tri-sialic acids in A3 fraction glycans can be elucidated considering the characteristic fragment ion of $m/z = 1329.8$ ((NeuAc4-Hex6-HexNAc3) (2H⁺)) (Figure 7—A3-4, A3-13).

In the tetra-sialylated (A4) fraction, 3 glycans (A4-5, 7, and 11) were identified and quantified. All of these glycans had core fucose, and 2 of them (A4-5 and A4-7) had a tetra-antennary structure.

The presence of tetra-sialic acids in A4 fraction glycans can be elucidated considering the characteristic fragment ion of $m/z = 1557.0$ ((NeuAc4-Hex7-HexNAc4) (2H⁺)) (Figure 7—A4-5).

3.4. Investigating the Glycans Significantly Differentiated between Males and Female in Core Glycome

Given a restricted number of samples to compare male and female groups, I employed bootstrapping as a means of multiple sampling to enhance the statistical tests' strength and yield more reliable outcomes in comparing the two genders.

I generated a thousand random samples by resampling our initial core glycome dataset, each with a replacement. I then computed the difference between the mean values of the male and female groups for each glycan structure in each bootstrapped sample and used it to create a distribution. This distribution was used to assess the significant differences between the two groups by computing the p -value.

The bootstrapped data revealed that out of 58 glycans, 5 exhibited considerable variation between the male and female groups. Of the 5, 4 (A2BG(4)2, A2G(4)2S(3,6)2, A2G(4)2S(3)2, and

F(6)A2F(3)G3S1) had significantly higher levels in females compared to males, while F(6)A3G(4)3S4_2 had notably higher levels in males than in females.

It is worth noting that the bootstrapping technique was effective in confirming the significant difference shown by the Wilcoxon test (p -value < 0.05) for 2 glycans (A2BG(4)2, F(6)A2BG(4)2S(6)2), as demonstrated in Figure 8A,D. Moreover, the technique detected a significant difference for three glycans (A2G(4)2S(3,6)2, A2G(4)2S(3)2, and F(6)A3G(4)3S4_2) that were not identified as significant in the original samples by the Wilcoxon test, which is also known as false negatives. (Figure 8B,C,E). Notably, the distribution of bootstrapped means differences (Figure 8—bottom) showed that a 95% confidence interval (CI) (denoted by a bold horizontal line) did not contain 0 for all significantly differentiated glycans.

Concerning the characteristics of these glycans, four out of the five distinct glycans contained sialic acid. Among these four glycans, two were categorized as fucosylated (F(6)A2BG(4)2S(6)2, and F(6)A3G(4)3S4_2) and two (A2G(4)2S(3,6)2 and A2G(4)2S(3)2) were classified as A-fucosylated.

The female glycans exhibited relatively greater variation than those in males. This variation in females could potentially be due to fluctuations in the secretion of ovarian hormones.

It should be noted that the differences in the glycans between males and females may be related to their binding to gender-specific proteins or sex hormones. For instance, A2BG(4)2 (H5Hn5PA1) may be attached to proteins that are highly expressed in females, such as immunoglobulins [36], or female enriched proteins, such as Choriogonadotropin alpha and beta chains [37], which could explain why these glycans are more abundant in females than in males.

On the other hand, a further investigation of the F(6)A3G(4)3S4_2 glycan in the GlyConnect database (<https://glyconnect.expasy.org/browser/compositions/1238> (accessed on 8 December 2022)) revealed that they only attach to either Erythropoietin or Alpha-1-antitrypsin proteins. These proteins may positively contribute to the abundance of the F(6)A3G(4)3S4_2 glycan (N4H6Hn5dH1PA1) in males compared to females.

3.5. Investigating the Glycans Significantly Correlated with Age in the Core Glycome

It is widely recognized that men and women utilize physiological pathways to achieve longevity, with women generally living longer than men. Therefore, I studied the connection between gender and glycan values at various ages. Our findings revealed that in females, the relative abundances of three glycans (F(6)M2, A1[3]G(4)1S(6)1, and F(6)A2BG(4)2[6]S(3)1) were negatively correlated with age (Figure 9C–E), whereas the relative abundances of two glycans (M9 and A3G(4)3S3_1) showed a positive correlation with age (Figure 9A–B).

In males, the relative abundance of F(6)A1[3]G(4)1S1 showed a negative correlation with age (Figure 10). All negative correlations have a Pearson correlation coefficient ($R < -0.8$) and p -value < 0.05 . Additionally, all positive correlations have a Pearson correlation coefficient ($R > 0.8$) and p -value < 0.05 . Our results showed that there is an interaction between age and sex in the urine N -glycosylation features, with more dynamic changes in females than males.

To confirm the glycans that were significantly correlated with age and to identify false negatives that were missed in the original data, the bootstrapping technique was used. The process involved creating a thousand random samples by resampling the initial core glycome dataset, each with replacement. The R and p -values were then calculated for each core glycan in each bootstrapped sample for a specific gender. The frequency of positively correlated bootstrapped samples ($R >$

0.8), negatively correlated bootstrapped samples ($R < -0.8$), and significantly correlated bootstrapped samples (p -value < 0.05) were determined for each glycan in both the male and female groups. The results, as shown in Figures 10 and 11, indicated that the most frequent glycans in the bootstrapping analysis were the ones that displayed a significant correlation with age in the original data for males or females.

The glycans' association with age could potentially be explained by the age-related associations of their precursor proteins. Research examining the plasma proteomic profiles of adults revealed a group of proteins and pathways that were significantly linked to chronological age and were better indicators of biological age [38]. For instance, the study found that proteins such as FSH, LH, and SHGB were positively correlated with age only in women, while netrin-4 was significantly negatively associated with age only in men.

Previous research on the urinary glycome has highlighted the differentiated urinary glycans in different genders and ages. Li et al. (2020) conducted a comprehensive MS analysis of *N*-glycans present in urine samples from both adult and pediatric populations. The *N*-glycans released by PNGase F were isolated, labeled with aminobenzoic acid, and methylamidated before being analyzed using LC-MS/MS. The authors were able to detect 116 *N*-glycan compositions, out of which 46 were reproducibly detected and quantified. I checked the existence of these 46 glycans in our core glycome, which consists of 41 glycan compositions corresponding to 58 core glycan structures. I found that $>70\%$ of the glycan compositions are common between both studies; however, our study provides more information at the glycan structural level. For instance, there is agreement between both studies that the most abundant glycan in urine is the N2H5Hn4 glycan composition, as it represents $\sim 21\%$ of the total glycome signal. Yet, I indicated that the A2G(4)2S(6)2 glycan structure is the most abundant among others that have the same composition,

as it represents ~18% of the total glycome signal, and other glycan structures (A2G(4)2S(3,6)2 and A2G(4)2S(3)2) represent the minority, where A2G(4)2S(3,6)2 represents ~10% of the abundance of the A2G(4)2S(6)2 glycan and A2G(4)2S(3)2 represents ~2% of the A2G(4)2S(3)2 glycan signal.

Additionally, they found that 42 glycan compositions out of 46 showed a significant difference between different ages and sex groups, but our study found only a small number of glycans that differed significantly between genders and ages at the glycan structure level. Another recent study also suggested that male and female urine *N*-glycan profiles have few differences [39]. The discrepancies observed in these studies could be attributed to different factors, such as the sample size, methodology, and data analysis. For instance, Li et al. (2020) utilized PNGase F for glycan isolation, while I used hydrazinolysis. Additionally, they used aminobenzoic acid for labeling, while I used PA. Moreover, I used the Wilcoxon test to detect the differences in the glycan relative abundances between males and females, since glycan relative abundances are not normally distributed. However, Li et al. (2020) used the t-test to detect the differences of glycan MS1 peak areas between males and females.

I also acknowledge that there is great variety in the living environments and eating habits between the cohorts of our study and others, which may account for individual differences and lead to new findings. It is worth noting that the gender and age differences in this study could be affected by the limited sample size.

In light of the biomarker discovery, different studies indicate different candidate biomarkers for different human diseases in terms of the glycan type or glycan composition. For instance, Ganglong Yang et al. [40] revealed that terminal GalNAc and Gal, core-fucosylated *N*-glycans and high mannose-type *N*-glycans, were more highly expressed in bladder cancer cells and tissues than

in normal cells. However, identifying glycan biomarkers at the structural level can provide higher sensitivity and specificity. Additionally, structural information can differentiate between different glycan isomers, which is important in the development of targeted therapies. Thus, the quantification data of the core glycome presented in this study can serve as a potential reference for future studies interested in discovering glycan biomarkers and developing targeted therapies for various human diseases at the glycan structure level.

4. Conclusions

Urine biofluid outperformed other biofluids, such as blood, as it can be collected non-invasively in large volumes with high stability and less complexity. Moreover, the urinary glycome can reflect both the systemic and urogenital physiology, as it is linked to proteins that come from systemic circulation, as well as those released from the kidney and the urogenital tract. Thus, the human glycome profile was investigated in urine under normal physiological conditions using LC-MS/MS. Urinary glycans were fractionated by DEAE HPLC and reversed-phase (RP)-LC before MS-MS/MS analysis to reduce the sample complexity. Mainly mass spectrometry data were used to identify 67 distinct compositions of the urinary *N*-glycan. The retention time of PA-glycans from the C18 stationary phase was used to elucidate the structural features of these PA-glycans and to distinguish among different glycan isomers, where the addition of certain monosaccharides to PA-glycan contributed either positively or negatively to the RP retention time. Consequently, 109 distinct glycan structures were identified. Of them, 58 distinct glycan structures showed a tendency to be identified in at least 80% of samples. Additionally, some characteristic fragment ions from the MS/MS data were used to elucidate the structural features of the *N*-glycans, such as the characteristic fragment ions that validate the existence of core fucose or bisecting GlcNAc in the identified *N*-glycan. The comparative glycome profile between urine and serum showed that approximately 50% of the urinary *N*-glycome is uniquely detected in urine, shedding light on some perspective candidate biomarkers for diseases related to the kidney and urinary tract. On the other hand, the other 50% of urinary *N*-glycans are shared with serum; this can be explained by the incomplete reabsorption of these *N*-glycans in tubules. Additionally, gender and age differences were also observed in the urinary *N*-glycan profile. This urinary *N*-glycan profiling can aid future

glycan studies in the discovery of novel biomarkers for diagnosing different diseases in the context of gender and age differences.

Biological significance of the study:

Biomarker discovery: Urine is an excellent source for biomarker discovery due to its ability to reflect both systemic and urogenital physiology. The study's thorough analysis of urinary N-glycome using LC-MS/MS opens up new avenues for identifying potential biomarkers associated with various physiological and pathological conditions. These biomarkers can aid in the early detection and monitoring of diseases, leading to improved diagnostic and therapeutic approaches.

Age and sex-related differences: The correlation between age/sex and the relative abundances of urinary N-glycome suggests that the glycomic profile in urine can be influenced by age and gender-specific factors. This finding highlights the importance of considering age and sex in future biomarker studies, as these variables may impact the interpretation and diagnostic potential of urinary glycome-based biomarkers.

Kidney and urinary tract origin: The study's observation that approximately 50% of the urinary glycome could originate from the kidney and urinary tract is significant. This finding sheds light on the specific contributions of these organs to the overall composition of the urinary glycome, providing valuable information about their glycosylation patterns and potential involvement in disease processes.

Future prospects:

Clinical applications: The identified N-glycans that are commonly present in urine and serum could serve as potential candidates for several disease biomarkers. Further research is warranted to validate these glycan markers in large patient cohorts to assess their diagnostic, prognostic, and predictive capabilities for various diseases, such as kidney disorders, urinary tract infections, and even systemic conditions.

Personalized medicine: The correlation between age/sex and the urinary N-glycome opens up the possibility of incorporating glycomic profiling into personalized medicine approaches. Understanding the glycomic variations associated with age and sex can help tailor treatments and interventions according to an individual's specific needs and susceptibilities.

In summary, this study significantly advances our knowledge of urinary N-glycome profiling and its potential as a source for biomarker discovery. The findings lay the foundation for future research aiming to utilize glycomic information to improve diagnostic and therapeutic approaches in various medical conditions.

Thesis Figures

Figure 1. Anion exchange HPLC of human urine N-glycans.

The result for the sample 036 is presented as a representative example. Other samples showed similar profiles. The peaks indicated by N, A1 to A4 were fractionated as a neutral, monoanionic, dianionic, trianionic, and tetraanionic PA-glycans, respectively. The arrowheads from S0 to S4 indicate the elution positions of standard N-glycans prepared from α 1-acid glycoproteins, and these numbers correspond to the number of sialic acids. The mark x shows a non-glycan peak.

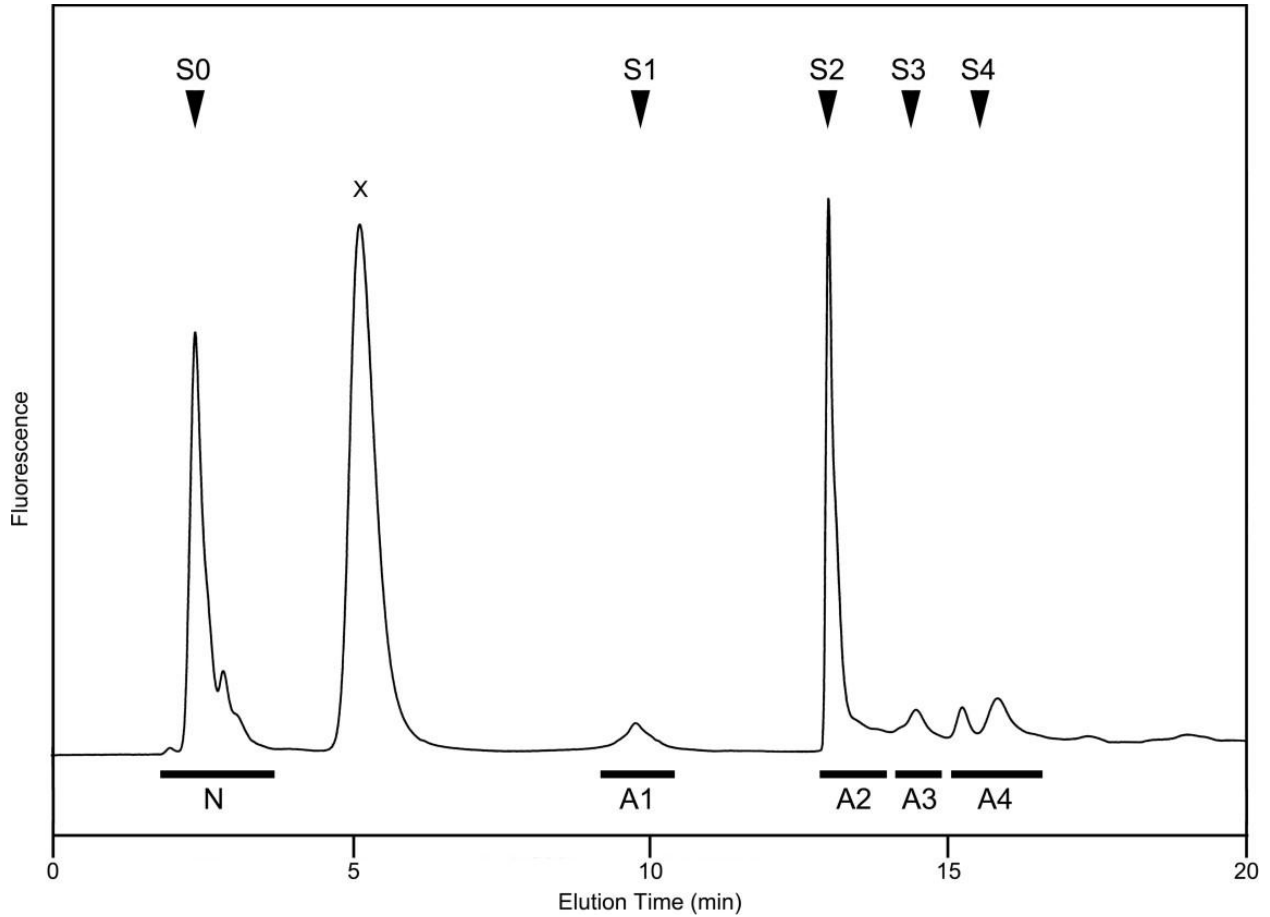
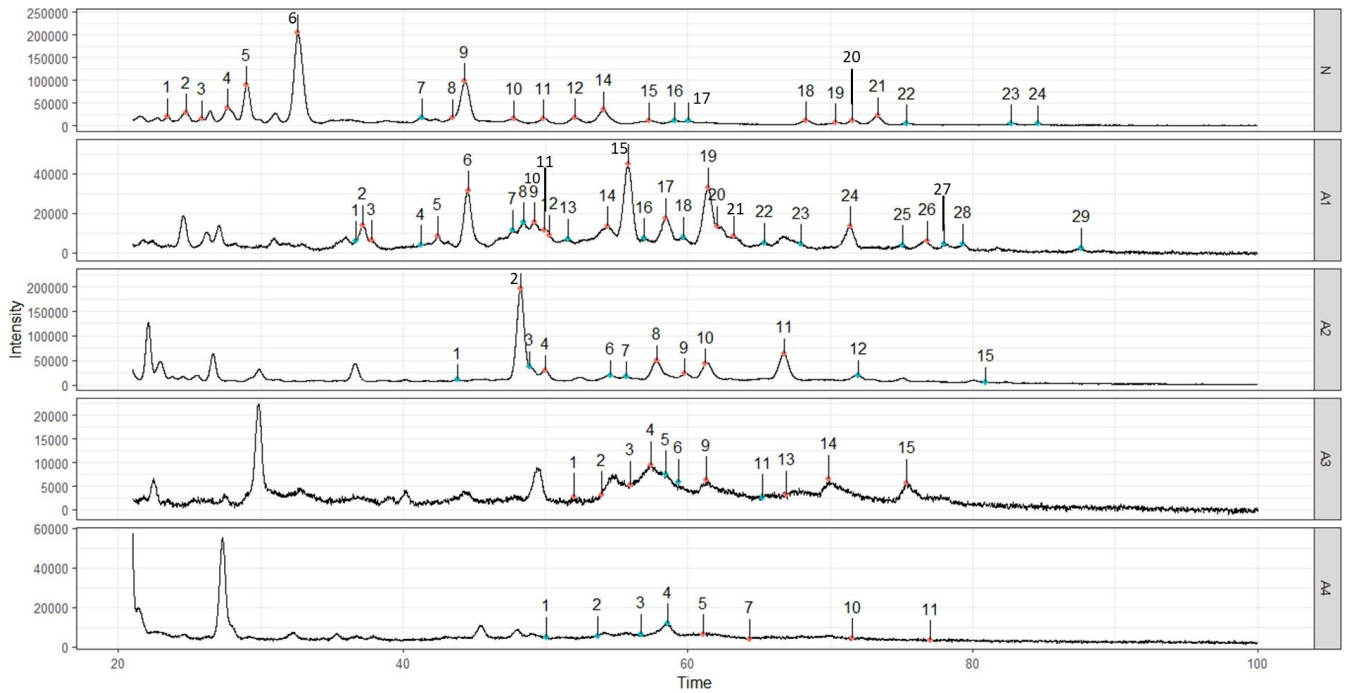


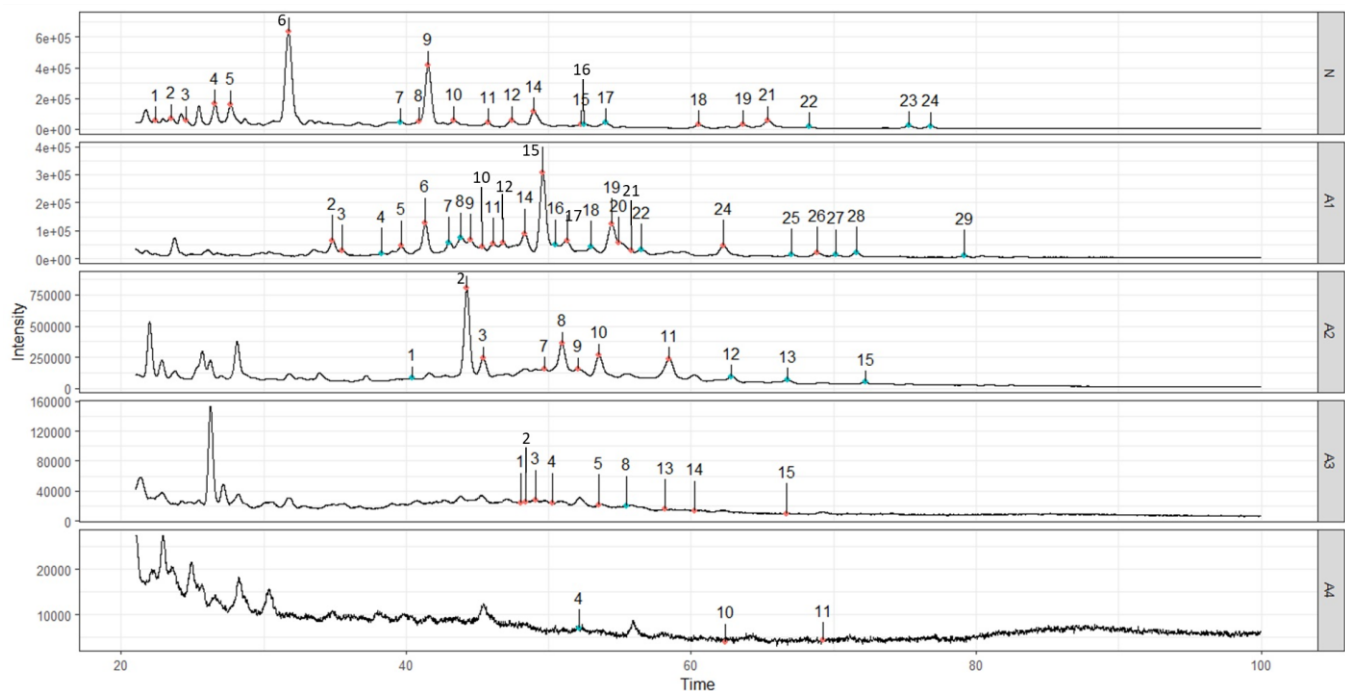
Figure 2. Chromatograms of reversed phase HPLC for each sample.

Each fraction (N, A1, A2, A3, A4) separated on DEAE HPLC were developed further on reversed phase HPLC. The peaks were colored with 2 different colors; red color for the peaks detected in at least 10 in 12 samples (Core glycome), blue color for the peaks detected in less than 10 samples. The peaks in each fraction was labeled by numbers referring to certain identified glycan. All identification and quantification data for these labeled peaks can be shown in Table S2. The unlabeled peaks were considered as PA derivatives of *O*-glycans, glucose oligomers or artificial products from *N*-glycans.

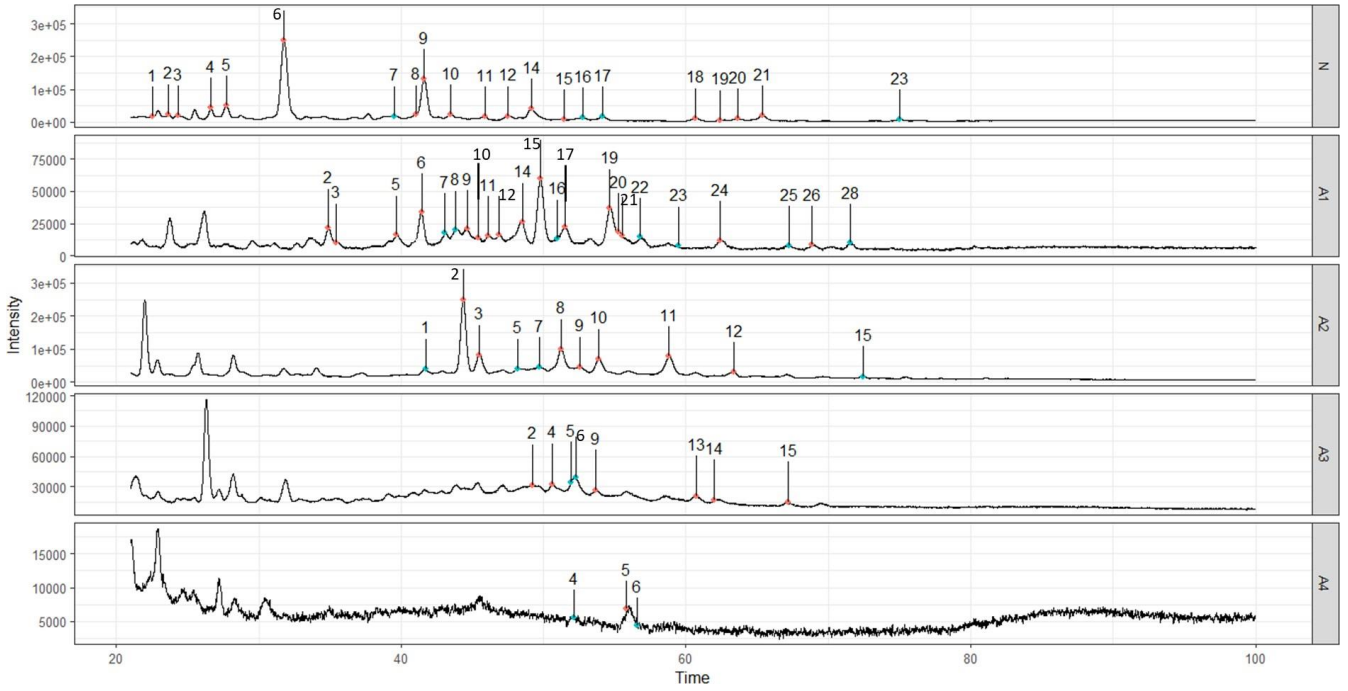
028



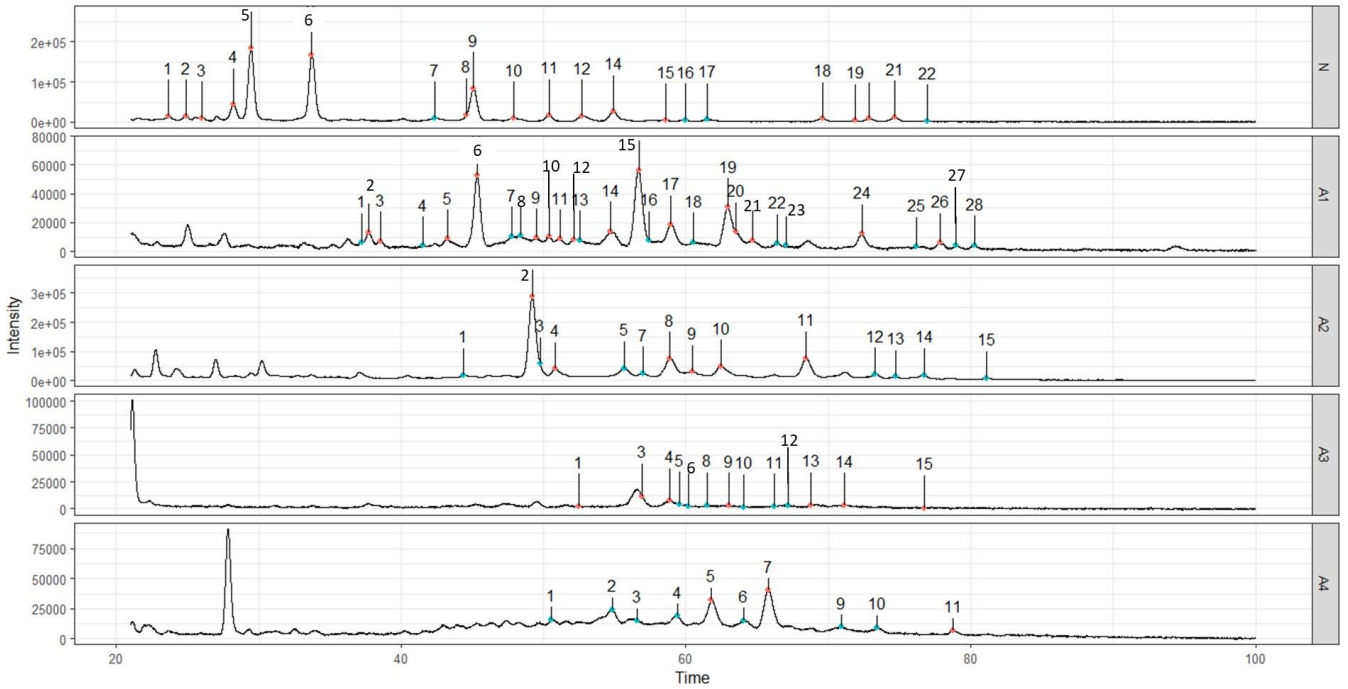
031



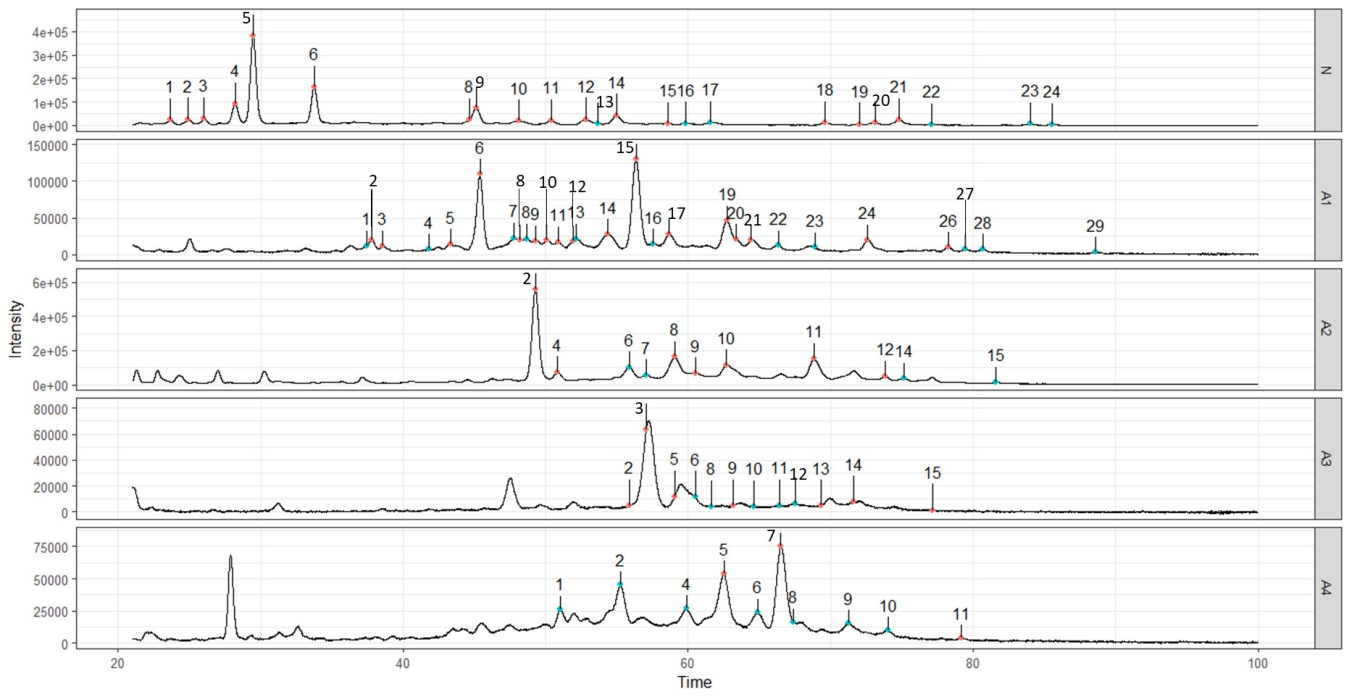
035



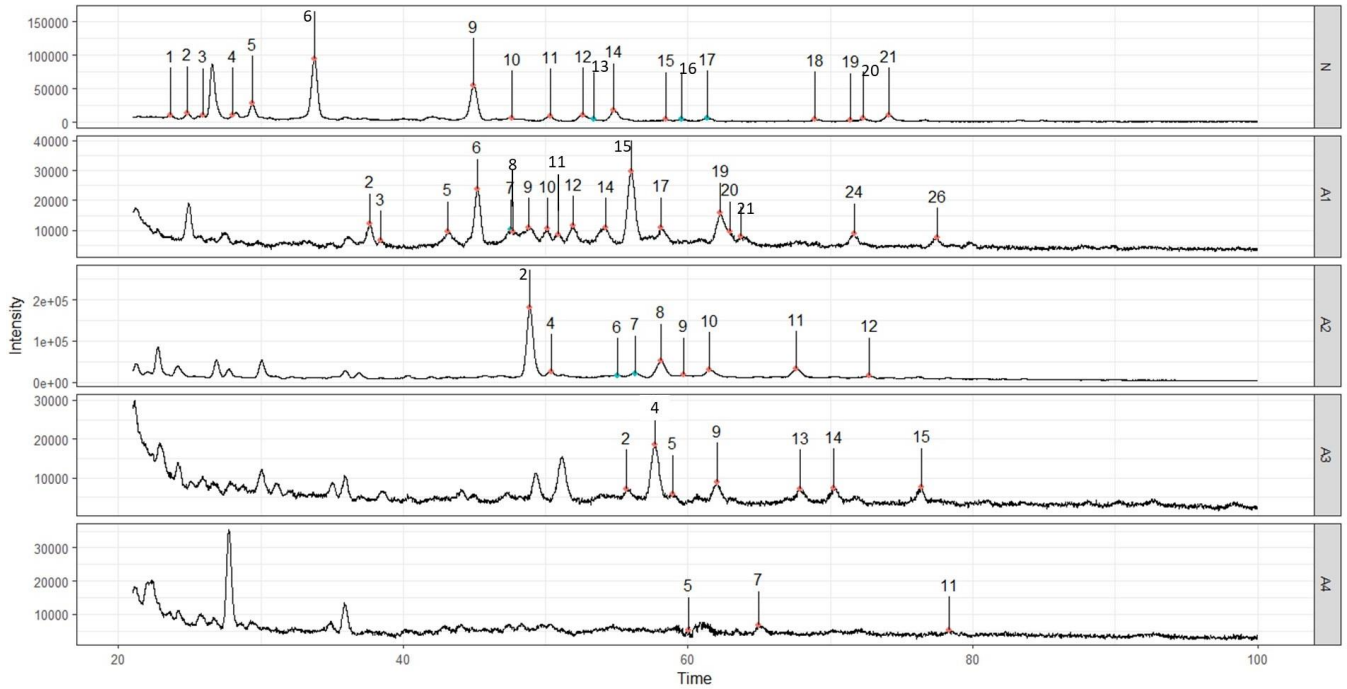
030



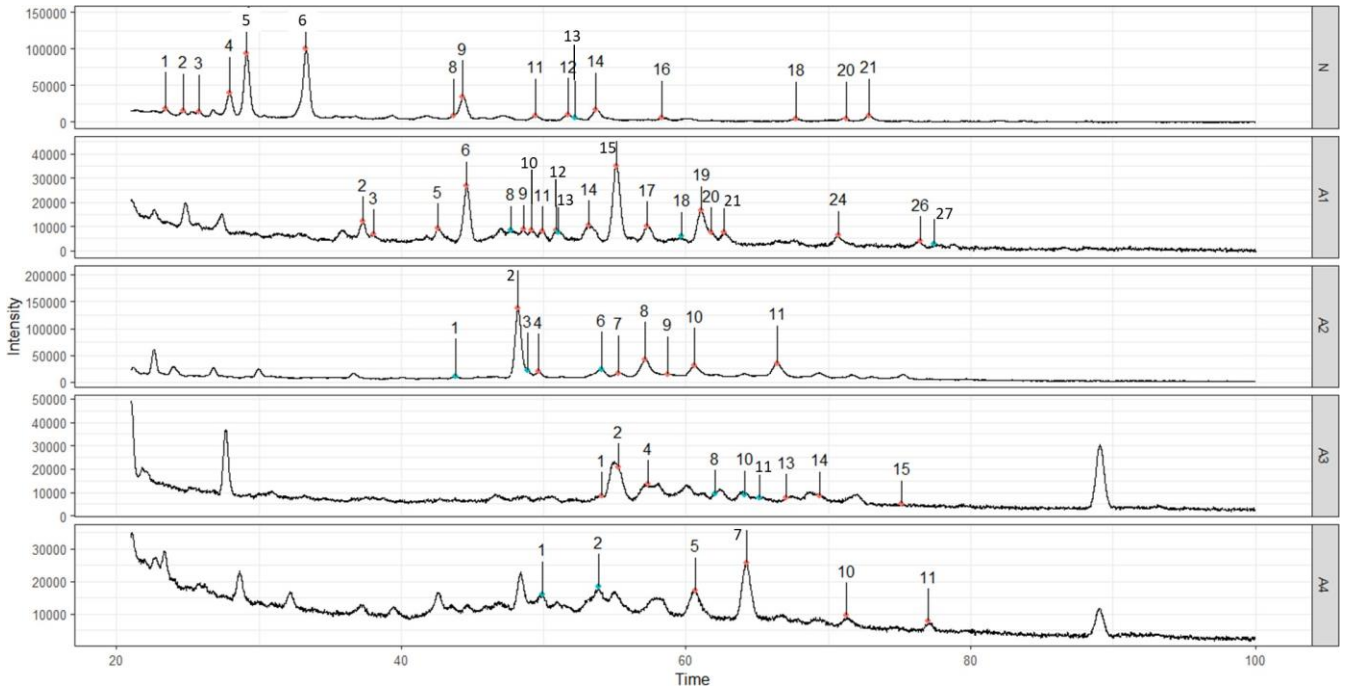
038



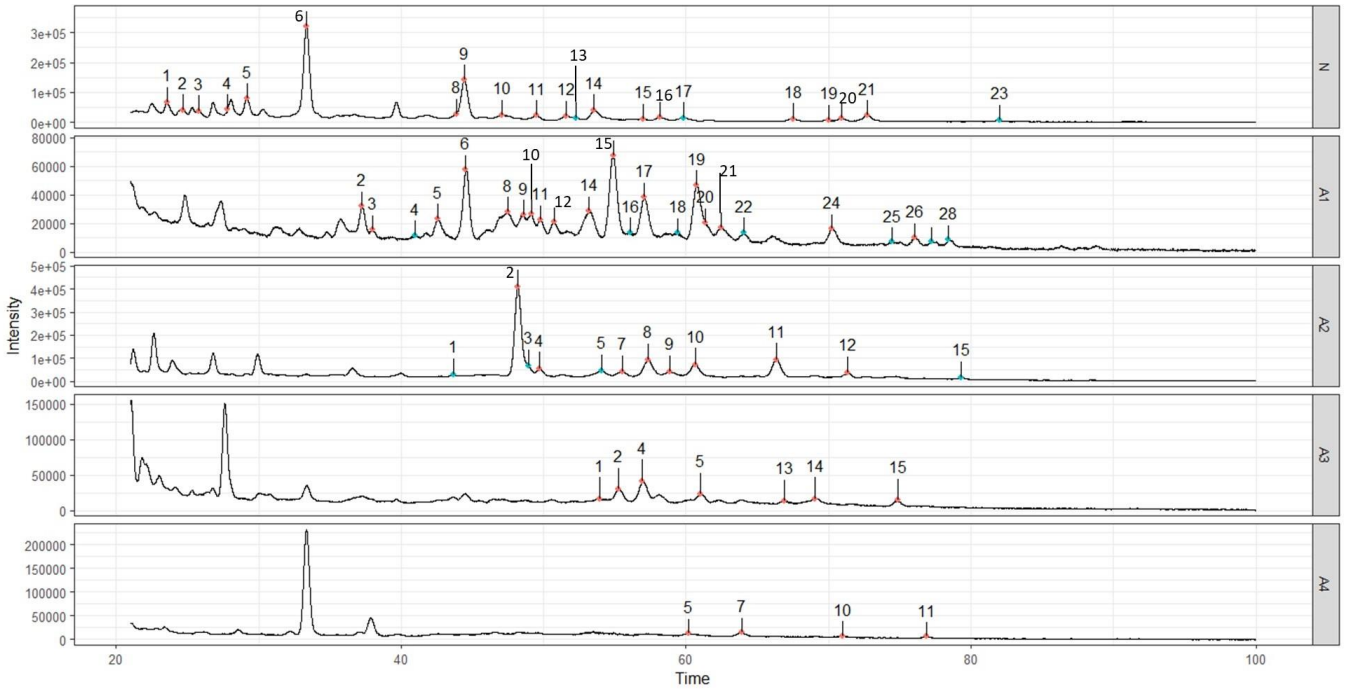
042



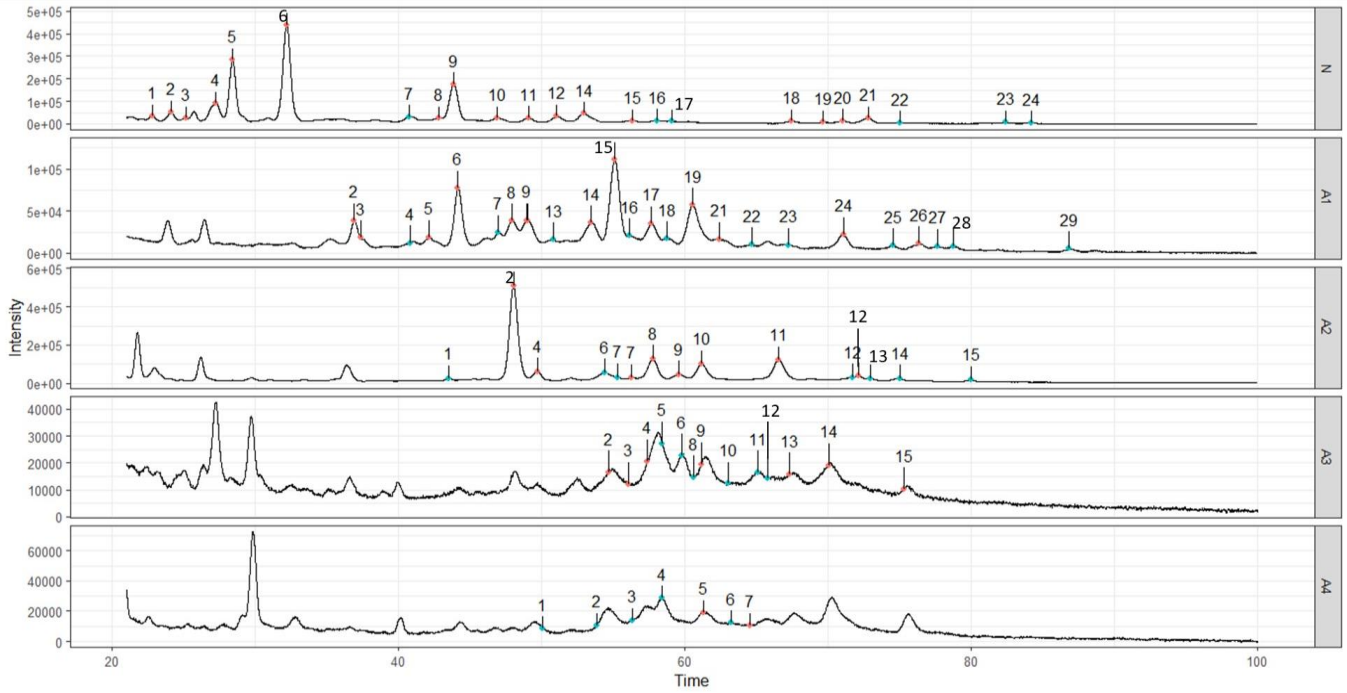
040



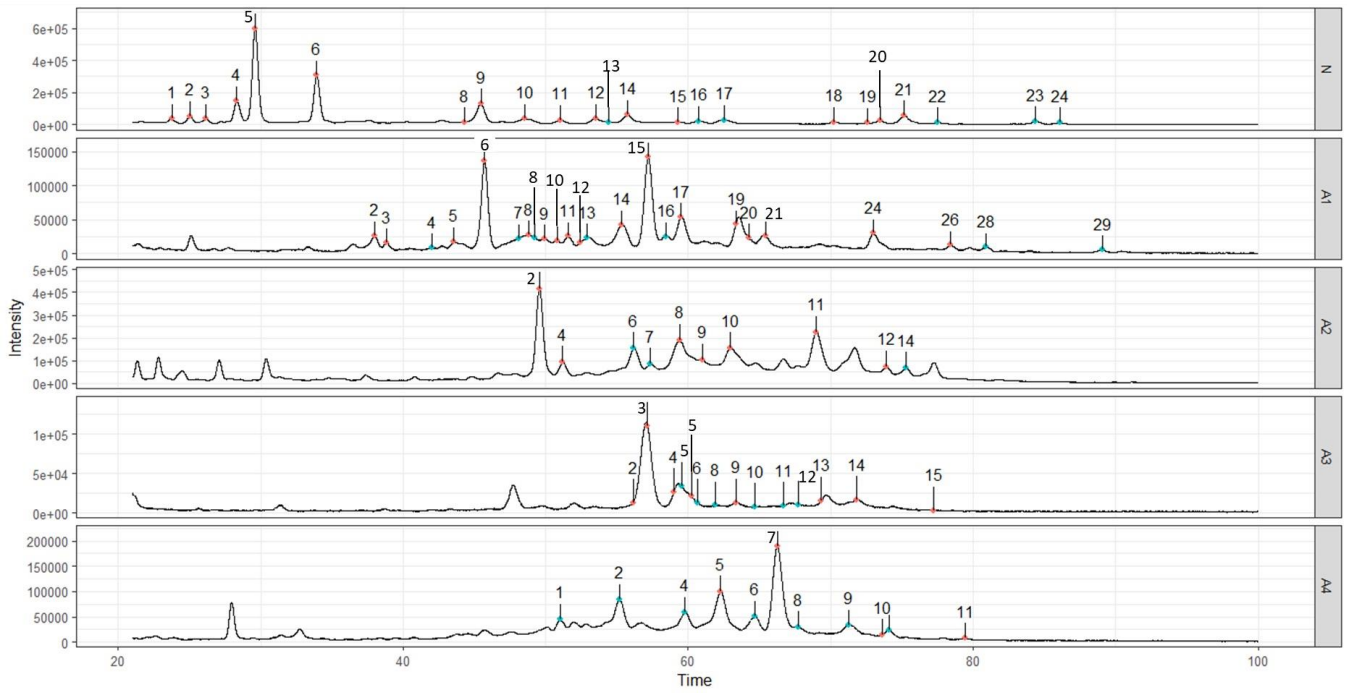
023



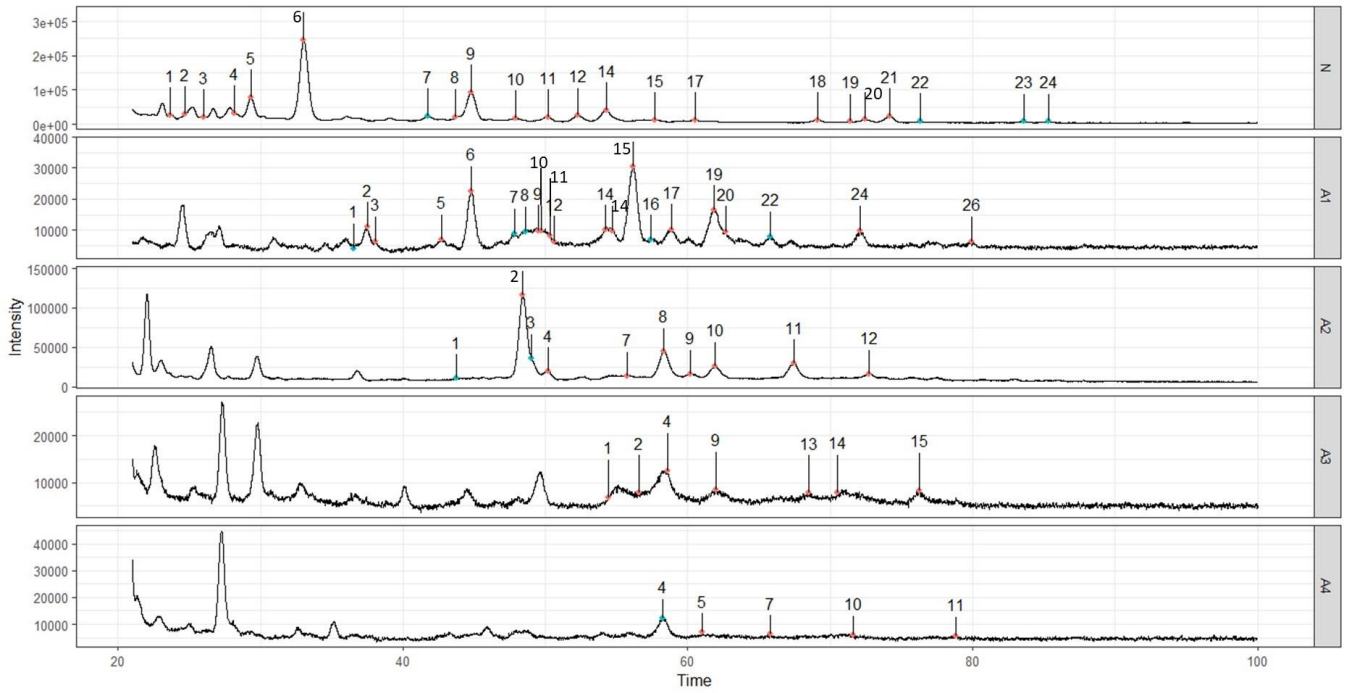
014



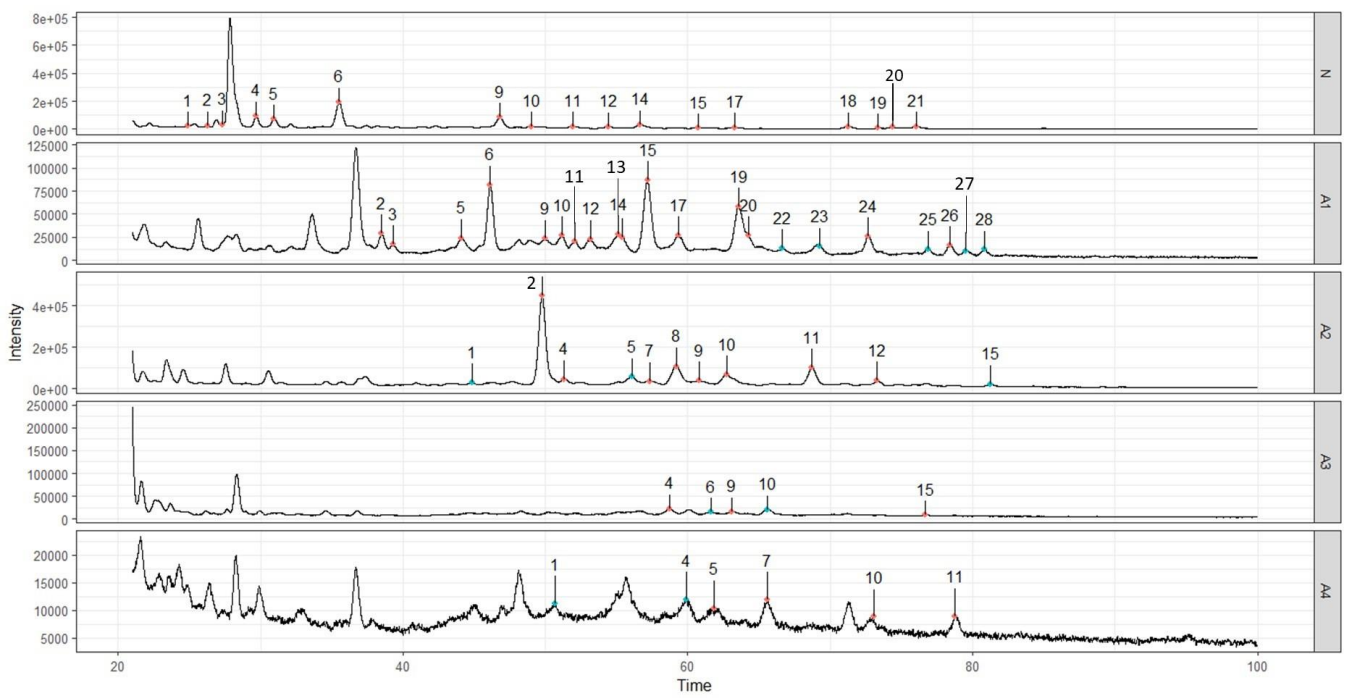
095



027



036



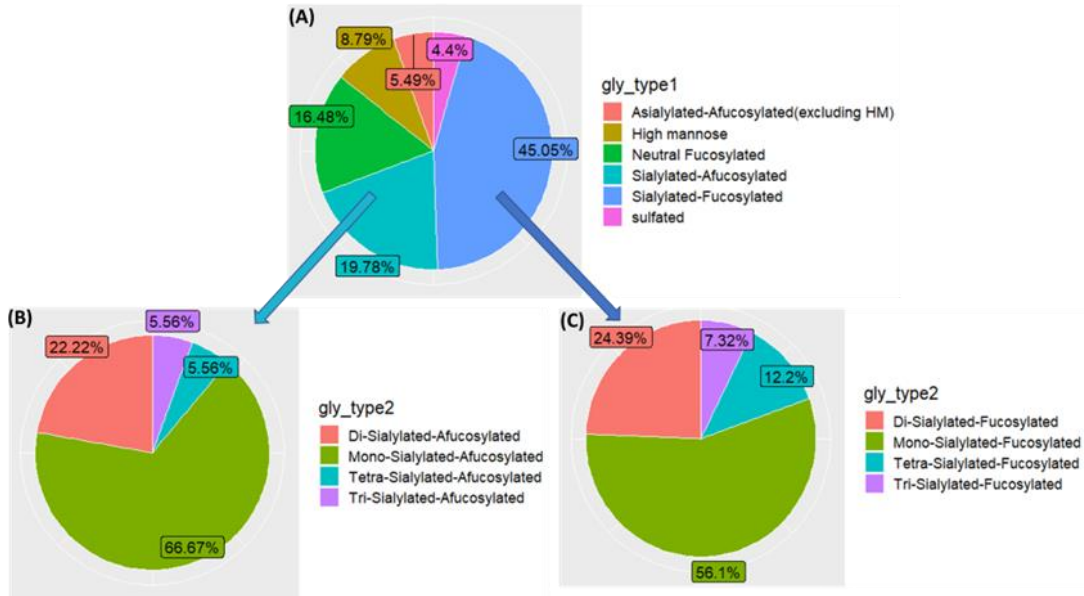


Figure 3. (A) Pie chart showing the distribution of the identified *N*-glycans through different glycan classes; (B) and (C) show the distribution of the sialic acid count for only sialylated glycans.

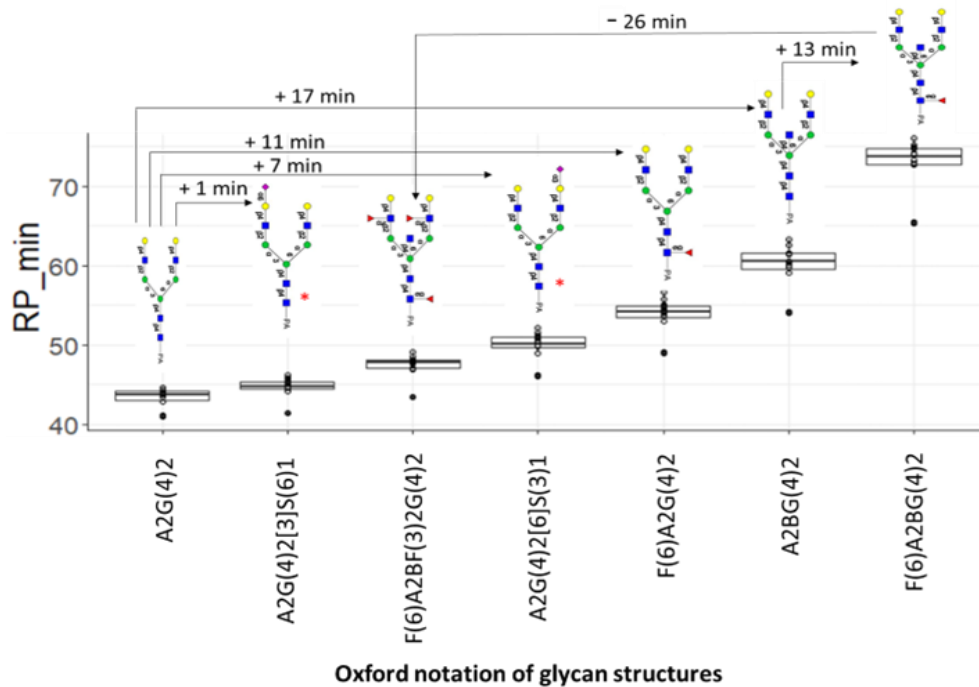


Figure 4. Boxplots showing the distribution of different PA- *N*-glycans elution times in minutes across samples. Line arrows indicate the time shift of the elution positions of PA- *N*-glycans by the addition of certain glycan residues on a certain position. Glycans with * in red are glycan isoforms with the same composition.

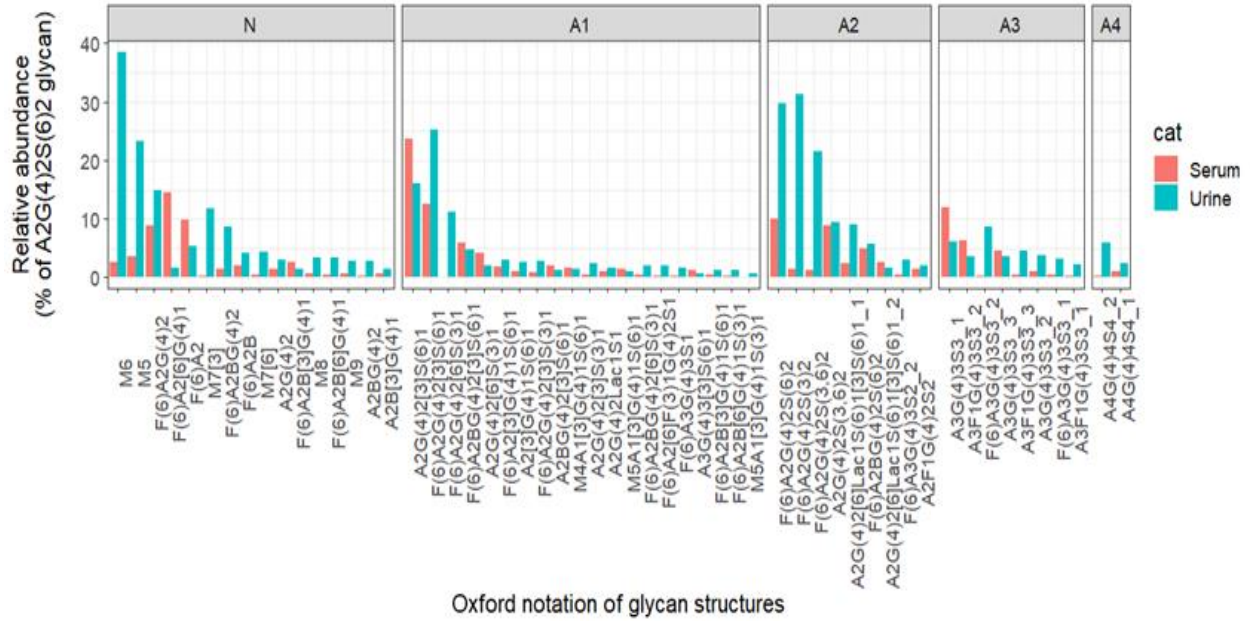


Figure 5. Bar plot showing the difference of relative abundances of common glycan in serum and urine in different fractions as a percent of A2G(4)2S(6)2 glycan.

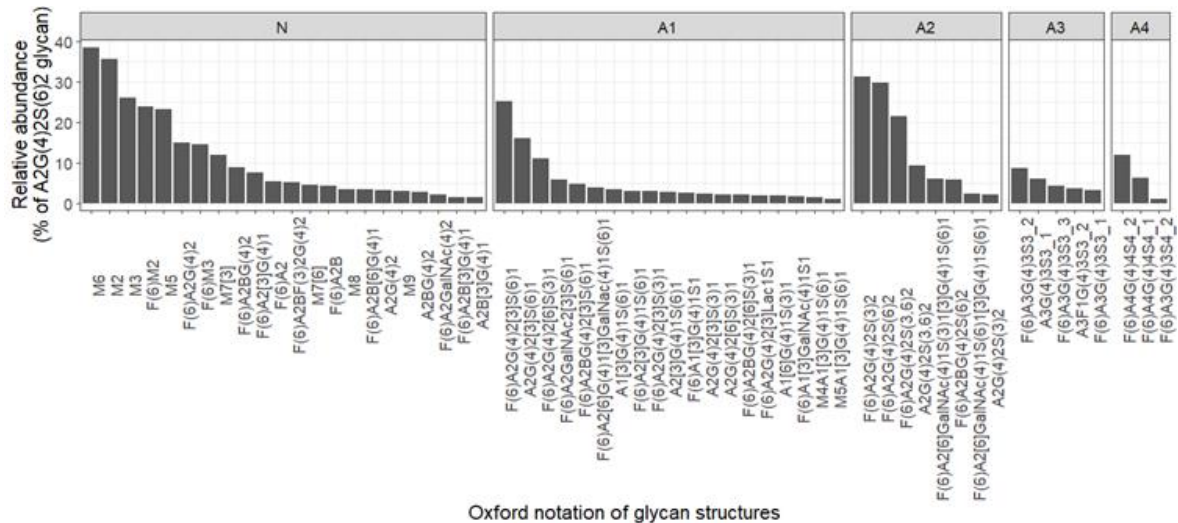


Figure 6. Bar plot showing the average of the relative abundances of 58 glycans in the urinary core glycome.

Figure 7:

MS and MS/MS spectra for some of the glycans detected in at least 10 samples (the core urinary glycome) in each fraction (N, A1, A2, A3, A4).

Figures N-1 : N-21. glycans in Neutral fraction (N).

Figures A1-2 : A1-24. glycans in Mono-silylated fraction(A1).

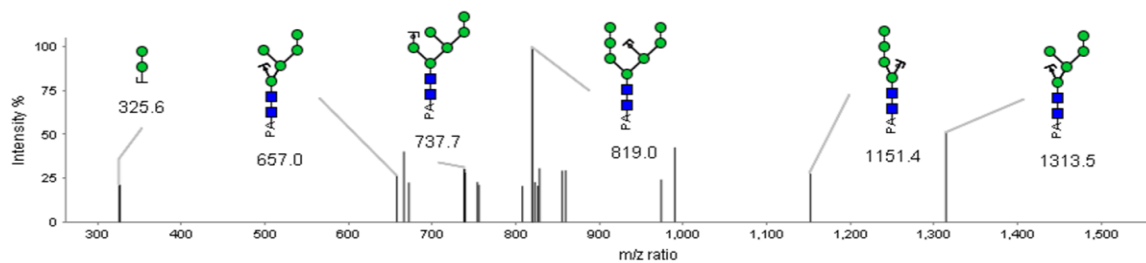
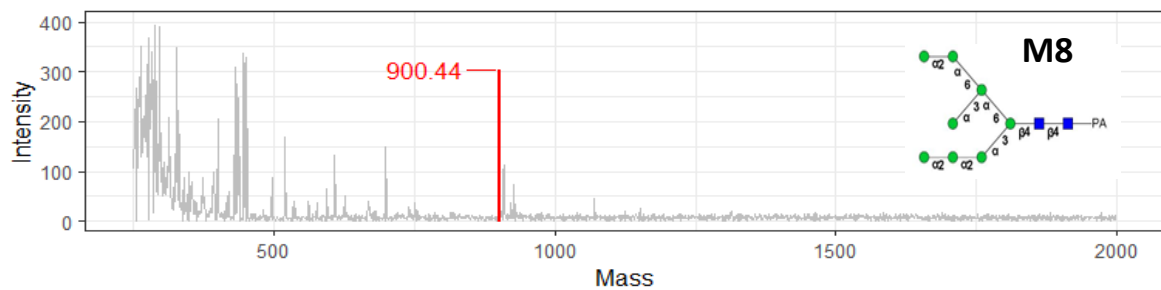
Figures A2-2 : A2-12. glycans in Di-silylated fraction (A2).

Figures A3-4 , A3-13. glycans in Tri-silylated fraction (A3).

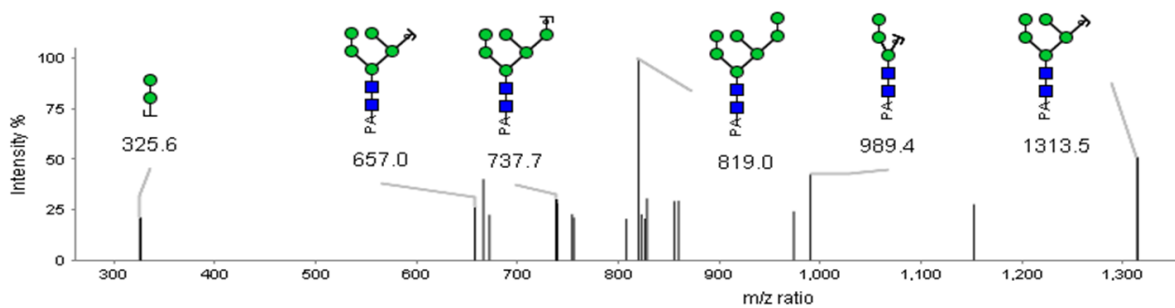
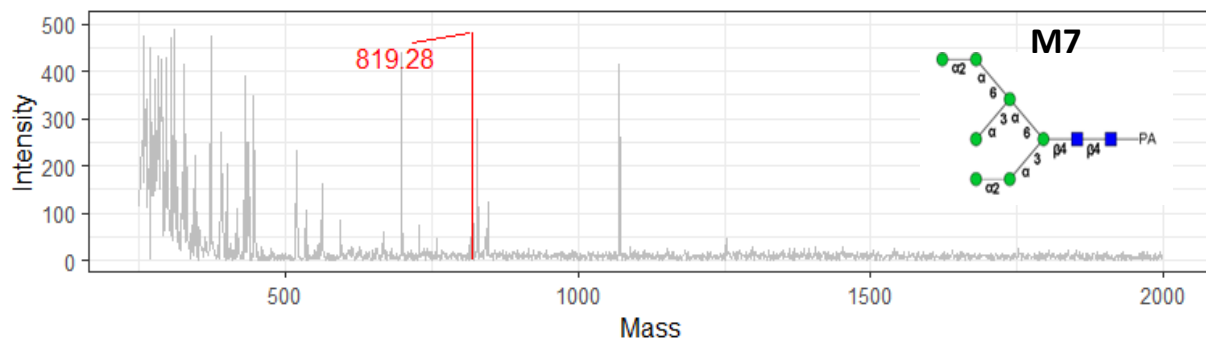
Figures A4-5. glycans in Tetra-silylated fraction (A4).

GlycoWorkbench software was used to draw the glycan structure and to assign the fragment ions to their precursors.

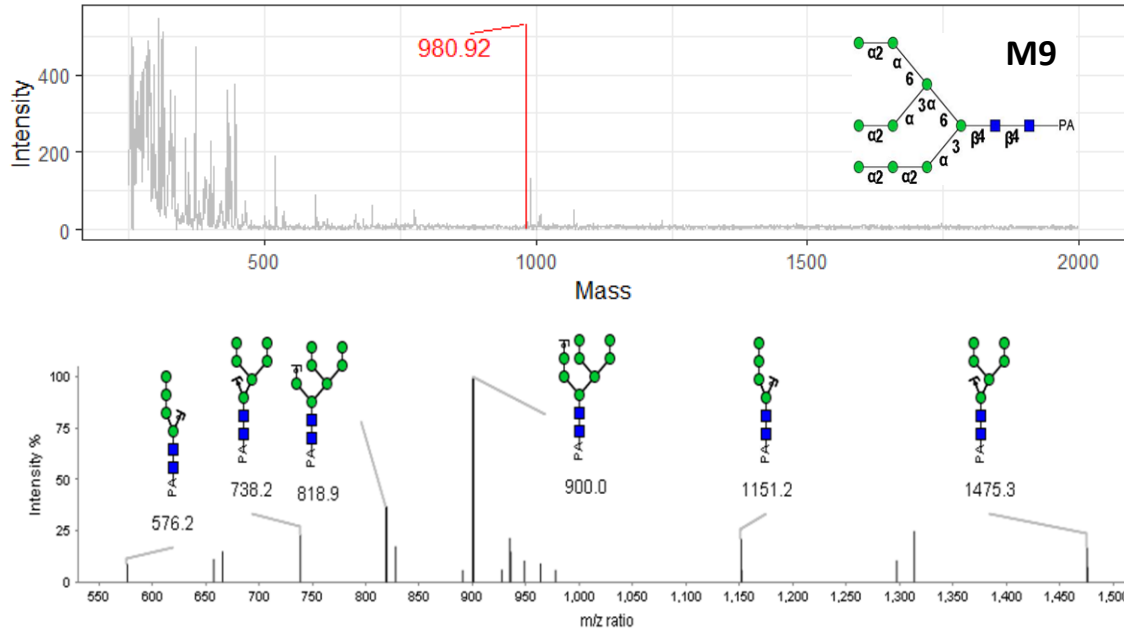
N-1



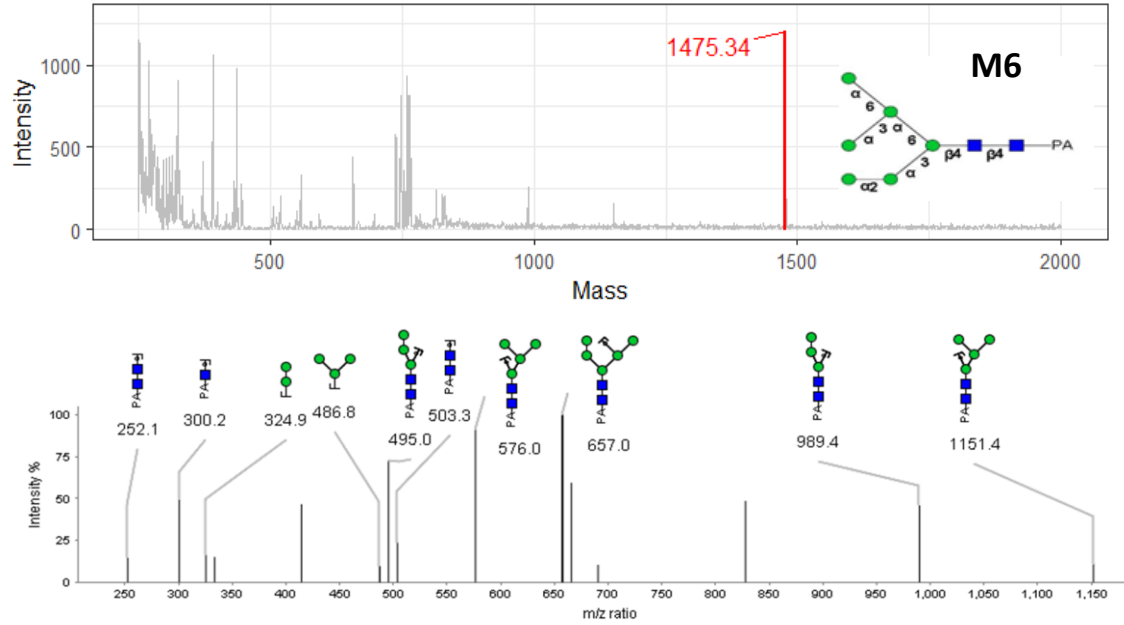
N-2



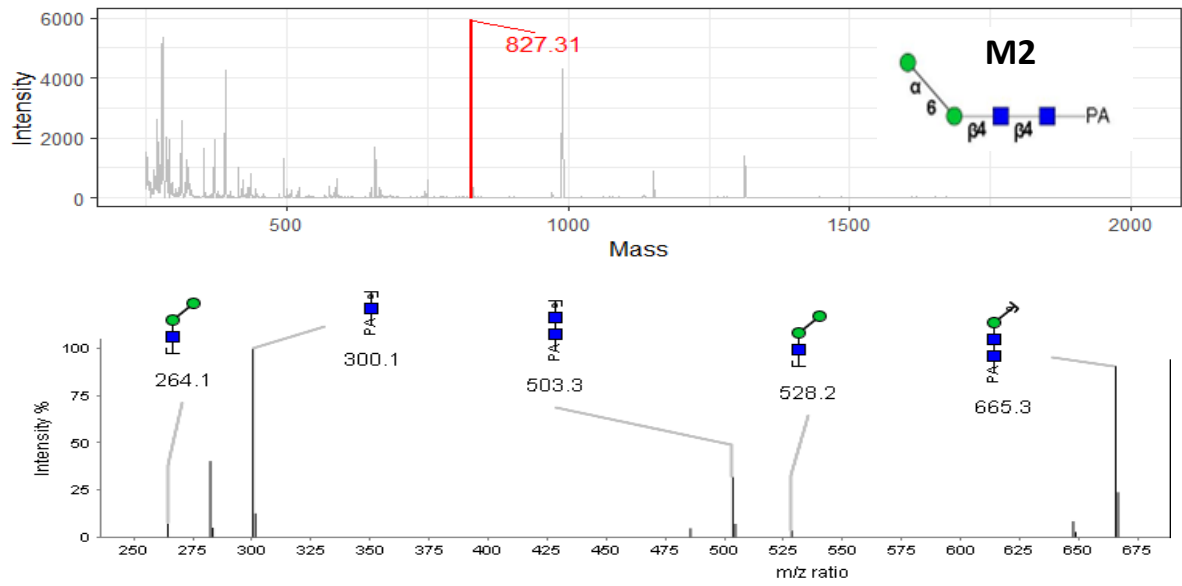
N-3



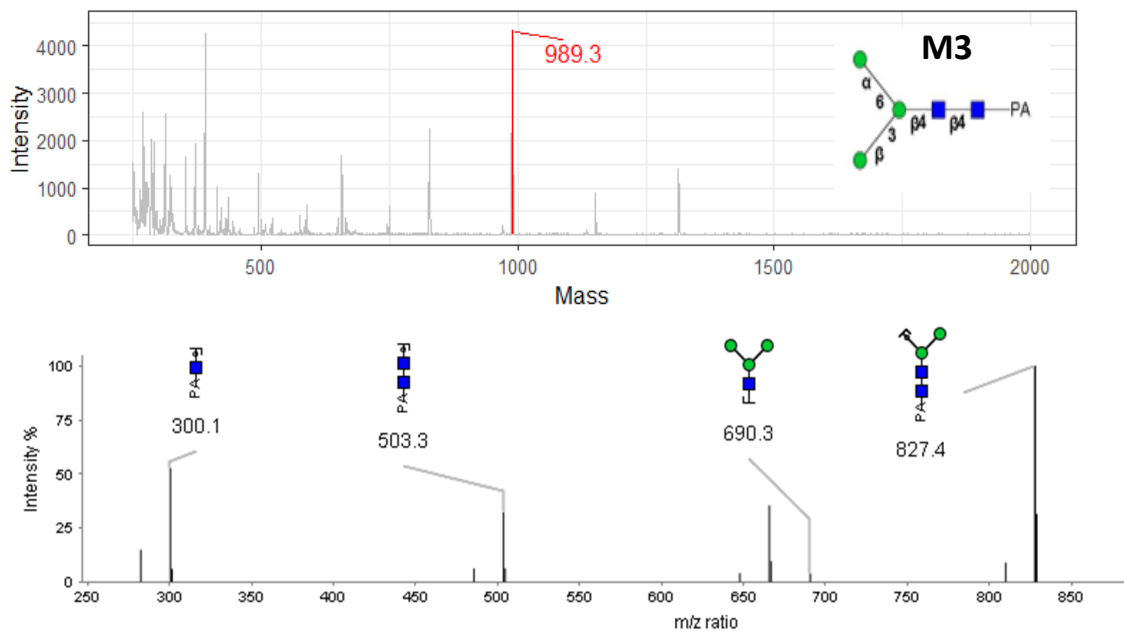
N-5



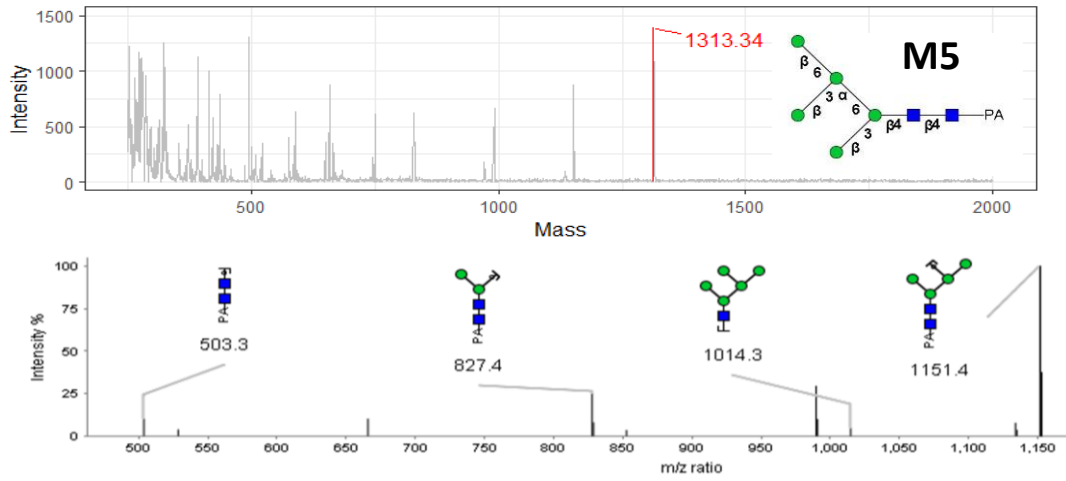
N-6-1



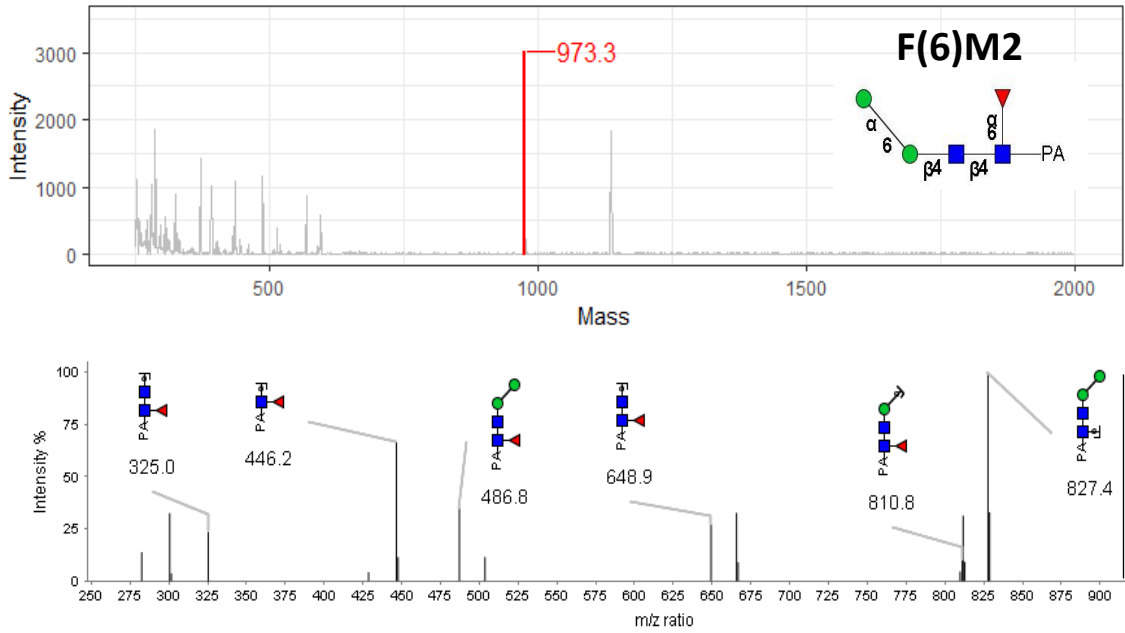
N-6-2



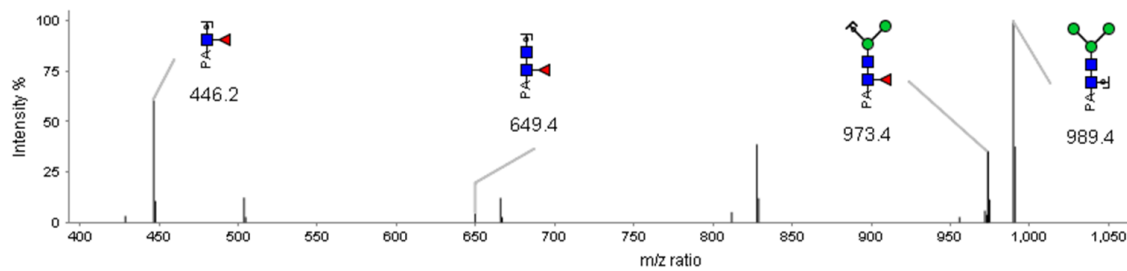
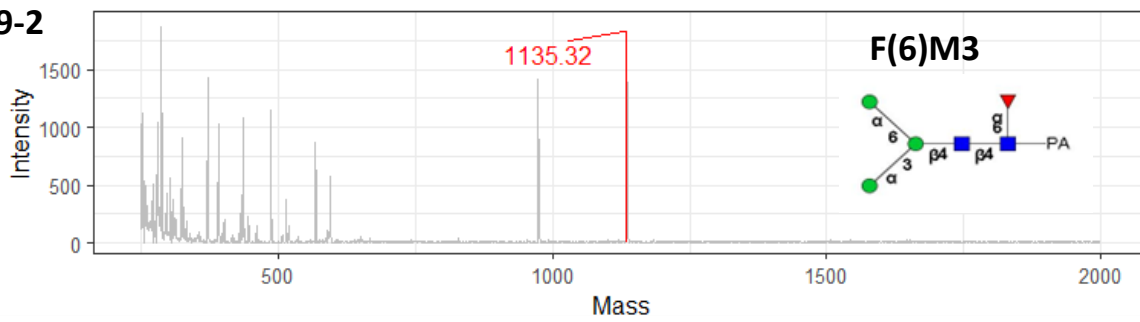
N-6-3



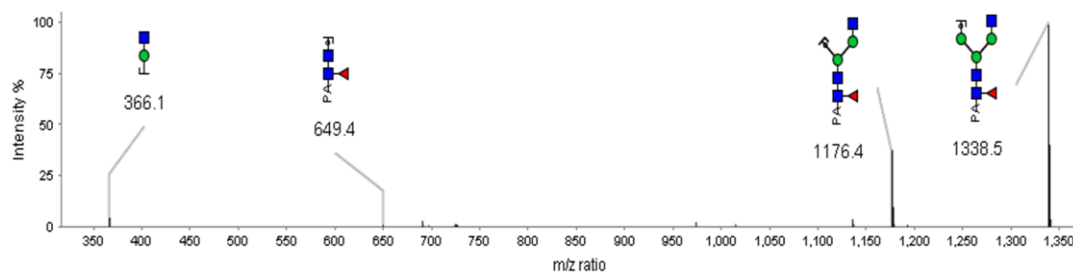
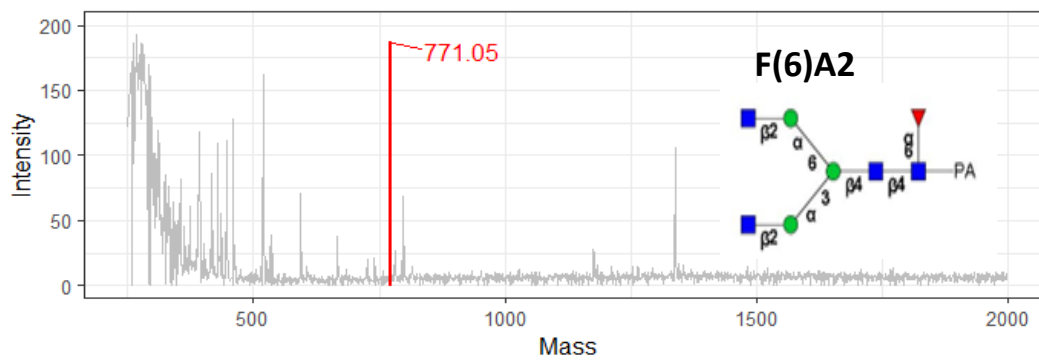
N-9-1



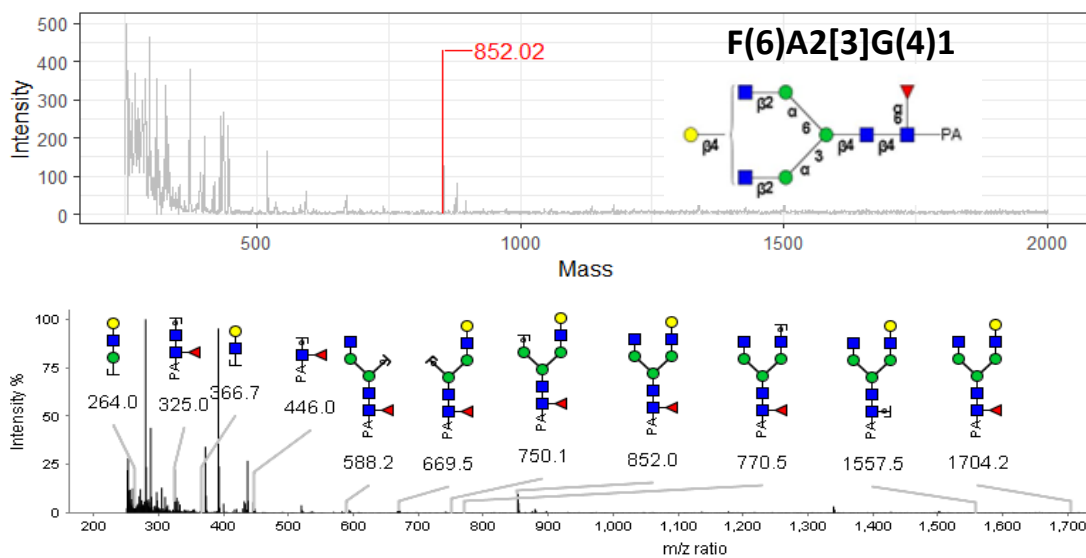
N-9-2



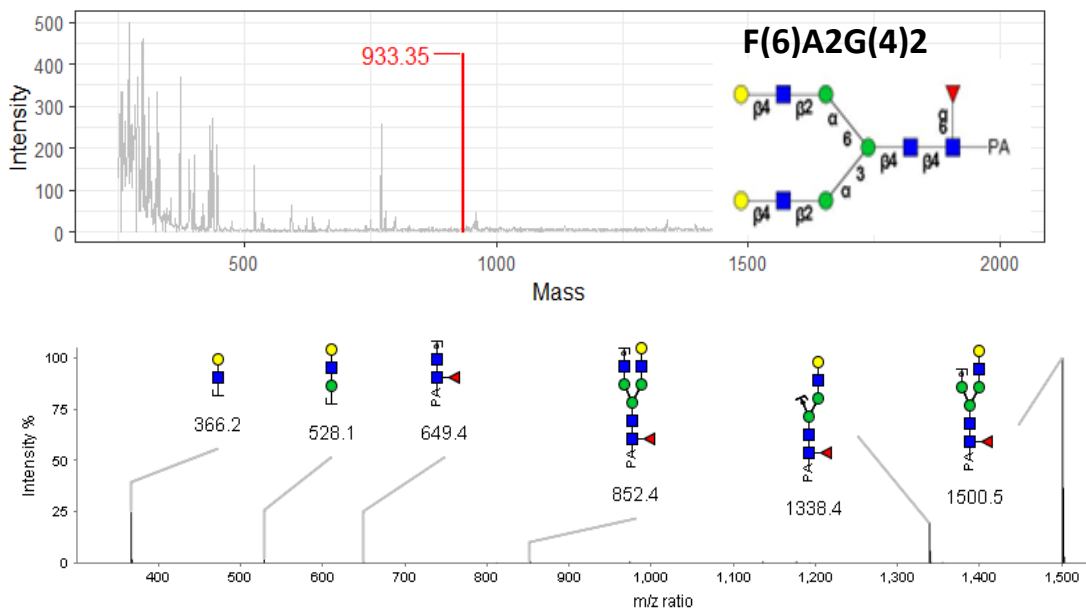
N-11



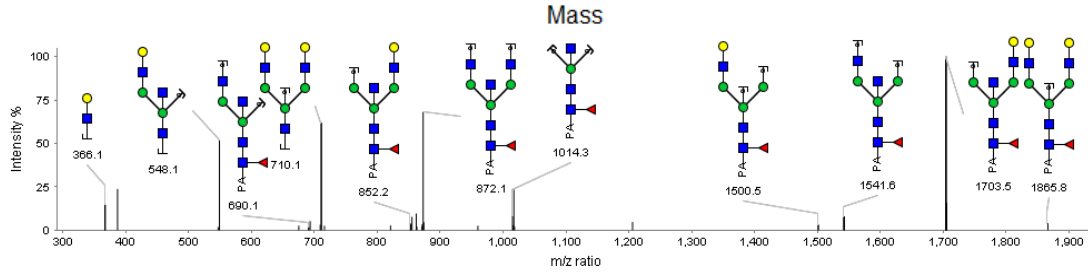
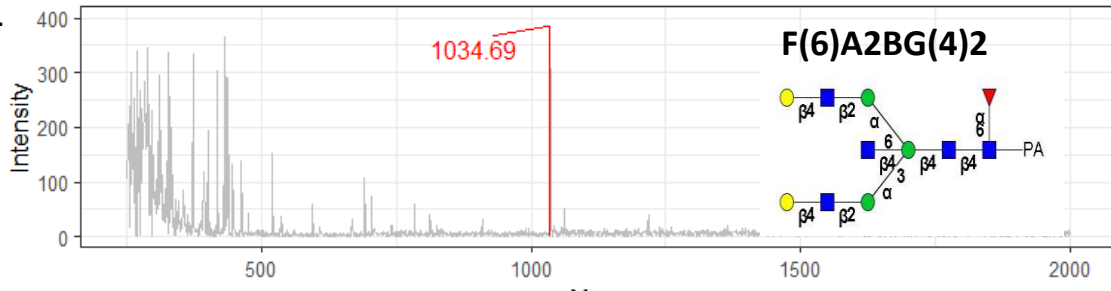
N-12



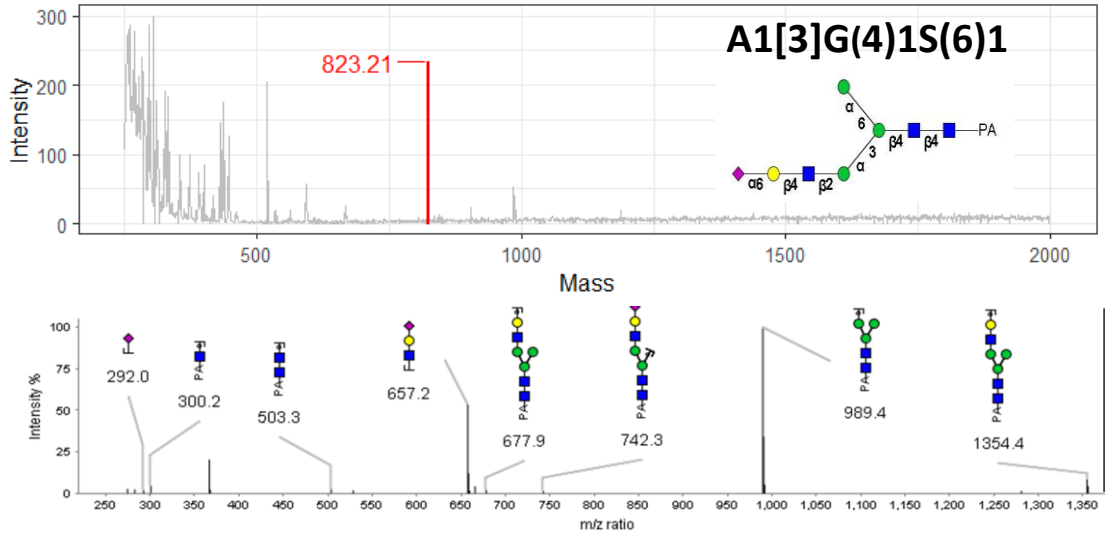
N-14



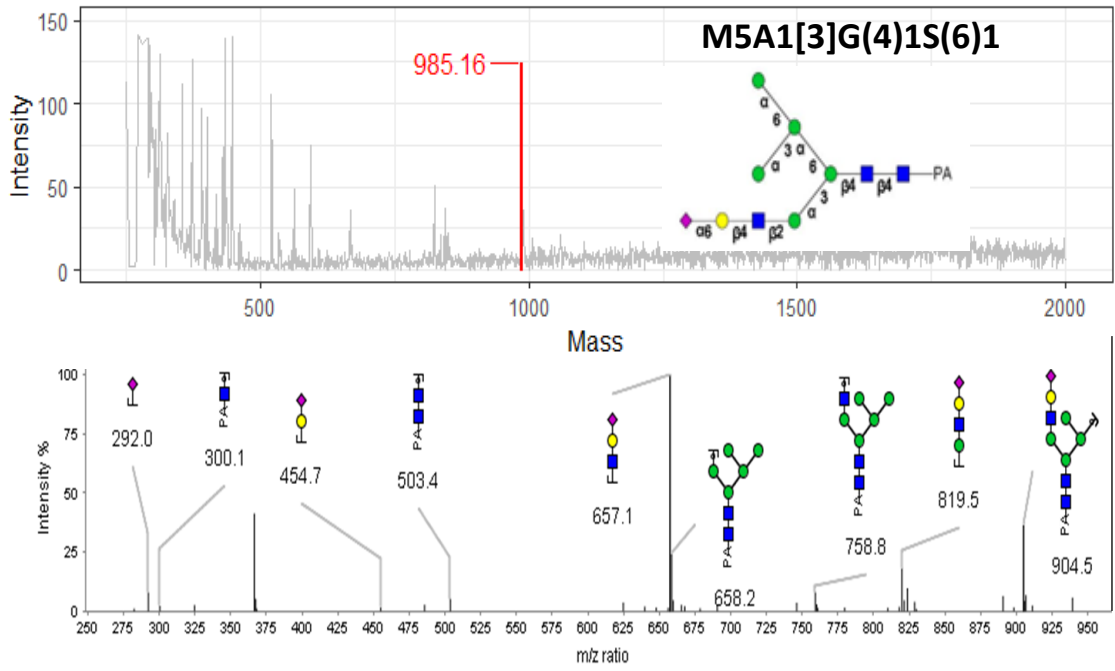
N-21



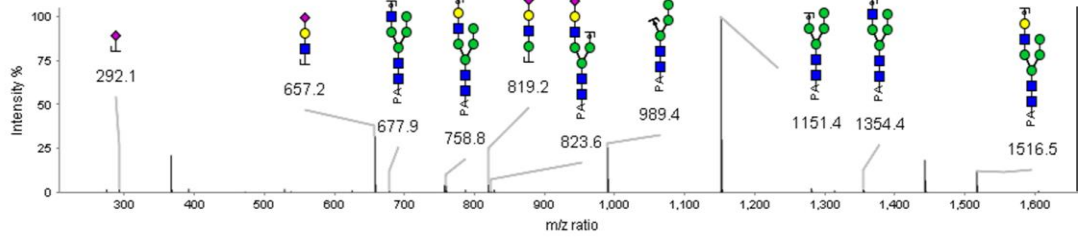
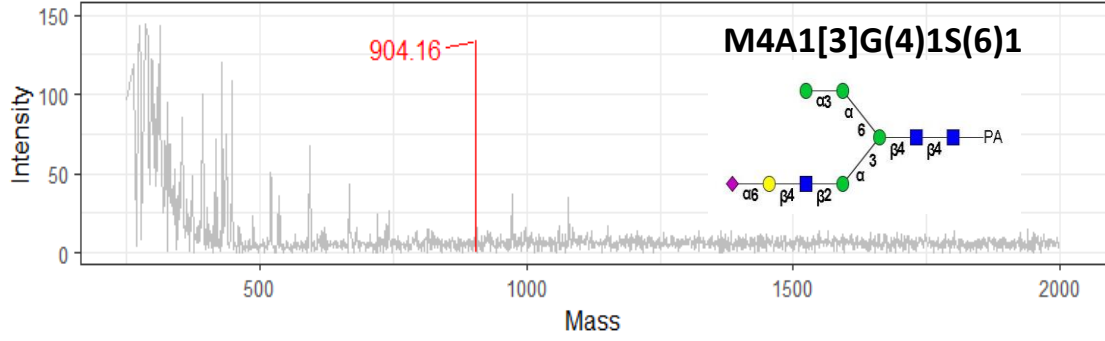
A1-2-1



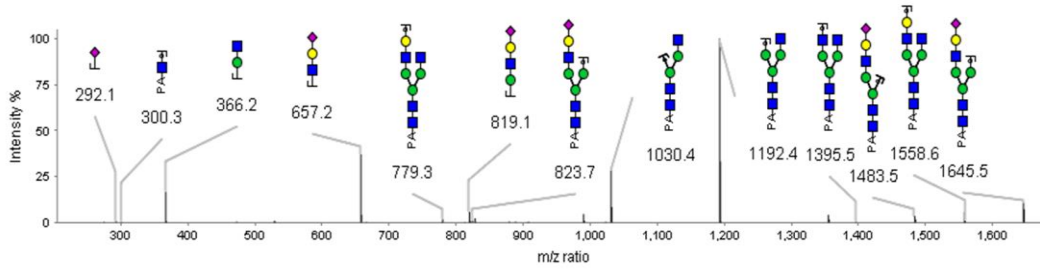
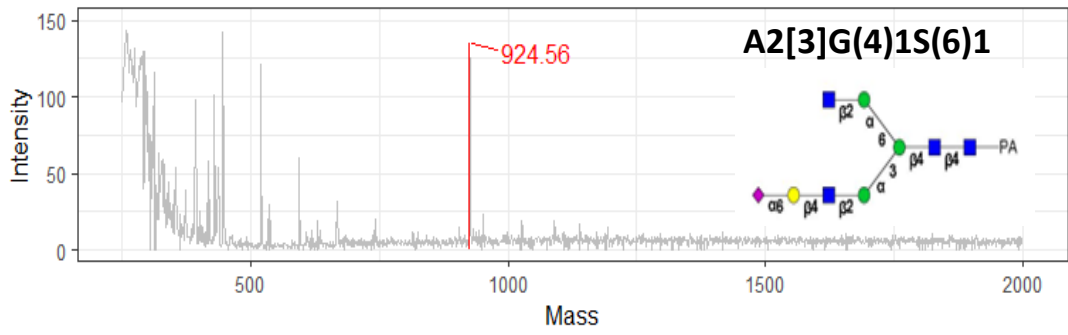
A1-2-2



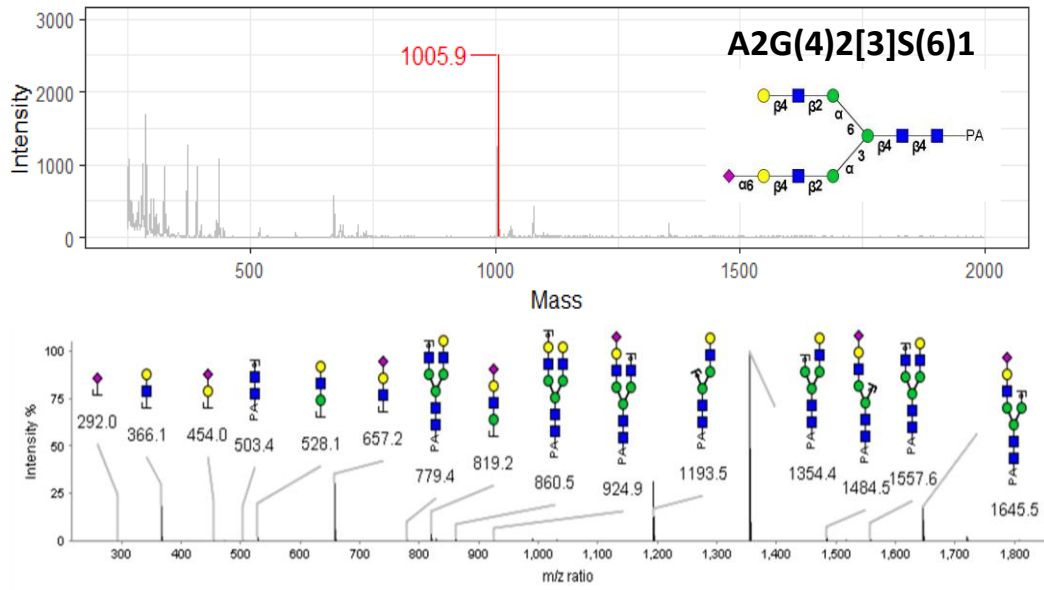
A1-3



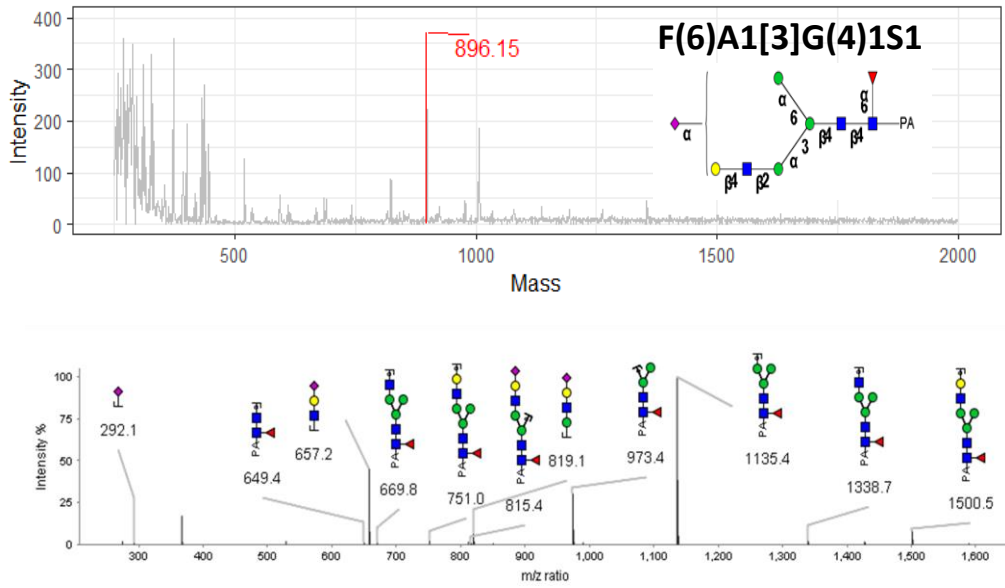
A1-5



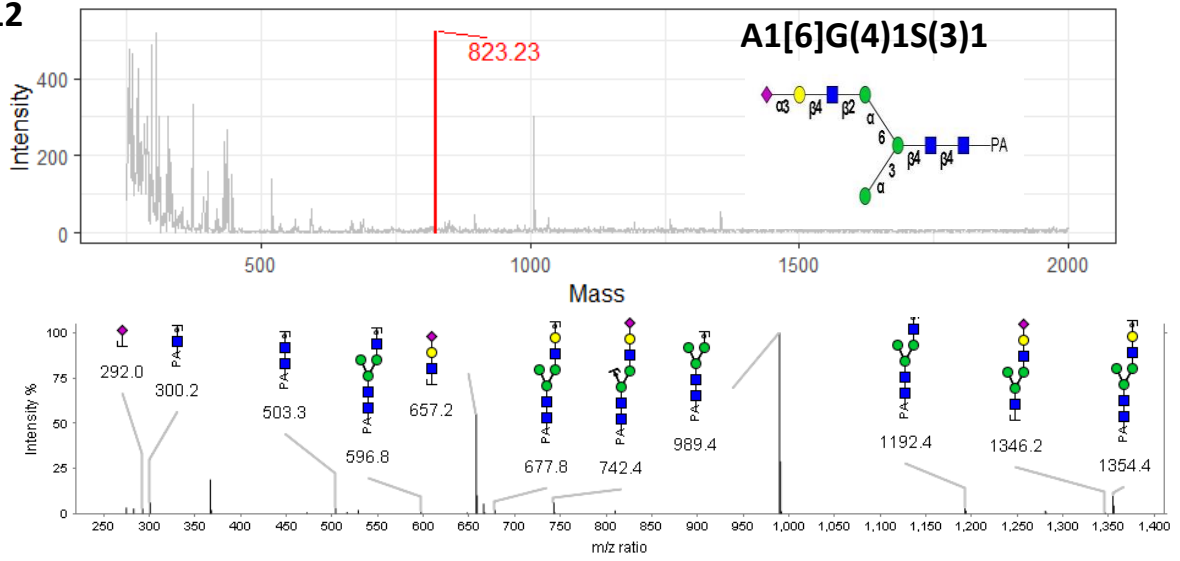
A1-6



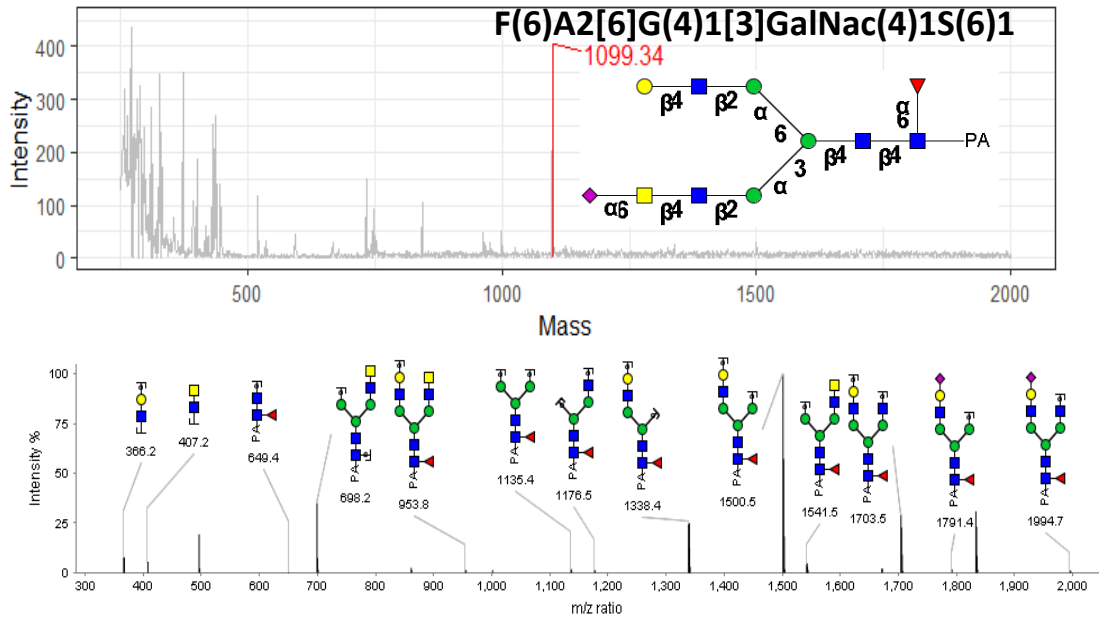
A1-9



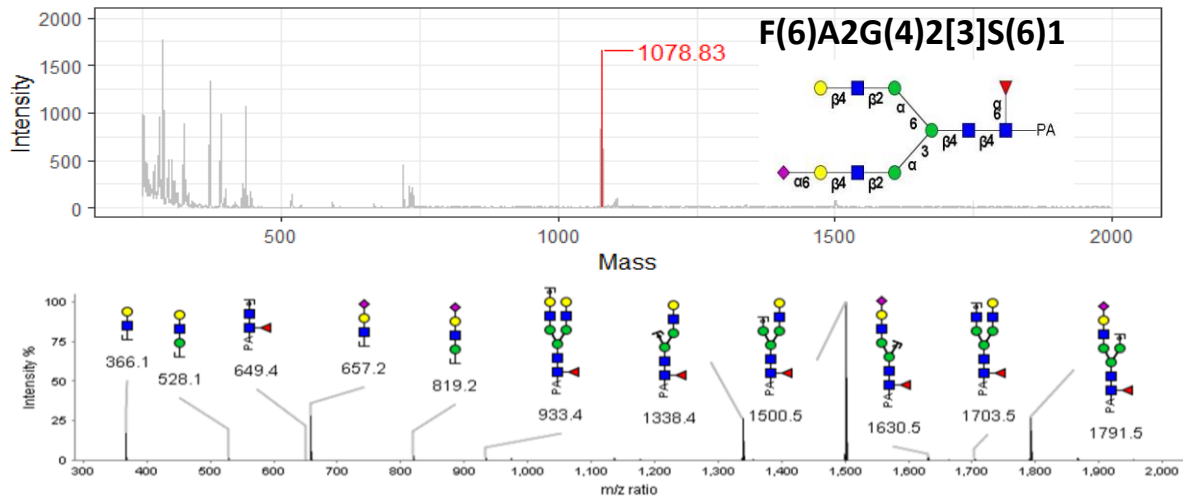
A1-12



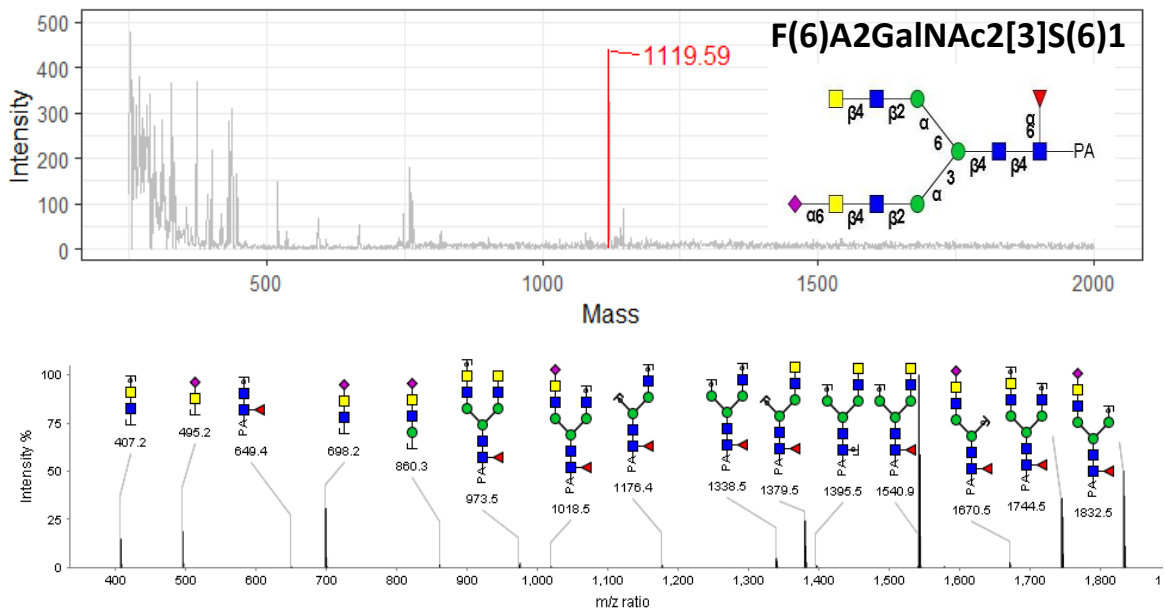
A1-14-2



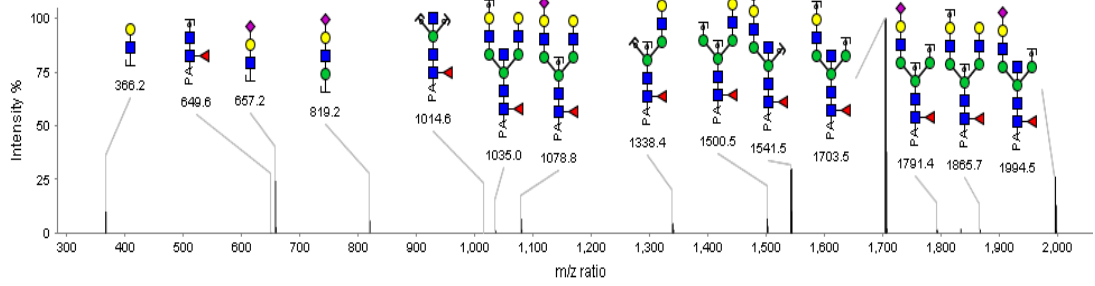
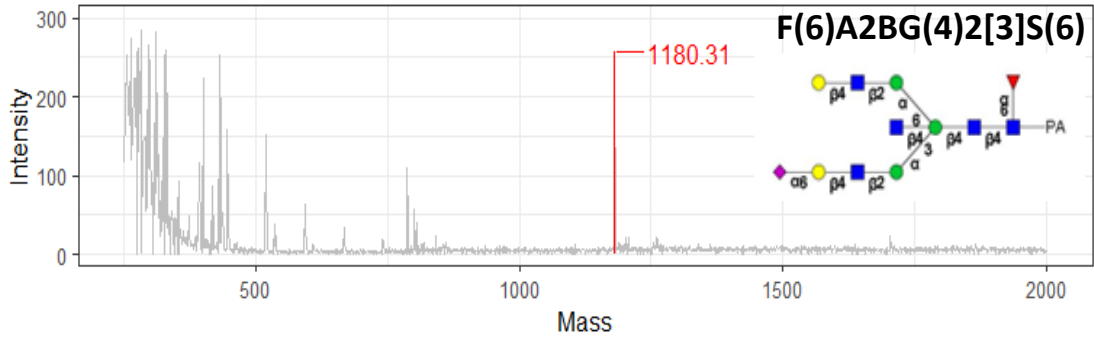
A1-15



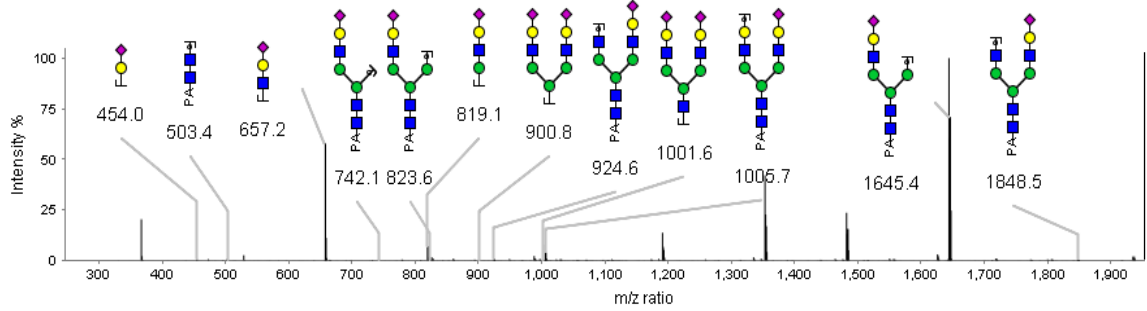
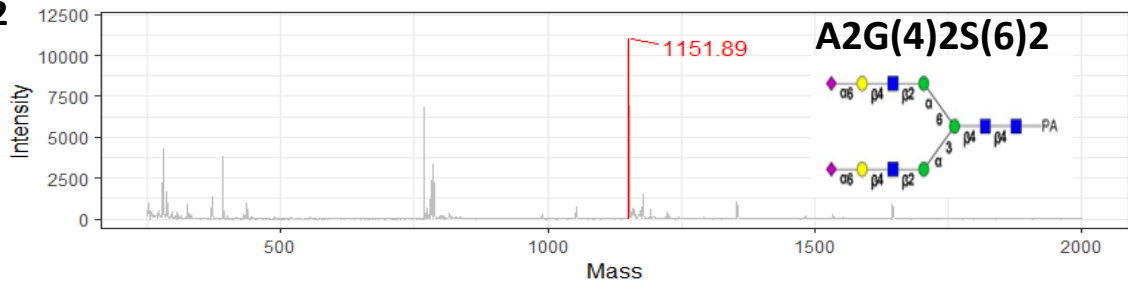
A1-17



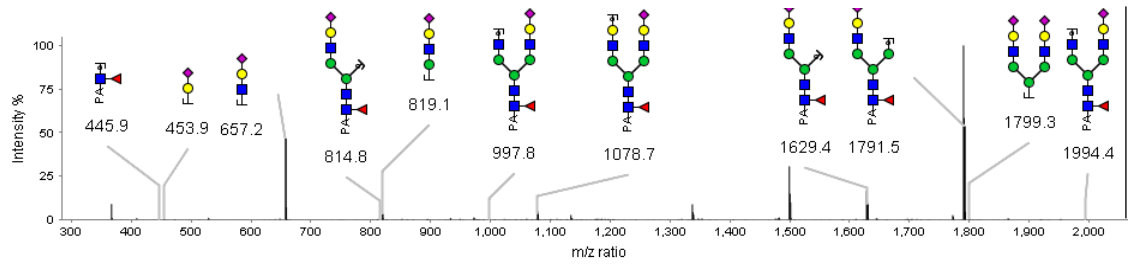
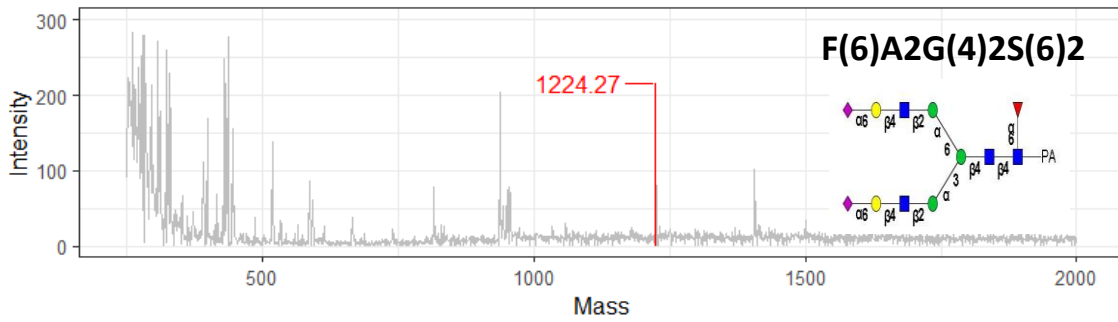
A1-24

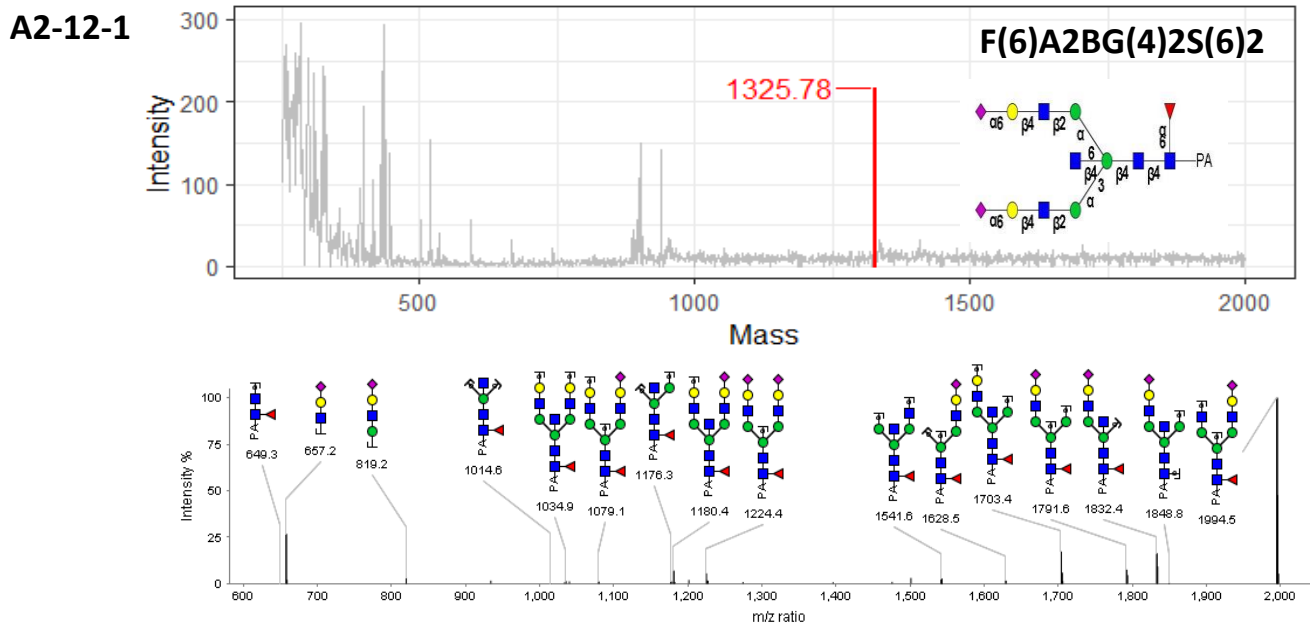
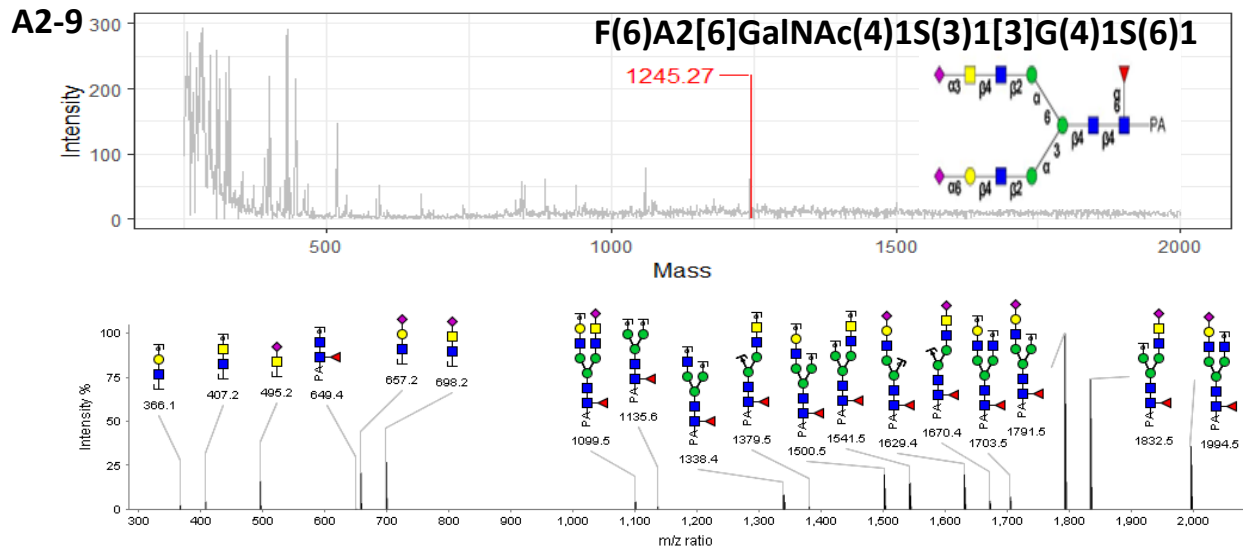


A2-2

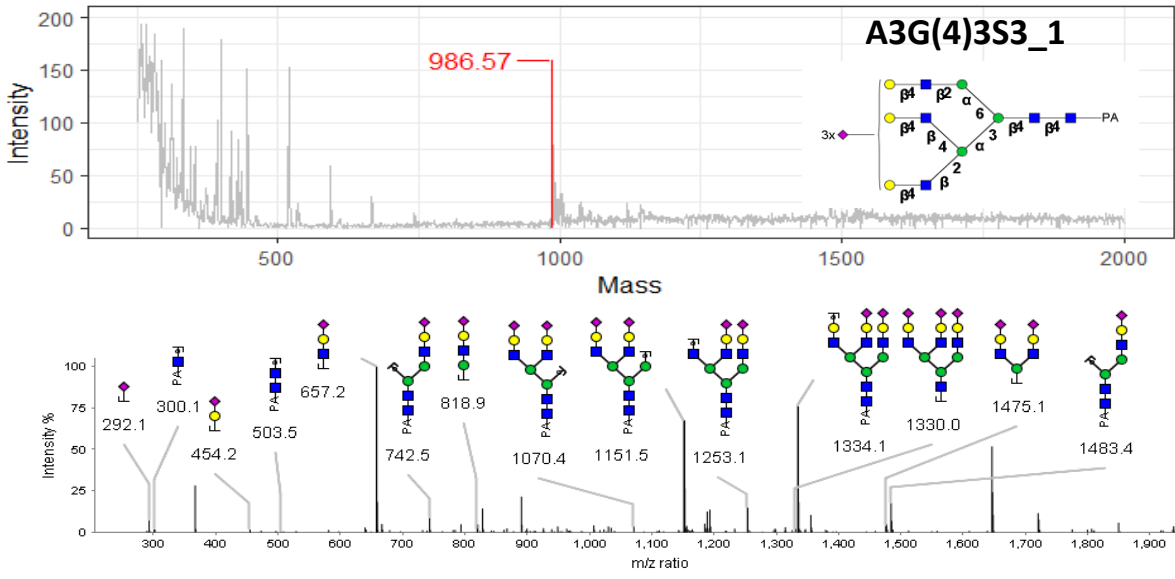


A2-8

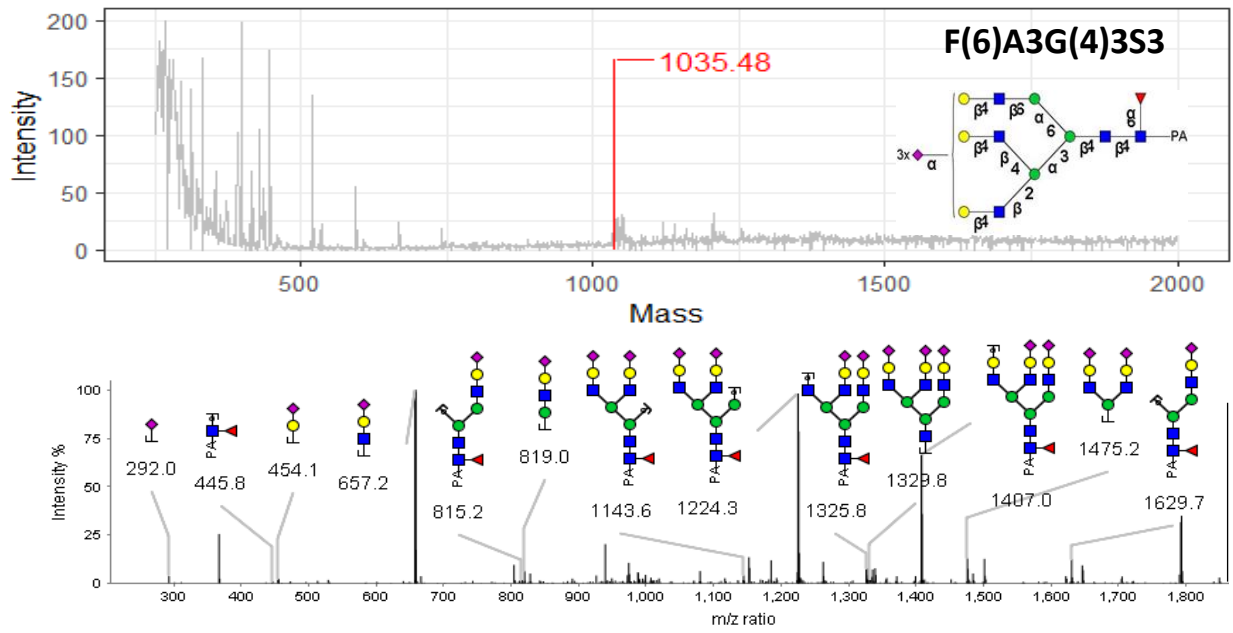




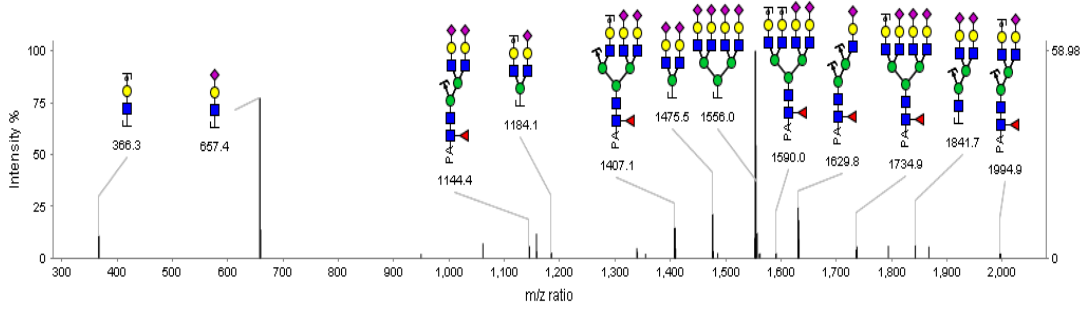
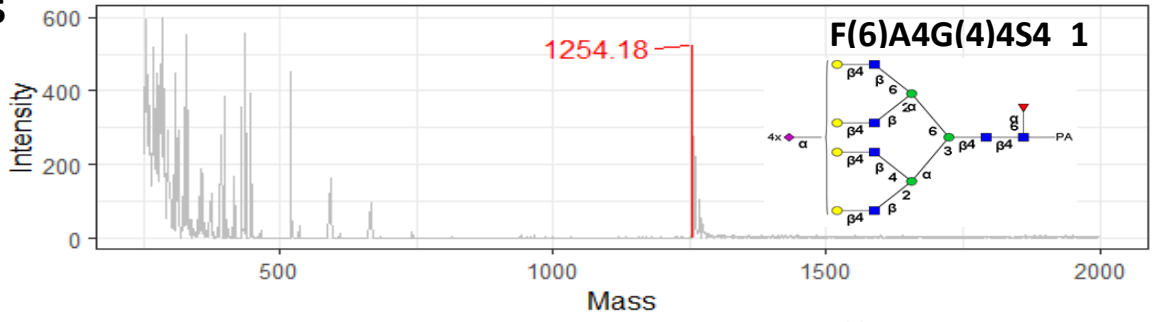
A3-4



A3-13



A4-5



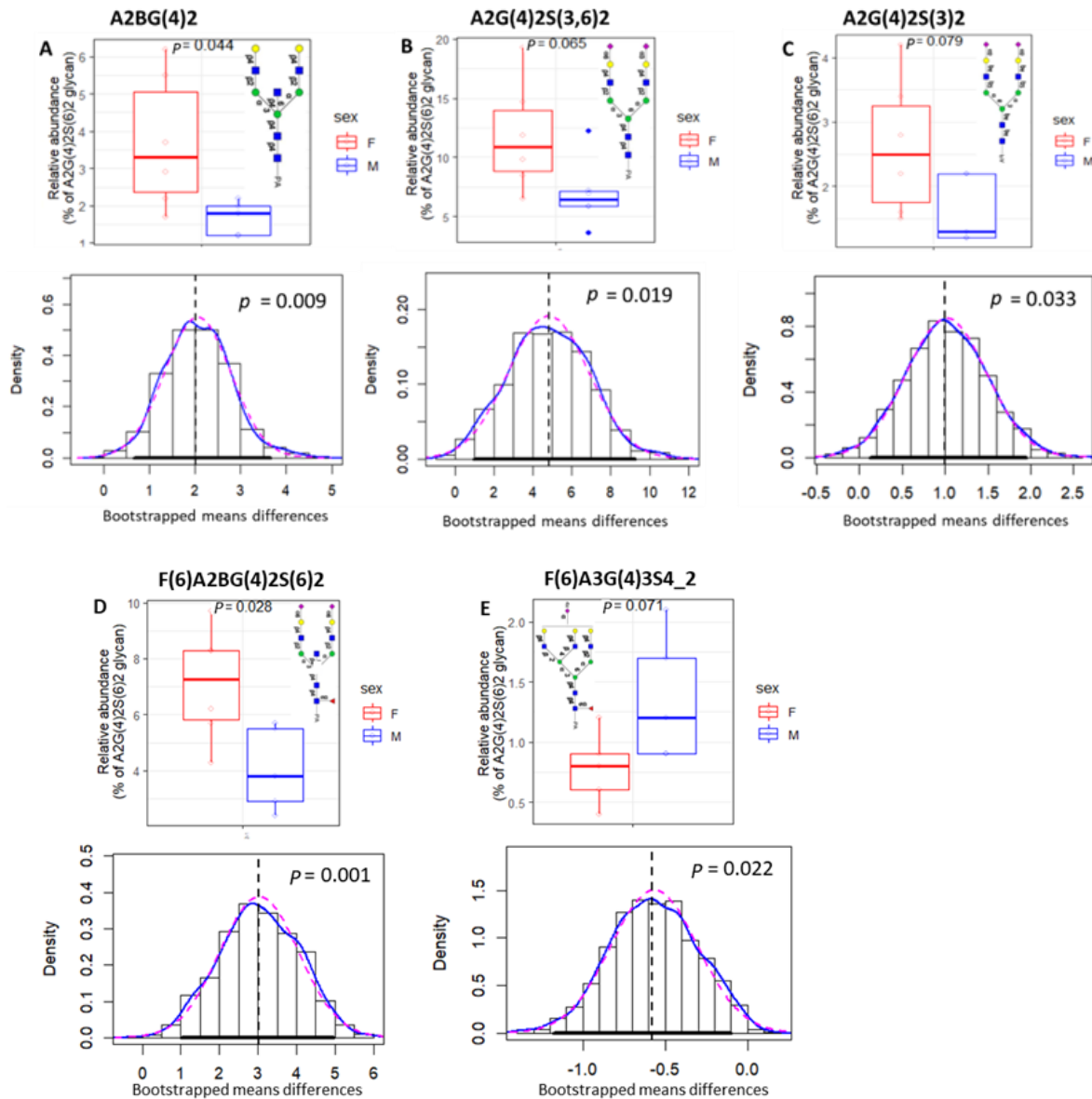


Figure 8. Each glycan was represented by an upper boxplot showing the distribution of the original data combined with the calculated p -value and a bottom density plot showing the distribution of the mean differences of the bootstrapped samples combined with the calculated p -value. The dashed vertical line represents the mean difference in the original data, the bold horizontal line represents the 95% confidence interval (CI), the dotted red line represents normal density, and the blue one represents kernel density. (A–D) show the significantly elevated glycans in females ($N = 6$) compared to males ($N = 6$) (p -value < 0.05) in bootstrapped samples. (E) shows the significantly elevated glycan structures in males compared to females (p -value < 0.05) in bootstrapped samples.

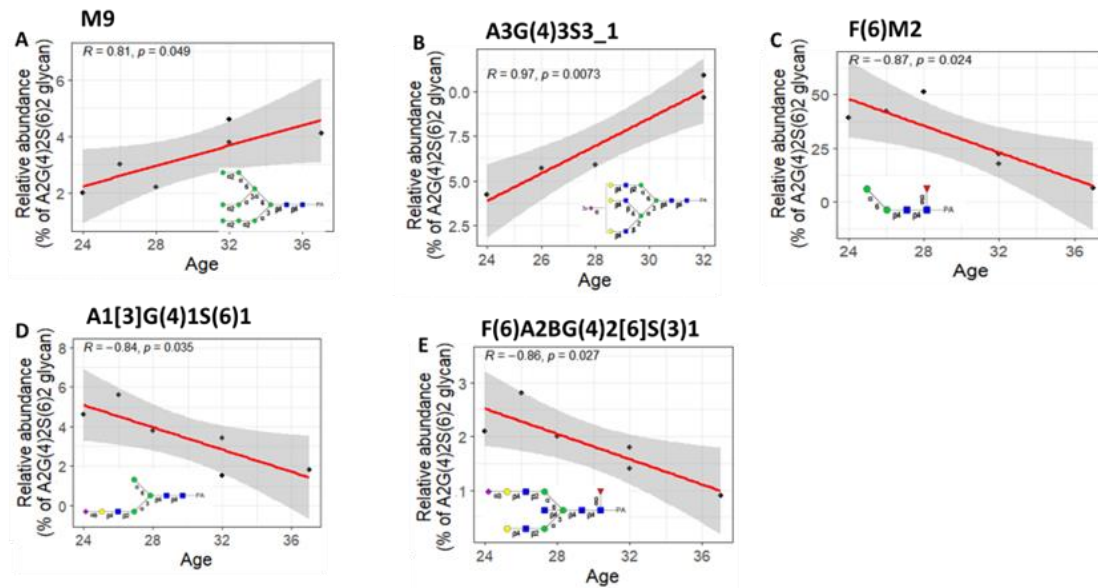


Figure 9. (A,B) Correlation plot showing a significant positive correlation ($R > 0.8$ & $p < 0.05$) between relative abundances of the M9 and A3G(4)3S3_1 glycans and age in females ($N = 6$). (C–E) Correlation plot showing a significant negative correlation ($R < -0.8$ & $p < 0.05$) between relative abundances of the F(6)M2, A1[3]G(4)1S(6)1, and F(6)A2BG(4)2[6]S(3)1 glycans and age in female.

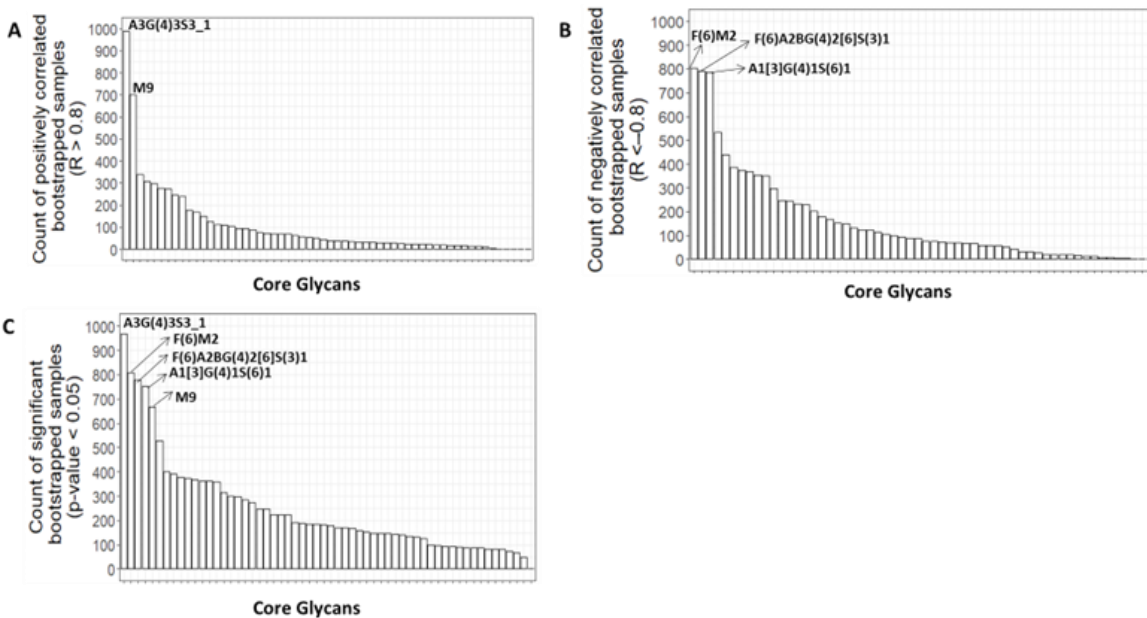


Figure 10. (A) Bar plot displaying the number of positively correlated bootstrapped samples ($R > 0.8$) between each core glycan and age in females ($N = 6$). (B). Bar plot displays the number of negatively correlated bootstrapped samples ($R < -0.8$) between each core glycan and age in females. (C) Bar plot displaying the number of significantly correlated bootstrapped samples ($p\text{-value} < 0.05$) between each core glycan and age in females.

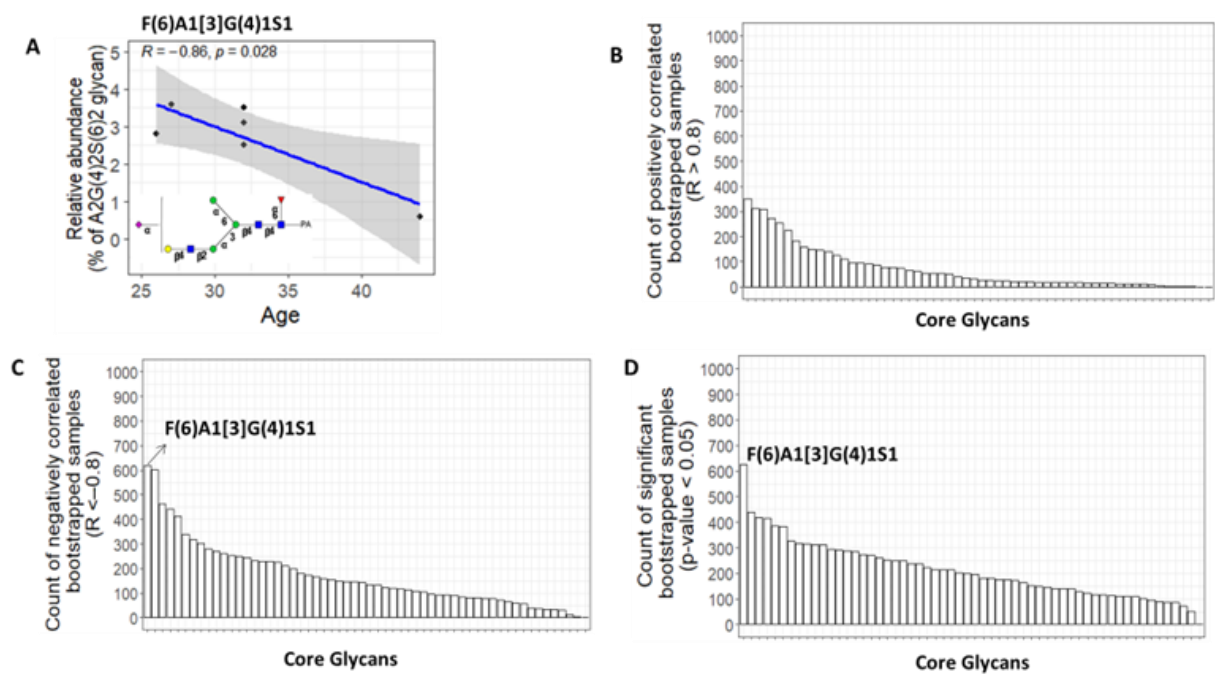





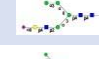











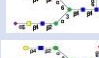




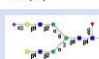










Figure 11. (A) Correlation plot showing a significant negative correlation ($R < -0.8$ & $p < 0.05$) between the relative abundance of the F(6)A1[3]G(4)1S1 glycan and age in males ($N = 6$). (B) Bar plot displaying the number of positively correlated bootstrapped samples ($R > 0.8$) between each core glycan and age in males. (C) Bar plot displaying the number of negatively correlated bootstrapped samples ($R < -0.8$) between each core glycan and age in males. (D) Bar plot displaying the number of significantly correlated bootstrapped samples ($p\text{-value} < 0.05$) between each core glycan and age in males.

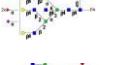










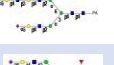

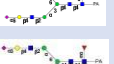






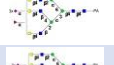
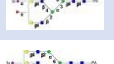
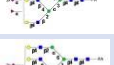




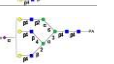



Table 1. Human urine sample information.

Sample symbol	Sex	Age
014	male	32
023	female	32
027	female	28
028	male	27
030	male	44
031	female	26
035	female	24
036	male	32
038	female	37
040	male	32
042	male	26
095	female	32

Table 2. List of 109 urinary N-glycans detected from human urine samples.
The glycans commonly detected in more than 80% of the urine samples are shown in blue background as the core glycome.

Fraction of DEAE HPLC	Fraction of RP-HPLC	Peak on MS analysis	Glycan ID	Glucose unit on RP-HPLC	MZ	Ion form	MS	Composition ¹	Proposed glycan structure ²	Oxford notation of glycan structure ³	014	023	027	028	030	031	035	036	038	040	042	095	Number of samples detected	Average of the ratios (%)	The ratio of human serum N-glycans
N	1		N-1	5.16	900.33	2H ⁺	1756.65	H8Hn2PA1		M8	2.5	7.5	5.4	3.5	2.0	1.2	0.9	0.9	3.1	6.5	2.4	4.8	12	3.38	0.73
N	2		N-2	5.36	819.31	2H ⁺	1636.60	H7Hn2PA1		M7[6]	5.2	2.3	6.3	10.1	2.3	4.3	2.8	1.1	3.4	4.1	2.9	8.3	12	4.42	0.42
N	3		N-3	5.54	981.36	2H ⁺	1960.70	H9Hn2PA1		M9	1.5	3.8	2.2	2.2	0.9	3.0	2.0	3.4	4.1	5.1	1.8	4.6	12	2.88	0.66
N	4		N-4	5.93	819.31	2H ⁺	1636.60	H7Hn2PA1		M7[3]	13.5	2.3	6.7	18.5	10.3	15.4	10.5	2.1	13.7	19.1	2.0	27.7	12	11.82	0.19
N	5		N-5	6.16	738.28	2H ⁺	1474.54	H6Hn2PA1		M6	36.2	12.0	44.3	37.9	48.7	12.6	13.9	11.0	58.8	52.7	10.3	123.2	12	38.47	2.68
N	6	1	N-6-1	7.02	827.34	H ⁺	826.33	H2Hn2PA1		M2	28.0	34.3	104.1	60.4	12.5	41.7	68.3	19.3	3.4	28.8	19.7	6.9	12	35.62	ND
N	6	2	N-6-2	7.02	989.39	H ⁺	988.39	H3Hn2PA1		M3	20.1	25.2	52.3	49.6	13.4	35.6	32.3	15.2	8.2	19.7	19.4	22.3	12	28.12	ND
N	6	3	N-6-3	7.02	1313.50	H ⁺	1312.49	H5Hn2PA1		M5	26.9	18.2	67.0	27.1	19.2	23.3	21.6	6.7	12.5	17.5	5.3	33.6	12	23.24	3.52
N	7		N-7	9.56	1192.47	H ⁺	1191.47	H3Hn3PA1		A1[6]	3.3	ND	14.2	6.1	3.6	1.8	3.3	ND	ND	ND	ND	ND	6	5.38	ND
N	8		N-8	9.91	860.33	2H ⁺	1718.65	H9Hn4PA1		A2G(4)2	1.1	3.4	9.8	3.8	2.2	2.7	1.9	ND	1.3	2.4	ND	2.2	10	3.07	1.37
N	9	1	N-9-1	10.13	973.40	H ⁺	972.39	H2Hn2nH1PA1		F(6)M2	18.3	22.4	51.2	32.8	13.1	42.2	39.2	9.9	6.4	12.9	21.7	17.7	12	23.97	ND
N	9	2	N-9-2	10.13	1135.45	H ⁺	1134.44	H3Hn2nH1PA1		F(6)M3	12.4	14.4	26.9	24.2	12.6	19.2	16.7	6.5	5.9	7.9	8.8	17.2	12	14.40	ND
N	10		N-10	11.12	1180.96	2H ⁺	2359.90	H5Hn5nH3PA1		F(6)A2BF(3)2G(4)2	3.5	3.2	11.0	6.6	3.9	4.0	5.2	2.7	3.9	ND	2.6	10.0	11	5.14	ND
N	11		N-11	11.92	771.31	2H ⁺	1540.60	H3Hn4nH1PA1		F(6)A2	3.3	4.6	12.0	8.3	4.8	3.2	3.5	4.3	3.3	5.1	3.9	7.0	12	5.29	9.92
N	12		N-12	12.78	852.33	2H ⁺	1702.66	H4Hn4nH1PA1		F(6)A2[3]G(4)1	5.3	4.8	18.7	9.3	6.6	7.3	4.9	3.3	5.5	6.7	6.8	10.0	12	7.42	ND
N	13		N-13	12.98	852.33	2H ⁺	1702.66	H4Hn4nH1PA1		F(6)A2[6]G(4)1	0.0	1.7	ND	0.0	ND	ND	ND	ND	1.0	1.4	2.0	1.9	5	1.15	14.50
N	14		N-14	13.56	933.36	2H ⁺	1864.71	H5Hn4nH1PA1		F(6)A2G(4)2	5.3	11.0	36.9	23.3	7.6	16.3	18.3	8.3	9.6	11.9	12.4	18.7	12	14.97	8.85
N	15		N-15	14.96	880.85	2H ⁺	1759.68	H4Hn5PA1		A2B[3]G(4)1	2.1	0.8	2.2	3.8	0.7	1.4	0.8	0.6	0.8	ND	0.8	1.6	11	1.42	0.64
N	16	1	N-16-1	15.62	974.39	2H ⁺	1946.76	H3Hn6nH1PA1		F(6)A2GalNAc(4)2	1.9	2.9	ND	2.0	0.7	1.0	2.6	ND	1.5	2.8	0.8	3.4	10	1.97	ND
N	16	2	N-16-2	15.62	1107.93	2H ⁺	2213.85	H5Hn5nH2PA1		F(6)A2BF(3)1G(4)2_1	0.6	ND	ND	1.2	0.2	0.9	1.2	ND	0.3	ND	0.8	0.8	8	0.76	ND
N	17	1	N-17-1	16.23	961.87	2H ⁺	1921.73	H5Hn5PA1		A2BG(4)2	1.2	2.2	6.2	1.8	1.2	3.7	2.9	2.0	1.7	ND	2.2	5.5	11	2.79	0.31
N	17	2	N-17-2	16.45	1107.93	2H ⁺	2213.85	H5Hn5nH2PA1		F(6)A2BF(3)1G(4)2_2	0.1	1.6	ND	0.3	0.9	1.6	3.6	ND	1.5	ND	1.5	4.1	9	1.69	ND
N	18		N-18	20.66	872.85	2H ⁺	1743.68	H3Hn5nH1PA1		F(6)A2B	2.3	2.7	8.6	7.3	2.9	4.6	6.3	4.1	2.5	3.1	2.5	3.8	12	4.21	2.06
N	19		N-19	22.27	953.87	2H ⁺	1905.73	H4Hn5nH1PA1		F(6)A2B[3]G(4)1	0.7	1.1	1.8	2.6	0.5	3.9	1.0	1.1	0.9	ND	0.8	1.9	11	1.49	2.65
N	20		N-20	23.02	953.87	2H ⁺	1905.73	H4Hn5nH1PA1		F(6)A2B[6]G(4)1	1.7	2.7	6.3	4.7	2.3	ND	2.7	2.9	2.2	2.6	2.5	5.8	11	3.31	0.41
N	21		N-21	24.42	1034.90	2H ⁺	2067.79	H5Hn5nH1PA1		F(6)A2BG(4)2	4.8	6.0	18.7	14.1	4.5	9.1	9.3	4.6	5.4	7.0	6.3	15.1	12	8.75	1.40
N	22		N-22	26.99	1144.44	2H ⁺	2286.86	H6Hn6PA1		A3BG(4)3	0.5	ND	3.5	2.0	0.4	2.2	ND	ND	0.9	ND	ND	4.0	7	1.93	ND
N	23		N-23	35.17	1290.50	2H ⁺	2578.98	H6Hn6nH2PA1		F(6)A3BF(3)1G(4)3	1.0	1.3	3.2	2.8	ND	3.3	2.8	ND	1.1	ND	ND	5.0	8	2.56	ND
N	24		N-24	38.18	1217.47	2H ⁺	2432.92	H8Hn6nH1PA1		F(6)A3BG(4)3	0.7	ND	3.6	1.3	ND	2.4	ND	ND	0.9	ND	ND	2.8	6	1.94	ND

A1	1		A1-1	7.93	1188.45	2H+	2374.88	N1H6H5PA1		A3G(4)3[3]S(6)1	ND	ND	0.8	1.1	0.3	ND	ND	ND	0.8	ND	ND	ND	4	0.76	1.22
A1	2	1	A1-2-1	8.04	823.31	2H+	1644.61	N1H4H3PA1		A1[3]G(4)1S(6)1	3.6	3.4	3.8	3.9	1.2	5.6	4.6	3.0	1.8	6.3	3.0	1.5	12	3.48	ND
A1	2	2	A1-2-2	8.04	985.37	2H+	1968.72	N1H6H3PA1		M5A1[3]G(4)1S(6)1	1.0	0.8	0.8	1.1	0.3	0.6	1.1	1.0	0.7	1.2	0.8	2.7	12	1.02	1.54
A1	3		A1-3	8.22	904.34	2H+	1806.67	N1H5H3PA1		M4A1[3]G(4)1S(6)1	1.4	0.9	1.1	1.7	0.7	1.4	1.3	1.9	1.3	2.1	0.9	1.8	12	1.39	1.68
A1	4		A1-4	9.08	985.37	2H+	1968.72	N1H6H3PA1		M5A1[3]G(4)1S(3)1	0.7	0.6	ND	0.5	0.4	0.5	ND	ND	0.5	ND	ND	0.8	7	0.58	0.13
A1	5		A1-5	9.54	924.85	2H+	1847.69	N1H4H4PA1		A2[3]G(4)1S(6)1	2.1	3.5	2.1	1.9	1.3	3.6	2.4	3.1	2.2	4.2	3.3	2.2	12	2.67	1.14
A1	6		A1-6	10.19	1005.88	2H+	2009.75	N1H5H4PA1		A2G(4)2[3]S(6)1	13.3	13.2	19.3	15.4	16.1	14.5	10.5	14.4	17.7	16.9	9.2	31.7	12	16.03	23.75
A1	7		A1-7	11.19	1261.48	2H+	2520.94	N1H6H5dH1PA1		F(6)A3G(4)3S1	1.1	ND	1.2	1.3	1.5	3.2	2.1	ND	1.1	ND	2.2	1.9	9	1.73	0.37
A1	8	1	A1-8-1	11.33	916.86	2H+	1831.70	N1H3H4dH1PA1		F(6)A1[3]GalNac(4)1S1	1.6	2.5	ND	2.4	1.4	1.3	0.8	ND	0.7	1.0	1.2	4.1	10	1.69	ND
A1	8	2	A1-8-2	11.33	1151.94	2H+	2301.86	N1H5H4dH2PA1		F(6)A2[6]F(3)1G(4)2S1	2.0	ND	2.4	3.1	0.3	2.8	2.1	ND	1.3	1.9	ND	2.2	9	2.01	0.32
A1	9		A1-9	11.61	896.34	2H+	1750.67	N1H4H3dH1PA1		F(6)A1[3]G(4)1S1	2.5	2.1	3.0	3.6	0.6	2.5	2.1	3.1	0.7	3.5	2.8	3.2	12	2.48	ND
A1	10		A1-10	11.82	1005.88	2H+	2009.75	N1H5H4PA1		A2G(4)2[6]S(3)1	1.7	2.3	2.2	2.0	0.6	1.1	1.0	3.7	1.9	3.2	2.5	1.7	12	2.00	4.16
A1	11		A1-11	12.10	1005.88	2H+	2009.75	N1H5H4PA1		A2G(4)2[3]S(3)1	2.3	1.8	2.2	2.2	0.7	2.3	1.3	2.3	1.7	2.9	1.6	7.0	12	2.35	0.44
A1	12		A1-12	12.29	823.31	2H+	1644.61	N1H4H3PA1		A1[6]G(4)1S(3)1	1.5	1.9	1.6	1.6	0.6	1.7	1.4	2.9	1.0	2.9	3.9	0.6	12	1.80	ND
A1	13		A1-13	12.63	1188.45	2H+	2374.88	N1H6H5PA1		A2G(4)2[LacNac]1S1	0.7	ND	ND	1.2	0.5	ND	ND	ND	3.1	0.6	ND	3.5	6	1.60	1.07
A1	14	1	A1-14-1	13.53	997.88	2H+	1993.75	N1H4H3dH1PA1		F(6)A2[3]G(4)1S(6)1	3.2	3.4	3.8	1.7	2.2	4.9	3.6	3.7	2.0	3.5	2.1	1.7	12	2.98	1.80
A1	14	2	A1-14-2	13.61	1099.42	2H+	2196.83	N1H4H5dH1PA1		F(6)A2[6]G(4)1[3]GalNac(4)1S(6)1	2.3	3.5	4.0	4.2	3.0	3.4	3.7	4.2	3.6	3.7	2.1	9.3	12	3.92	ND
A1	15		A1-15	14.24	1078.91	2H+	2155.80	N1H5H4dH1PA1		F(6)A2G(4)2[3]S(6)1	21.2	18.2	24.8	26.0	19.3	42.9	25.8	20.0	25.2	25.9	15.4	37.9	12	25.21	12.65
A1	16	1	A1-16-1	14.72	1107.42	2H+	2212.83	N1H5H5PA1		A2B[6]G(4)2[3]S(6)1	0.5	0.4	1.8	2.3	0.9	0.7	0.4	ND	0.5	ND	ND	3.0	9	1.16	2.11
A1	16	2	A1-16-2	14.72	1232.96	2H+	2463.91	N1H6H4dH2PA1		F(6)A2F(3)G3S1	0.4	ND	ND	ND	ND	0.5	ND	ND	ND	ND	ND	0.9	3	0.62	ND
A1	17		A1-17	15.23	1119.94	2H+	2237.86	N1H3H6dH1PA1		F(6)A2GalNac2[3]S(6)1	4.4	8.1	6.1	10.6	5.0	4.1	4.7	4.3	3.4	5.0	2.3	11.7	12	5.82	ND
A1	18		A1-18	15.98	997.88	2H+	1993.75	N1H4H3dH1PA1		F(6)A2[3]G(4)1S(3)1	1.6	0.9	ND	2.6	0.7	3.1	ND	ND	ND	1.2	ND	ND	6	1.68	ND
A1	19		A1-19	16.92	1078.91	2H+	2155.80	N1H5H4dH1PA1		F(6)A2G(4)2[6]S(3)1	10.7	11.3	13.2	15.8	7.8	13.1	10.5	12.7	8.5	9.9	6.9	13.0	12	11.11	0.12
A1	20		A1-20	17.28	1078.91	2H+	2155.80	N1H5H4dH1PA1		F(6)A2G(4)2[3]S(3)1	ND	2.5	3.3	4.7	1.7	4.5	2.3	3.3	1.6	2.6	2.0	2.7	11	2.84	0.92
A1	21	1	A1-21-1	17.81	1099.42	2H+	2196.83	N1H4H5dH1PA1		F(6)A2G(4)2S1	1.0	2.3	ND	1.4	0.4	1.4	ND	ND	0.6	0.9	1.2	0.0	8	1.01	ND
A1	21	2	A1-21-2	17.81	1261.48	2H+	2520.94	N1H6H5dH1PA1		F(6)A2G(4)2[3]Lac1S1	2.4	1.0	ND	1.8	0.8	0.8	1.2	ND	2.5	2.6	1.2	5.1	10	1.93	ND
A1	22		A1-22	18.79	1151.94	2H+	2301.86	N1H5H4dH2PA1		F(6)A2F(3)1G(4)2S1	0.6	1.6	4.5	2.4	0.9	2.7	3.5	1.3	0.9	ND	ND	ND	9	2.05	ND
A1	23		A1-23	20.65	1099.42	2H+	2196.83	N1H4H5dH1PA1		F(6)A2B[3]G(4)1S(6)1	0.7	ND	ND	1.5	0.6	ND	0.7	3.3	0.6	ND	ND	ND	6	1.23	0.45
A1	24		A1-24	22.79	1180.45	2H+	2358.88	N1H5H5dH1PA1		F(6)A2B[6]G(4)2[3]S(6)1	3.9	3.7	5.8	8.2	2.9	6.7	4.7	4.9	3.1	4.0	2.3	6.8	12	4.76	5.84
A1	25		A1-25	25.85	1099.42	2H+	2196.83	N1H4H5dH1PA1		F(6)A2B[6]G(4)1S(3)1	0.9	0.5	ND	1.9	0.7	1.6	2.4	1.1	ND	ND	ND	0.0	7	1.12	0.31
A1	26		A1-26	27.69	1180.45	2H+	2358.88	N1H5H5dH1PA1		F(6)A2B[6]G(4)2[6]S(3)1	1.2	1.4	2.0	3.6	1.5	2.8	2.1	2.7	0.9	2.1	1.6	1.8	12	1.98	0.46

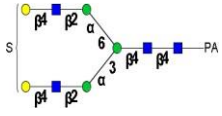
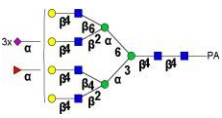
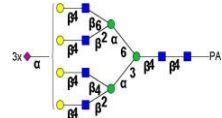
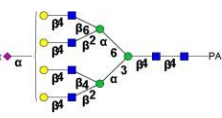
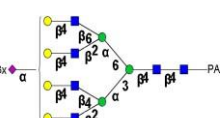
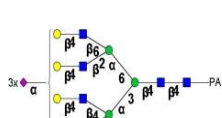
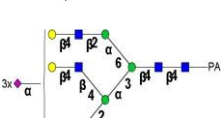
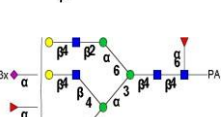
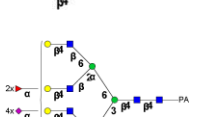
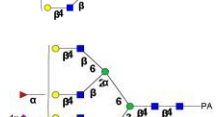
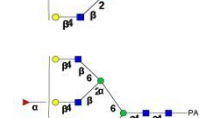
A1	27	1	A1-27-1	29.21	1006.38	3H ⁺	3016.13	N1H6Hn6dH3PA1		F(6)A3F2BG(4)3S1	0.3	0.3	ND	0.6	0.1	0.5	ND	ND	0.3	1.1	ND	0.0	7	0.40	ND	
A1	27	2	A1-27-2	29.21	1099.42	2H ⁺	2196.83	N1H4Hn5dH1PA1		F(6)A2B(3)G(4)1S(3)1	0.2	0.4	ND	1.0	0.5	0.8	ND	1.2	0.3	ND	ND	0.0	7	0.56	ND	
A1	28		A1-28	30.72	1180.45	2H ⁺	2358.88	N1H5n5dH1PA1		F(6)A2BG(4)2(3)S(3)1	0.7	0.9	ND	1.6	0.9	3.1	3.3	1.4	0.7	ND	ND	1.5	9	1.55	ND	
A1	29		A1-29	43.79	957.70	3H ⁺	2870.07	N1H6Hn6dH2PA1		F(6)A3F1BG(4)3S1	0.9	ND	ND	1.3	ND	1.3	ND	ND	0.4	ND	ND	1.2	5	1.04	ND	
A2	1		A2-1	9.97	1224.46	2H ⁺	2446.90	N2H5Hn4dH1PA1		A2F1G(4)2S2	1.8	1.7	1.5	1.8	1.5	0.8	4.4	2.0	ND	2.9	ND	ND	9	2.05	1.41	
A2	2		A2-2	11.47	1151.43	2H ⁺	2300.84	N2H5Hn4PA1		A2G(4)2S(6)2	100.0	100.0	100.0	100.0	100.0	100.0	100.0	100.0	100.0	100.0	100.0	100.0	100.0	12	100.00	100.00
A2	3		A2-3	11.11	1053.36	H ⁺	1052.35	S1H2Hn2dH1PA1		F(6)M2Sf1	ND	7.8	12.0	7.7	3.6	5.3	13.1	ND	ND	4.1	ND	ND	7	7.66	ND	
A2	4		A2-4	12.05	1151.43	2H ⁺	2300.84	N2H5Hn4PA1		A2G(4)2S(3,6)2	6.9	6.5	9.8	12.2	5.9	14.7	11.9	3.6	8.5	7.2	5.9	19.3	12	9.36	8.94	
A2	5		A2-5	1035.72		3H ⁺	3104.15	N2H6Hn5dH3PA1		F(6)A3F2G(4)3S2	ND	7.3	ND	ND	5.1	ND	5.8	11.5	ND	ND	ND	ND	4	7.43	ND	
A2	6		A2-6	13.84	1333.99	2H ⁺	2665.97	N2H6Hn5PA1		A2G(4)2(6)LacNac(1S)(6)1(3)S(6)1_1	6.1	ND	ND	6.6	4.4	ND	ND	ND	6.1	6.2	2.7	31.2	7	9.03	2.34	
A2	7	1	A2-7-1	14.34	1151.43	2H ⁺	2300.84	N2H5Hn4PA1		A2G(4)2S(3)2	1.2	2.8	3.4	2.2	1.2	1.6	2.2	ND	1.5	1.3	2.2	4.2	11	2.16	ND	
A2	7	2	A2-7-2	14.55	1244.97	2H ⁺	2487.93	N2H4Hn5dH1PA1		F(6)A2(6)GalNAc(4)1S(6)1(3)G(4)1S(6)1	1.1	5.8	ND	0.8	0.6	0.7	3.1	4.8	1.2	ND	3.6	2.3	10	2.38	ND	
A2	7	3	A2-7-3	14.23	1333.99	2H ⁺	2665.97	N2H6Hn5PA1		A2G(4)2(6)LacNac(1S)(6)1(3)S(6)1_2	1.1	ND	ND	2.2	0.5	ND	1.7	ND	1.3	ND	2.9	1.3	7	1.55	2.56	
A2	8		A2-8	15.21	1224.46	2H ⁺	2446.90	N2H5Hn4dH1PA1		F(6)A2G(4)2S(6)2	22.7	26.5	40.2	24.1	21.8	30.7	24.2	30.4	30.8	33.1	33.3	38.5	12	29.70	10.03	
A2	9		A2-9	16.00	1244.97	2H ⁺	2487.93	N2H4Hn5dH1PA1		F(6)A2(6)GalNAc(4)1S(3)1(3)G(4)1S(6)1	4.0	5.8	7.1	8.5	2.6	6.7	6.9	5.6	3.3	5.6	4.3	11.1	12	5.95	ND	
A2	10		A2-10	16.81	1224.46	2H ⁺	2446.90	N2H5Hn4dH1PA1		F(6)A2G(4)2S(3,6)2	16.5	20.4	19.9	26.1	10.7	24.5	20.9	12.6	21.3	20.6	12.9	52.0	12	21.53	1.31	
A2	11		A2-11	20.01	1224.46	2H ⁺	2446.90	N2H5Hn4dH1PA1		F(6)A2G(4)2S(3)2	26.3	25.3	27.3	40.6	27.6	33.9	34.0	24.4	22.9	25.2	17.3	70.6	12	31.29	1.46	
A2	12	1	A2-12-1	23.66	1326.00	2H ⁺	2649.98	N2H5Hn5dH1PA1		F(6)A2BG(4)2S(6)2	2.9	5.7	8.3	5.5	2.4	6.2	8.3	5.7	4.3	ND	3.8	9.7	11	5.71	5.03	
A2	12	2	A2-12-2	23.66	1407.02	2H ⁺	2812.03	N2H6Hn5dH1PA1		F(6)A3G(4)3S2_1	1.5	ND	ND	2.1	1.0	1.8	ND	ND	ND	ND	ND	ND	4	1.61	ND	
A2	13		A2-13	24.68	1407.02	2H ⁺	2812.03	N2H6Hn5dH1PA1		F(6)A3G(4)3S2_2	1.6	ND	ND	ND	1.9	5.7	ND	ND	ND	ND	ND	ND	3	3.05	0.41	
A2	14		A2-14	26.28	1407.02	2H ⁺	2812.03	N2H6Hn5dH1PA1		F(6)A3G(4)3S2_3	2.3	ND	ND	ND	0.3	ND	ND	ND	2.5	ND	ND	10.3	4	3.86	ND	
A2	15		A2-15	31.98	1326.00	2H ⁺	2649.98	N2H5Hn5dH1PA1		F(6)A2BG(4)2S(3)2	1.8	2.2	ND	3.5	1.5	3.1	3.3	2.6	1.5	ND	ND	ND	8	2.43	ND	
A3	1		A3-1	13.08	1035.38	3H ⁺	3103.13	N3H6Hn5dH1PA1		A3F1G(4)3S3_1	ND	0.9	1.7	1.0	0.9	3.3	ND	ND	ND	5.7	ND	ND	6	2.24	0.25	
A3	2		A3-2	13.80	1035.38	3H ⁺	3103.13	N3H6Hn5dH1PA1		A3F1G(4)3S3_2	5.6	4.2	0.8	4.0	ND	2.9	5.5	ND	2.4	2.4	1.9	7.2	10	3.68	6.33	
A3	3		A3-3	14.36	1035.38	3H ⁺	3103.13	N3H6Hn5dH1PA1		A3F1G(4)3S3_3	0.9	ND	ND	0.9	1.0	18.0	ND	ND	1.2	ND	ND	5.0	6	4.50	0.50	
A3	4		A3-4	14.99	986.70	3H ⁺	2957.07	N3H6Hn5PA1		A3G(4)3S3_1	3.0	9.7	5.9	3.9	2.1	5.7	4.2	3.7	ND	7.8	10.1	10.9	11	6.10	11.89	
A3	5	1	A3-5-1	15.35	1139.40	2H ⁺	2276.79	S1N1H4Hn5dH1PA1		F(6)A2(6)GalNAc(4)1(3)G(4)1S1Sf1	2.7	ND	ND	0.8	0.8	ND	1.9	ND	ND	ND	ND	5.0	5	2.24	ND	
A3	5	2	A3-5-2	15.57	986.70	3H ⁺	2957.07	N3H6Hn5PA1		A3G(4)3S3_2	1.6	4.1	ND	2.3	1.2	3.4	ND	ND	6.9	ND	1.3	9.6	8	3.81	1.08	
A3	6		A3-6	15.85	1157.09	3H ⁺	3468.26	N3H7Hn6dH1PA1		F(6)A4G(4)4S3_1	0.5	ND	ND	0.9	1.4	ND	2.0	1.3	1.7	ND	ND	5.9	7	1.97	ND	
A3	8		A3-8	16.39	1157.09	3H ⁺	3468.26	N3H7Hn6dH1PA1		F(6)A4G(4)4S3_2	0.5	ND	ND	ND	0.8	8.6	ND	ND	2.7	2.8	ND	7.8	6	3.86	ND	
A3	9		A3-9	16.96	986.70	3H ⁺	2957.07	N3H6Hn5PA1		A3G(4)3S3_3	2.5	ND	2.8	2.0	1.5	ND	3.1	4.9	4.8	ND	3.1	7.7	9	3.60	4.54	

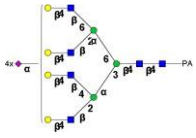
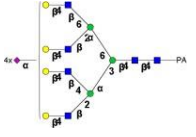
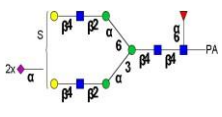
A3	10	A3-10	17.70	1157.09	3H+	3468.26	N3H7H6dH1PA1		F(6)A4G(4)4S3_3	0.6	ND	ND	0.0	1.6	ND	ND	3.5	4.4	4.7	ND	12.9	6	3.95	ND	
A3	11	A3-11	18.74	1157.09	3H+	3468.26	N3H7H6dH1PA1		F(6)A4G(4)4S3_4	1.0	ND	ND	2.5	2.9	ND	ND	ND	6.9	0.9	ND	13.0	6	4.54	ND	
A3	12	A3-12	19.42	1157.09	3H+	3468.26	N3H7H6dH1PA1		F(6)A4G(4)4S3_5	0.7	ND	ND	ND	0.6	ND	ND	ND	2.2	ND	ND	3.4	4	1.70	ND	
A3	13	A3-13	20.35	1035.38	3H+	3103.13	N3H6H5dH1PA1		F(6)A3G(4)3S3_1	2.5	1.6	1.5	0.9	1.2	5.8	3.7	ND	4.9	3.9	2.5	7.6	11	3.27	0.45	
A3	14	A3-14	22.02	1035.38	3H+	3103.13	N3H6H5dH1PA1		F(6)A3G(4)3S3_2	6.3	2.6	1.5	24.2	5.5	8.0	1.5	ND	11.9	8.4	2.4	23.2	11	8.69	0.24	
A3	15	A3-15	26.87	1035.38	3H+	3103.13	N3H6H5dH1PA1		F(6)A3G(4)3S3_3	3.5	2.7	1.5	3.7	2.6	6.3	2.5	0.5	4.5	6.6	2.3	15.1	12	4.32	ND	
A4	1	A4-1	12.08	1205.44	3H+	3613.30	N4H7H6PA1		A4G(4)4S4_1	0.5	ND	ND	0.7	1.4	ND	ND	0.7	2.7	2.7	ND	7.7	7	2.35	1.08	
A4	2	A4-2	13.59	1205.44	3H+	3613.30	N4H7H6PA1		A4G(4)4S4_2	0.9	ND	ND	1.2	4.7	ND	ND	ND	6.3	5.4	ND	17.1	6	5.92	0.35	
A4	3	A4-3	14.34	1524.90	3H+	4571.67	N4H7H610dH1PA1		A4F1G(4)4LacdNac2S4	0.5	ND	ND	0.7	6.6	ND	ND	ND	ND	ND	ND	ND	3	2.61	ND	
A4	4	A4-4	15.46	1054.34	2H+	2106.67	S2H3H6dH1PA1		F(6)A2GalNac(4)2S1I2	3.4	ND	4.0	5.0	2.8	2.3	7.8	4.1	3.4	ND	ND	10.5	9	4.81	ND	
A4	5	A4-5	16.68	1254.13	3H+	3759.35	N4H7H6dH1PA1		F(6)A4G(4)4S4_1	1.8	2.2	0.9	1.8	7.6	ND	2.7	0.8	9.7	10.1	3.9	25.9	11	6.12	ND	
A4	6	A4-6	17.79	1321.82	3H+	3962.43	N4H7H7dH1PA1		F(6)A4G(4)4A1S4	0.5	ND	ND	ND	2.5	ND	1.4	ND	3.4	ND	ND	9.2	5	3.41	ND	
A4	7	A4-7	18.62	1254.13	3H+	3759.35	N4H7H6dH1PA1		F(6)A4G(4)4S4_2	1.2	3.0	0.7	1.4	13.0	ND	ND	1.5	15.8	16.9	2.8	62.2	10	11.85	ND	
A4	8	A4-8	19.44	1375.84	3H+	4124.49	N4H8H7dH1PA1		F(6)A4G(4)4LacNac1S4_1	ND	ND	ND	ND	ND	ND	ND	1.7	ND	ND	4.5	2	3.12	ND		
A4	9	A4-9	21.85	1375.84	3H+	4124.49	N4H8H7dH1PA1		F(6)A4G(4)4LacNac1S4_2	ND	ND	ND	ND	2.3	ND	ND	ND	2.7	ND	ND	7.7	3	4.22	ND	
A4	10	1	A4-10-1	23.20	1132.41	3H+	3394.22	N4H6H5dH1PA1		F(6)A3G(4)3S4_1	ND	1.0	0.7	1.1	1.1	0.7	ND	0.7	0.7	3.3	ND	1.2	9	1.16	ND
A4	10	2	A4-10-2	23.20	1447.00	2H+	2891.99	S1N2H6H5dH1PA1		F(6)A3G(4)3S2S1I1	ND	ND	ND	ND	0.7	ND	ND	ND	0.5	ND	ND	3.0	3	1.37	ND
A4	11	A4-11	29.03	1132.41	3H+	3394.22	N4H6H5dH1PA1		F(6)A3G(4)3S4_2	ND	1.2	0.6	0.9	1.2	0.8	ND	0.9	0.4	2.1	1.7	0.9	10	1.06	ND	

1. Abbreviations of the composition are N for NeuAc, H for hexose, Hn for N-acetylhexosamine, dH for deoxyhexose(fucose), S for sulfate, PA for pyridylamino residue.
2. Proposed Glycan structure. Symbols was explained as follows: PA: pyridylamino- or 2-aminopyridine; blue square: GlcNAc; yellow square: GalNAc; green circle: mannose; yellow circle: galactose; red triangle: fucose; purple diamond: sialic acid (NeuAc); S: sulfur. GlycoWork-bench software was used to draw the glycan structure and their linkage information.
2. Abbreviations of the Oxford notation are M for Mannose, A for any GlcNAc comes after core GlcNAcs, B for Bisecting GlcNAc, F for fucose(F at the start of the abbreviation indicates a core fucose).
G for galactose, S for sialic acid, S1I for Sulfate.
- free numbers after certain glycan element e.g. A2 are used to indicate the number of that element in glycan structure
- [3]or [6] e.g. [6]G1 indicate that the glycan element comes after is on the antenna of the α -1-3 or α -1-6 mannose.
- Numbers in brackets e.g. F(6) are used to indicate linkages, where known.

Table 3. List of 24 unique serum N -glycans

NO.	Fraction of DEAE HPLC	Glucose unit on RP-HPLC	M/Z	ion form	MS	Composition ¹	Proposed structure ²	Oxford notation of glycans ³	The ratio of human serum N -glycans
1	N	6.67	1062.39	2H ⁺	2122.76	H10Hn2PA1		M9Gu	0.13%
2	N	6.89	758.79	2H ⁺	1515.57	H5Hn3PA1		M5[3]A1	0.16%
3	N	15.06	880.85	2H ⁺	1759.68	H4Hn5PA1		A2B[6]G(4)1	0.35%
4	A1	13.42	1026.39	2H ⁺	2050.77	N1H4Hn5PA1		A2B[3]G(4)1S(6)1	1.12%
5	A1	15.86	1078.91	2H ⁺	2155.8	N1H5Hn4dH1PA1		A2G(4)2[6]S(6)1	0.38%
6	A1	23.65	1261.48	2H ⁺	2520.94	N1H6Hn5dH1PA1		F(6)A3G(4)3S1	0.29%
7	A1	24.95	909.01	3H ⁺	2724.02	N1H6Hn6dH1PA1		F(6)A2BG(4)2 LacNac1S1	0.15%
8	A2	10.55	1011.38	3H ⁺	3031.11	N2H7Hn6PA1		A4G(4)4S2	0.77%
9	A2	13.02	1407.02	2H ⁺	2812.03	N2H6Hn5dH1PA1		F(6)A3G(4)3S2	1.21%
10	A2	18.39	1333.99	2H ⁺	2665.97	N2H6Hn5PA1		A3G(4)3S2	0.11%

11	A2	25.09	900.31	2H ⁺	1798.61	S1H5Hn4PA1		A2G(4)2S1f1	0.26%
12	A3	10.44	1157.09	3H ⁺	3468.26	N3H7Hn6dH1PA1		A4F1G(4)4S3	0.42%
13	A3	11.28	1108.41	3H ⁺	3322.2	N3H7Hn6PA1		A4G(4)4S3	0.84%
14	A3	11.55	1108.41	3H ⁺	3322.2	N3H7Hn6PA1		A4G(4)4S3	0.79%
15	A3	11.78	1108.41	3H ⁺	3322.2	N3H7Hn6PA1		A4G(4)4S3	0.42%
16	A3	12.19	1108.41	3H ⁺	3322.2	N3H7Hn6PA1		A4G(4)4S3	0.21%
17	A3	17.62	1479.54	2H ⁺	2957.07	N3H6Hn5PA1		A3G(4)3S3	0.47%
18	A3	18.57	1084.07	3H ⁺	3249.18	N3H6Hn5dH2PA1		F(6)A3F1G(4)3S3	0.51%
19	A4	10.18	1302.81	3H ⁺	3905.41	N4H7Hn6dH2PA1		A4F2G(4)4S4	0.15%
20	A4	10.63	1254.13	3H ⁺	3759.35	N4H7Hn6dH1PA1		A4F1G(4)4S4	0.26%
21	A4	11.02	1254.13	3H ⁺	3759.35	N4H7Hn6dH1PA1		A4F1G(4)4S4	0.55%

22	A4	11.47	1205.44	3H ⁺	3613.3	N4H7Hn6PA1		A4G(4)4S4	0.23%
23	A4	11.91	1205.44	3H ⁺	3613.3	N4H7Hn6PA1		A4G(4)4S4	0.54%
24	A2	14.20	1264.46	2H ⁺	2526.86	S1N2H5Hn4dH1PA1		F(6)A2G(4)2 S2S1f1	0.22%

1. Abbreviations of the composition are N for NeuAc, H for hexose, Hn for N -acetylhexosamine, dH for deoxyhexose(fucose), S for sulfate, PA for pyridylamino residue.

2. Proposed Glycan structure. Symbols was explained as follows: PA: pyridylamino- or 2-aminopyridine; blue square: GlcNAc; yellow square: GalNAc; green circle: mannose; yellow circle: galactose; red triangle: fucose; purple diamond:sialic acid (NeuAc); blue circle: Glucose.

S: sulfur. GlycoWork-bench software was used to draw the glycan structure and their linkage information.

2. Abbreviations of the Oxford notation are M for Mannose, A for the number of antennae (GlcNAc) on the trimannosyl core , B for Bisecting GlcNAc, F for fucose(F at the start of the abbreviation indicates a core fucose), G for galactose, S for sialic acid, Gu for Glucose, S1f for Sulfate.

- free numbers after certain glycan element e.g. A2 are used to indicate the number of that element in glycan structure.

- [3]or [6] e.g. [6]G1 indicate that the glycan element comes after is on the antenna of the α 1-3 or α 1-6 mannose.

- Numbers in brackets e.g. F(6) are used to indicate linkages, where known.

References

1. Stanley, P.; Cummings, R.D. Structures Common to Different Glycans. In *Essentials of Glycobiology*, 3rd ed.; Varki, A., Cummings, R.D., Esko, J.D., Stanley, P., Hart, G.W., Aebi, M., Darvill, A.G., Kinoshita, T., Packer, N.H., Prestegard, J.H., et al., Eds.; Cold Spring Harbor Laboratory Press: Cold Spring Harbor, NY, USA, 2015; pp. 161–178. <https://doi.org/10.1101/glycobiology.3e.014>.
2. Dotz, V.; Wuhrer, M. N-glycome signatures in human plasma: Associations with physiology and major diseases. *FEBS Lett.* **2019**, *593*, 2966–2976. <https://doi.org/10.1002/1873-3468.13598>.
3. An, H.J.; Froehlich, J.W.; Lebrilla, C.B. Determination of glycosylation sites and site-specific heterogeneity in glycoproteins. *Curr. Opin. Chem. Biol.* **2009**, *13*, 421–426. <https://doi.org/10.1016/j.cbpa.2009.07.022>.
4. Helm, J.; Hirtler, L.; Altmann, F. Towards Mapping of the Human Brain N-Glycome with Standardized Graphitic Carbon Chromatography. *Biomolecules* **2022**, *12*, 85. <https://doi.org/10.3390/biom12010085>.
5. Ohtsubo, K.; Marth, J.D. Glycosylation in cellular mechanisms of health and disease. *Cell* **2006**, *126*, 855–867. <https://doi.org/10.1016/j.cell.2006.08.019>.
6. Xiao, K.; Han, Y.; Tian, Z. Large-scale identification and visualization of human liver N-glycome enriched from LO₂ cells. *Anal. Bioanal. Chem.* **2018**, *410*, 4195–4202. <https://doi.org/10.1007/s00216-018-1070-2>.

7. Stumpo, K.A.; Reinhold, V.N. The N-glycome of human plasma. *J. Proteome Res.* **2010**, *9*, 4823–4830. <https://doi.org/10.1021/pr100528k>.
8. Li, H.; Patel, V.; DiMartino, S.E.; Froehlich, J.W.; Lee, R.S. An in-depth Comparison of the Pediatric and Adult Urinary N-glycomes. *Mol. Cell Proteom. MCP* **2020**, *19*, 1767–1776. <https://doi.org/10.1074/mcp.RA120.002225>.
9. Zhao, J.; Li, S.; Li, C.; Wu, S.L.; Xu, W.; Chen, Y.; Shameem, M.; Richardson, D.; Li, H. Identification of Low Abundant Isomeric N-Glycan Structures in Biological Therapeutics by LC/MS. *Anal. Chem.* **2016**, *88*, 7049–7059. <https://doi.org/10.1021/acs.analchem.6b00636>.
10. Abrahams, J.L.; Campbell, M.P.; Packer, N.H. Building a PGC-LC-MS N-glycan retention library and elution mapping resource. *Glycoconj. J.* **2018**, *35*, 15–29. <https://doi.org/10.1007/s10719-017-9793-4>.
11. Tomiya, N.; Awaya, J.; Kurono, M.; Endo, S.; Arata, Y.; Takahashi, N. Analyses of N-linked oligosaccharides using a two-dimensional mapping technique. *Anal. Biochem.* **1988**, *171*, 73–90. [https://doi.org/10.1016/0003-2697\(88\)90126-1](https://doi.org/10.1016/0003-2697(88)90126-1).
12. Natsuka, S.; Masuda, M.; Sumiyoshi, W.; Nakakita, S. Improved method for drawing of a glycan map, and the first page of glycan atlas, which is a compilation of glycan maps for a whole organism. *PLoS ONE* **2014**, *9*, e102219. <https://doi.org/10.1371/journal.pone.0102219>.
13. Vreeker, G.C.; Wührer, M. Reversed-phase separation methods for glycan analysis. *Anal. Bioanal. Chem.* **2017**, *409*, 359–378. <https://doi.org/10.1007/s00216-016-0073-0>.

14. Suzuki, N.; Abe, T.; Hanzawa, K.; Natsuka, S. Toward robust N-glycomics of various tissue samples that may contain glycans with unknown or unexpected structures. *Sci. Rep.* **2021**, *11*, 6334. <https://doi.org/10.1038/s41598-021-84668-x>.
15. Saito, S.; Hirao, Y.; Quadery, A.F.; Xu, B.; Elguoshy, A.; Fujinaka, H.; Koma, S.; Yamamoto, K.; Yamamoto, T. The Optimized Workflow for Sample Preparation in LC-MS/MS-Based Urine Proteomics. *Methods Protoc.* **2019**, *2*, 46. <https://doi.org/10.3390/mps2020046>.
16. Yosizawa, Z.; Sato, T.; Schmid, K. Hydrazinolysis of alpha-1-acid glycoprotein. *Biochim. Biophys. Acta* **1966**, *121*, 417–420. [https://doi.org/10.1016/0304-4165\(66\)90134-6](https://doi.org/10.1016/0304-4165(66)90134-6).
17. Natsuka, S.; Hase, S. Analysis of N- and O-glycans by pyridylamination. *Methods Mol. Biol.* **1998**, *76*, 101–113. <https://doi.org/10.1385/0-89603-355-4:101>.
18. Hase, S.; Ikenaka, T.; Matsushima, Y. Structure analyses of oligosaccharides by tagging of the reducing end sugars with a fluorescent compound. *Biochem. Biophys. Res. Commun.* **1978**, *85*, 257–263. [https://doi.org/10.1016/s0006-291x\(78\)80037-0](https://doi.org/10.1016/s0006-291x(78)80037-0).
19. Kuraya, N.; Hase, S. Release of O-linked sugar chains from glycoproteins with anhydrous hydrazine and pyridylamination of the sugar chains with improved reaction conditions. *J. Biochem.* **1992**, *112*, 122–126. <https://doi.org/10.1093/oxfordjournals.jbchem.a123850>.
20. Natsuka, S.; Hirohata, Y.; Nakakita, S.; Sumiyoshi, W.; Hase, S. Structural analysis of N-glycans of the planarian *Dugesia japonica*. *FEBS J.* **2011**, *278*, 452–460. <https://doi.org/10.1111/j.1742-4658.2010.07966.x>.

21. Harvey, D.J.; Merry, A.H.; Royle, L.; Campbell, M.P.; Dwek, R.A.; Rudd, P.M. Proposal for a standard system for drawing structural diagrams of N- and O-linked carbohydrates and related compounds. *Proteomics* **2009**, *9*, 3796–3801. <https://doi.org/10.1002/pmic.200900096>.
22. Doherty, M.; Theodoratou, E.; Walsh, I.; Adamczyk, B.; Stockmann, H.; Agakov, F.; Timofeeva, M.; Trbojevic-Akmacic, I.; Vuckovic, F.; Duffy, F.; et al. Plasma N-glycans in colorectal cancer risk. *Sci. Rep.* **2018**, *8*, 8655. <https://doi.org/10.1038/s41598-018-26805-7>.
23. Chen, W.C.; Lin, H.S.; Chen, H.Y.; Shih, C.H.; Li, C.W. Effects of Tamm-Horsfall protein and albumin on calcium oxalate crystallization and importance of sialic acids. *Mol. Urol.* **2001**, *5*, 1–5. <https://doi.org/10.1089/109153601750124186>.
24. Kukulski, W. A glycoprotein in urine binds bacteria and blocks infections. *Science* **2020**, *369*, 917–918. <https://doi.org/10.1126/science.abd7124>.
25. Kipp, A.; Olinger, E. What Does Uromodulin Do? *Clin. J. Am. Soc. Nephrol.* **2021**, *16*, 150–153. <https://doi.org/10.2215/cjn.06390420>.
26. Volpi, N.; Galeotti, F.; Yang, B.; Linhardt, R.J. Analysis of glycosaminoglycan-derived, precolumn, 2-aminoacridone-labeled disaccharides with LC-fluorescence and LC-MS detection. *Nat. Protoc.* **2014**, *9*, 541–558. <https://doi.org/10.1038/nprot.2014.026>.
27. Tomiya, N.; Takahashi, N. Contribution of component monosaccharides to the coordinates of neutral and sialyl pyridylaminated N-glycans on a two-dimensional sugar map. *Anal. Biochem.* **1998**, *264*, 204–210. <https://doi.org/10.1006/abio.1998.2849>.

28. Thongboonkerd, V.; Malasit, P. Renal and urinary proteomics: Current applications and challenges. *Proteomics* **2005**, *5*, 1033–1042. <https://doi.org/10.1002/pmic.200401012>.
29. Parsons, C.L.; Proctor, J.; Teichman, J.S.; Nickel, J.C.; Davis, E.; Evans, R.; Zupkas, P.; Phillips, C.; Shaw, T.; Naidu, N.; et al. A multi-site study confirms abnormal glycosylation in the Tamm-Horsfall protein of patients with interstitial cystitis. *J. Urol.* **2011**, *186*, 112–116. <https://doi.org/10.1016/j.juro.2011.02.2699>.
30. Patabandige, M.W.; Go, E.P.; Desaire, H. Clinically Viable Assay for Monitoring Uromodulin Glycosylation. *J. Am. Soc. Mass Spectrom.* **2021**, *32*, 436–443. <https://doi.org/10.1021/jasms.0c00317>.
31. Dini, L.; Autuori, F.; Lentini, A.; Oliverio, S.; Piacentini, M. The clearance of apoptotic cells in the liver is mediated by the asialoglycoprotein receptor. *FEBS Lett.* **1992**, *296*, 174–178. [https://doi.org/10.1016/0014-5793\(92\)80373-O](https://doi.org/10.1016/0014-5793(92)80373-O).
32. Seow, Y.Y.; Tan, M.G.; Woo, K.T. Expression of a functional asialoglycoprotein receptor in human renal proximal tubular epithelial cells. *Nephron* **2002**, *91*, 431–438. <https://doi.org/10.1159/000064283>.
33. Lee, S.J.; Evers, S.; Roeder, D.; Parlow, A.F.; Risteli, J.; Risteli, L.; Lee, Y.C.; Feizi, T.; Langen, H.; Nussenzweig, M.C. Mannose receptor-mediated regulation of serum glycoprotein homeostasis. *Science* **2002**, *295*, 1898–1901. <https://doi.org/10.1126/science.1069540>.
34. Li, H.; Kostel, S.A.; DiMartino, S.E.; Hashemi Gheinani, A.; Froehlich, J.W.; Lee, R.S. Uromodulin Isolation and Its N-Glycosylation Analysis by NanoLC-MS/MS. *J. Proteome Res.* **2021**, *20*, 2662–2672. <https://doi.org/10.1021/acs.jproteome.0c01053>.

35. Jefferis, R.; Lund, J.; Mizutani, H.; Nakagawa, H.; Kawazoe, Y.; Arata, Y.; Takahashi, N. A comparative study of the N-linked oligosaccharide structures of human IgG subclass proteins. *Biochem. J.* **1990**, *268*, 529–537. <https://doi.org/10.1042/bj2680529>.
36. Takamatsu, S.; Katsumata, T.; Inoue, N.; Watanabe, T.; Fujibayashi, Y.; Takeuchi, M. Abnormal biantennary sugar chains are expressed in human chorionic gonadotropin produced in the choriocarcinoma cell line, JEG-3. *Glycoconj. J.* **2004**, *20*, 473–481. <https://doi.org/10.1023/B:GLYC.0000038293.37376.9f>.
37. Tanaka, T.; Biancotto, A.; Moaddel, R.; Moore, A.Z.; Gonzalez-Freire, M.; Aon, M.A.; Candia, J.; Zhang, P.; Cheung, F.; Fantoni, G.; et al. Plasma proteomic signature of age in healthy humans. *Aging Cell* **2018**, *17*, e12799. <https://doi.org/10.1111/accel.12799>.
38. Blaschke, C.R.K.; Hartig, J.P.; Grimsley, G.; Liu, L.; Semmes, O.J.; Wu, J.D.; Ippolito, J.E.; Hughes-Halbert, C.; Nyalwidhe, J.O.; Drake, R.R. Direct N-Glycosylation Profiling of Urine and Prostatic Fluid Glycoproteins and Extracellular Vesicles. *Front. Chem.* **2021**, *9*, 734280. <https://doi.org/10.3389/fchem.2021.734280>.
39. Yang, G.; Tan, Z.; Lu, W.; Guo, J.; Yu, H.; Yu, J.; Sun, C.; Qi, X.; Li, Z.; Guan, F. Quantitative glycome analysis of N-glycan patterns in bladder cancer vs normal bladder cells using an integrated strategy. *J. Proteome Res.* **2015**, *14*, 639–653. <https://doi.org/10.1021/pr5006026>.